

# Early phases in the stellar and substellar formation and evolution<sup>\*</sup>

## Infrared and submillimeter data in the Barnard 30 dark cloud

D. Barrado<sup>1</sup>, I. de Gregorio Monsalvo<sup>2,3</sup>, N. Huélamo<sup>1</sup>, M. Morales-Calderón<sup>1</sup>, A. Bayo<sup>4,5</sup>, A. Palau<sup>6</sup>, M.T. Ruiz<sup>7</sup>, P. Rivière-Marichalar<sup>8</sup>, H. Bouy<sup>1</sup>, Ó. Morata<sup>9</sup>, J.R. Stauffer<sup>10</sup>, C. Eiroa<sup>11,12</sup>, and A. Noriega-Crespo<sup>13</sup>

<sup>1</sup> Depto. Astrofísica, Centro de Astrobiología (INTA-CSIC), ESAC campus, Camino Bajo del Castillo s/n, E-28692 Villanueva de la Cañada, Spain e-mail: barrado@cab.inta-csic.es

<sup>2</sup> European Southern Observatory, Alonso de Córdova 3107, Vitacura, Santiago, Chile.

<sup>3</sup> Joint ALMA Observatory, Alonso de Córdova 3107, Vitacura, Santiago, Chile

<sup>4</sup> Departamento de Física y Astronomía, Facultad de Ciencias, Universidad de Valparaíso, Av. Gran Bretaña 1111, 5030 Casilla, Valparaíso, Chile

<sup>5</sup> ICM nucleus on protoplanetary disks, Universidad de Valparaíso, Av. Gran Bretaña 1111, Valparaíso, Chile

<sup>6</sup> Instituto de Radioastronomía y Astrofísica, Universidad Nacional Autónoma de México, P.O. Box 3-72, 58090 Morelia, Michoacán, México

<sup>7</sup> Depto. de Astronomía, Universidad de Chile, Camino del Observatorio 1515, Santiago, Chile.

<sup>8</sup> European Space Astronomy Centre (ESA), Camino Bajo del Castillo s/n, 28692 Villanueva de la Cañada, Madrid, Spain

<sup>9</sup> Institute of Astronomy and Astrophysics, Academia Sinica, 11F of AS/NTU Astronomy-Mathematics Building, No.1, Sec. 4, Roosevelt Rd, Taipei 10617, Taiwan

<sup>10</sup> Spitzer Science Center, California Institute of Technology, Pasadena, CA 91125, USA.

<sup>11</sup> Depto. Física Teórica, Fac. de Ciencias, Universidad Autónoma de Madrid, Campus Cantoblanco, 28049 Madrid, Spain.

<sup>12</sup> Unidad Asociada UAM-CAB/CSIC, Madrid, Spain.

<sup>13</sup> Space Telescope Science Institute, 3700 San Martin Dr., Baltimore, MD 21218, USA.

Received ; accepted

### ABSTRACT

**Aims.** The early evolutionary stage of brown dwarfs are not very well characterized, specially during the embedded phase. Our goal is to gain insight into the dominant formation mechanism of very low-mass objects and brown dwarfs.

**Methods.** We have conducted deep observations at 870  $\mu\text{m}$  obtained with the LABOCA bolometer at the APEX telescope in order to identify young submillimeter sources in the Barnard 30 dark cloud. We have complemented these data with multi-wavelength observations from the optical to the far-IR and compiled complete spectral energy distributions (SEDs) in order to identify the counterparts, characterize the sources and to assess their membership to the association and stellar or substellar status based on the available photometric information.

**Results.** We have identified 34 submillimeter sources and a substantial number of possible and probable Barnard 30 members within each individual APEX/LABOCA beam. They can be classified in three distinct groups. First, 15 out of these 34 have a clear optical or IR counterpart to the submm peak and nine of them are potential proto-BDs candidates. Moreover, a substantial number of them could be multiple systems. A second group of 13 sources comprises candidate members with significant infrared excesses located away from the central submm emission. All of them include brown dwarf candidates, some displaying IR excess, but their association with submm emission is unclear. In addition, we have found six starless cores and, based on the total dust mass estimate, three might be pre-substellar (or pre-BDs) cores. Finally, the complete characterization of our APEX/LABOCA sources, focusing on those detected at 24 and/or 70  $\mu\text{m}$ , indicates that in our sample of 34 submm sources there are, at least: two WTTs, four CTTs, five young stellar objects (YSOs), eight proto-BD candidates (with another three dubious cases), and one Very Low Luminosity objects (VeLLO).

**Conclusions.** Our findings provide additional evidence concerning the brown dwarf formation mechanism, which seems to be a downsized version of the stellar formation.

**Key words.** circumstellar matter – stars: formation – stars: low-mass, brown dwarfs – stars: pre-main sequence – infrared: stars – open clusters and associations: individual: Barnard 30 dark cloud

## 1. Introduction

The Barnard 30 dark cloud (B30, hereafter) is located at the rim of the Lambda Orionis star forming region (Murdin & Penston 1977), a complex structure at about 400 pc, which gives shape to

the head of Orion. Although bright, massive stars usually dominate stellar associations, swarms of low-mass objects, much less conspicuous, can be found inside them. Our aim is to unveil this population and to focus on the early phases of low-mass evolution by analyzing this moderately nearby and very interesting dark cloud, whose star formation and shape seems to be triggered and/or controlled by the O8 III  $\lambda$  Orionis star (actually, a binary, Bouy et al. 2009) and perhaps by a supernova event which took

Send offprint requests to: D. Barrado

\* Tables 3, 4, 5, 6 and 7 are only available in electronic form at the CDS via anonymous ftp to cdsarc.u-strasbg.fr (130.79.128.5) or via <http://cdsweb.u-strasbg.fr/cgi-bin/qcat?J/A+A/>

place a few Myr ago (see Maddalena & Morris 1987; Cunha & Smith 1996; Dolan & Mathieu 2002).

Although the age of B30 is not very well constrained (it is normally given as 2-3 Myr), it is very likely significantly younger than the central cluster, Collinder 69 (C69 hereafter) whose nominal age is 5-8 Myr (Barrado y Navascués et al. 2004; Bayo et al. 2011). We note, however, that an older value has been proposed for C69 (10-12 Myr, Bell et al. 2013; Bayo et al. 2011). While there are no Class I objects in C69 (Barrado y Navascués et al. 2007), the ratio of Class I to Class II objects in B30 is 1:2 (Morales-Calderón 2008, based on a Spitzer/IRAC color-color diagram (CCD), Allen et al. 2004). This schematic classification is described in Lada (1987) and Adams et al. (1987) and it is based on the spectral energy distribution (SED) and interpreted in an evolutionary scenario. Therefore, B30 is an excellent hunting ground to find embedded stars and, if deep infrared surveys are conducted, substellar objects (i.e., brown dwarfs or BDs, quasi stellar objects unable to burn hydrogen at any evolutionary stage. For solar metallicity, the mass is lower than  $\sim 0.072 M_{\odot}$ ).

Dolan & Mathieu (1999, 2001, 2002) and Koenig et al. (2015) carried out an extensive search of young, low-mass stars in the Lambda Orionis star forming region, including optical imaging and medium resolution spectroscopy. Their initial photometric search was centered around the central, massive star  $\lambda$  Orionis (the C69 cluster), and near the dark clouds B30 and Barnard 35, located northwest and east from C69, respectively. In the first case, their photometric survey and subsequent spectroscopic confirmation (via radial velocity and lithium detection) allowed the identification of 266 stellar members in an area around these three groups. Among them, 63 can be considered members of the B30 dark cloud. In the case of Koenig et al. (2015), they identified 544 photometric stellar candidates in a 200 sq.deg area. A subsample of 175 was confirmed spectroscopically either by them or by previous studies, with a pollution rate less than 24%. Regarding the central cluster, Bayo et al. (2011) includes 172 spectroscopically confirmed members for C69, and a significant number of them are very well inside the brown dwarf domain. Now, our focus is the significantly younger B30 cloud.

As shown by the aforementioned studies, the B30 complex is in a very early stage of star formation, and becomes an excellent testbed to search for the most embedded low-mass objects and brown dwarfs. Recent studies suggest that the particular environmental conditions of a star forming cloud may play an important role in determining the outcome of very low-mass objects and BDs in that cloud (e.g., Levine et al. 2006; Scholz et al. 2013; Polychroni et al. 2013; Drass et al. 2016). In low-mass star forming regions, which typically form objects in groups or loose associations, the main BD formation mechanisms are turbulent fragmentation (Padoan & Nordlund 2004; Hennebelle & Chabrier 2008), and ejection from multiple protostellar systems and/or fragmented disks (Reipurth & Clarke 2001; Bate et al. 2002; Matzner & Levin 2005; Whitworth & Stamatellos 2006). However, in the surroundings of high-mass stars, where objects typically form more closely packed, there are additional plausible mechanisms, namely photo-evaporation of cores near massive stars (e.g., Hester et al. 1996; Whitworth & Zinnecker 2004), and gravitational fragmentation of dense filaments formed in a nascent cluster (e.g., Bonnell et al. 2008; Bate 2012), suggesting that these clustered regions bathed by the feedback from high-mass stars could show higher BD-to-star ratios. From the observational point of view, the study of the most embedded and youngest BDs requires the use of the millimeter or submillimeter regime, where they emit the bulk of their energy, as they are

dominated by cold envelopes. Thus, it is necessary to conduct systematic multi-wavelength searches for BDs in clouds forming low-mass stars and also in clouds forming high-mass stars in closely packed environments.

Here we will mainly deal with four types of young objects. A young stellar object (YSO) contains an accreting hydrostatic core inside, whose final mass (after accretion and infall is finished) will be above  $75 M_{jup}$  (i.e., will form a star). In the literature it is possible to find restricted definitions, so a YSO would be in the Class 0 or I stages. A more flexible definition includes all the evolutionary stages that the hydrostatic core takes before reaching the main sequence (i.e., Class 0, I, II and III). A proto-BD also contains an embedded accreting hydrostatic core inside, whose final mass (after accretion and infall is finished) will be in the range  $13-75 M_{jup}$ . Thus, they are analogs to the Class 0/I protostars but in the substellar regime. An early phase would be a pre-BD, which is a dense core which will form a brown dwarf in a future but did not form an hydrostatic core yet (i.e., it is an analog to the "starless" cores for higher masses). Finally, a VeLLO (Very Low Luminosity objects) is a dense source with an accreting hydrostatic core inside, whose internal luminosity ( $L_{int}$ ) is equal or below  $0.1 L_{\odot}$ . We note that all proto-BDs are VeLLOs, but not all VeLLOs are proto-BDs.

Several works have been focused on the search for the youngest embedded brown dwarfs (proto-BDs), in different star forming regions. A number of VeLLOs have been identified as potential proto-BDs candidates (Young et al. 2004; di Francesco et al. 2007; Dunham et al. 2008). The first hydrostatic cores (FHCs), predicted by Larson (1969), might be classified as proto-BD candidates, since they are characterized by very low internal luminosities and very low masses, SEDs peaking at  $\sim 100 \mu\text{m}$ , and presence of low velocity outflows (e.g. Machida et al. 2008). To date, several FHCs have been identified (e.g. Onishi et al. 1999; Belloche et al. 2006a,b; Chen et al. 2010, 2012). However, the envelope masses of FHCs are too large so it seems unlikely that they will remain substellar (see Table 4 in Palau et al. 2014). Finally, observational studies using a multi-wavelength approach have provided several proto-BD candidates in different clouds and star forming regions (Barrado et al. 2009; Lee et al. 2009, 2013; Kauffmann et al. 2011; André et al. 2012; Palau et al. 2012, 2014; Morata et al. 2015; Liu et al. 2016; Riaz et al. 2016; de Gregorio-Monsalvo et al. 2016; Huélamo et al. 2017). Despite these efforts, the number of proto-BD candidates is still very small and the characterization incomplete.

In this work we present the results regarding a search of very young low-mass stars and BDs in one of the bright rims of the B30 dark cloud. The study is based on deep observations at  $870 \mu\text{m}$  obtained with the LABOCA bolometer array, installed on the Atacama Pathfinder EXperiment (APEX<sup>1</sup>) telescope, complemented with multi-wavelength observations from the optical to the far-infrared. The goal of the study is to gain insight into the dominant formation mechanism of very low-mass objects and BDs in this particular region of the Lambda Orionis star forming region. The data are described in Sect. 2, with a detailed description of the submillimeter imaging (subsect. 2.1). The master catalog for all possible counterparts to our B30 submillimeter sources is described in subsect. 2.6. In Sect. 3 we explain how we select cluster candidates from this list and discuss some in-

<sup>1</sup> This work is partially based on observations with the APEX telescope. APEX is a collaboration between the Max-Planck-Institute für Radioastronomie, the European Southern Observatory, and the Onsala Space Observatory

dividual cases in more detail. Sect. 4 summarizes the findings of this paper. A follow-up study based on ALMA observations is presented in Huélamo et al. (2017).

## 2. Observations and archival data

This work is focused on submm observations obtained with APEX/LABOCA at  $870\ \mu\text{m}$ . The region mapped by LABOCA (Fig. 1a) was selected based on the Spitzer nebulosity, as can be seen in Fig. 1b, where we display a Spitzer/MIPS image at  $24\ \mu\text{m}$  together with the APEX/LABOCA detections. This area contains a significant number of Class II objects (Morales-Calderón 2008; Bayo 2009). To complement the submm data, we have used both observations obtained by our group and data retrieved from public archives covering a broad wavelength range. These complementary observations are described in the following subsections, while their main characteristics (e.g. limiting magnitude, beam size, pointing accuracy) are summarized in Table 1.

### 2.1. APEX/LABOCA mapping at $870\ \mu\text{m}$

Continuum observations at  $870\ \mu\text{m}$  were carried out using APEX/LABOCA. The field of view (FOV) of the array is 11.4 arcmin, and the angular resolution of each beam is  $18.6\pm 1$  arcsec. APEX pointing errors, as quoted by the observatory<sup>2</sup>, are 2 arcsec, although our observations have smaller errors (see below).

Our data were acquired on 2008 October 09-10 within the Chilean program 082.F-0001B, under excellent weather conditions (zenith opacity values of 0.22 at  $870\ \mu\text{m}$ ). Observations were performed using a spiral raster mapping centered at  $\alpha = 05^{\text{h}}31^{\text{m}}18.96^{\text{s}}$ ,  $\delta = +12^{\circ}07'16.75''$  (J2000.0). This observing mode consist of a set of spirals with radii between 2 and 3 arcmin at a combination of nine and four raster positions separated by 60 arcsec in azimuth and elevation, with an integration time of 40 seconds per spiral. This mode provides a fully sampled and homogeneously covered map in an area of  $15\times 15$  arcmin. The total covered area has a quasi-circular shape with about 37 arcmin diameter. It represents about a 20-25% of the total projected size of the dark cloud, as seen by IRAS.

The total on source integration time was  $\sim 2.7$  hours. Calibration was performed using observations of Uranus as well as N2071R as secondary calibrator. The absolute flux calibration uncertainty is estimated to be  $\sim 8\%$ . The telescope pointing was checked every hour toward the source J0530+135, finding an rms pointing accuracy of  $\sim 1$  arcsec, smaller than the nominal pointing accuracy (2 arcsec) and the range quoted by Weiß et al. (2009), 3–4 arcsec, which was estimated with a Monte Carlo simulation.

We reduced the data using the BoA and MiniCRUSH software packages (see Kovács 2008). The pre-processing steps consisted of flagging dead or cross-talking channels, frames with too high telescope accelerations and with unsuitable mapping speed, as well as temperature drift correction using two blind bolometers. The data reduction process includes flat-fielding, opacity correction, calibration, correlated noise removal (atmospheric fluctuations seen by the whole array, as well as electronic noise originated in groups of detector channels), and de-spiking. Every scan was visually inspected to identify and discard corrupted data. We used an optimized data processing to recover faint sources, which smoothed the map to a final angular resolution of 27.6 arcsec.

<sup>2</sup> <http://www.apex-telescope.org/telescope/>

In total, we have detected 34 sources above a  $4\ \sigma$  detection threshold. The coordinates and the APEX/LABOCA fluxes at  $870\ \mu\text{m}$  are listed in Table 2. The APEX/LABOCA image of Barnard 30 is shown in Fig. 1a.

### 2.2. CAHA/Omega2000 near-IR

Deep near-IR data were acquired with the Omega2000 instrument at the CAHA 3.5m telescope (Calar Alto Observatory in Spain<sup>3</sup>), an imager with a  $15\times 15$  arcmin FOV. We collected a  $\sim 1^{\circ}\times 1^{\circ}$  grid in the *J*-band image, with a total ten minutes exposure per pointing. The data were obtained in December 2007 (a large mosaic in the *J* filter) and August 30th, 2011 (deep images in *JHKs* centered in the LABOCA pointing).

The initial data reduction was carried out with the "jitter" package from the eclipse library, version 5.0.0 (Devillard 1999, 1997), and involved flat field correction, bad pixel masking and frame combination. Typically, ten frames were available to combine, and we let jitter reject two to four frames per image to improve the final quality. The astrometry calibration was applied using Aladin with 2MASS as the reference catalog. Photometry was extracted using sextractor to detect the sources and to compute the aperture and PSF photometry for each detected object. An individual calibration was applied to each image, given the availability of 2MASS photometry. The process involves only zero point calibration, and we use well detected sources, with 2MASS magnitude not larger than 15 and quality flag A. The zero point error typically goes from 0.05 to 0.09 mag.

Due to their depth, our near-IR images include a very large number of detections. Based on the count number (see Fig. 2 for an example), the completeness and limiting magnitudes are  $J_{\text{compl}}\sim 18.75$  mag, and  $J_{\text{lim}}\sim 20.5$  mag in the case of the mosaic collected during December 2007. For the observations collected four years later, we have derived  $J_{\text{compl}}\sim 19.25$  mag,  $H_{\text{compl}}\sim 18.25$  mag,  $K_{\text{S compl}}\sim 16.25$  mag; and  $J_{\text{lim}}\sim 21.50$  mag,  $H_{\text{lim}}\sim 20.50$  mag,  $K_{\text{S lim}}\sim 18.25$  mag. The complete information is listed in Table 1.

### 2.3. WFC optical imaging

Morales-Calderón (2008) provides a detailed description of all of the optical and mid-IR observational data we have obtained for the Lambda Orionis star forming region (including the B30 dark cloud) and our basic data reduction procedures. Here we provide just a brief summary.

The optical survey on the Barnard 30 association was performed on 2005 December 24-26 with the 2.5m Isaac Newton Telescope at El Roque de los Muchachos Observatory (La Palma, Spain) and the Wide Field Camera<sup>4</sup>. Sloan-gunn *r* and *i* filters were used and 4 different pointings were observed covering the whole stellar cluster centered in Barnard 30. Short and long exposure times were used, in the first case, we exposed for 5 sec for each filter whereas the long exposure times were 600 and  $3\times 400$  sec for sloan-gunn *i* and *r* respectively.

<sup>3</sup> Based on observations collected at the Centro Astronomico Hispano Aleman (CAHA) at Calar Alto, operated jointly by the Max-Planck-Institut für Astronomie and the Instituto de Astrofísica de Andalucía (CSIC)

<sup>4</sup> Based on observations made through the Isaac Newton Groups' Wide Field Camera Survey Programme with the Isaac Newton Telescope operated on the island of La Palma by the Isaac Newton Group in the Spanish Observatorio del Roque de los Muchachos of the Instituto de Astrofísica de Canarias

The weather during the run was clear and the mean seeing as measured in the images is 1.5 arcsec. The reduction and photometry was performed with the CASU INT Wide Field Survey pipeline (see Irwin & Lewis 2001, for more information on the pipeline). We used an aperture of five pixels, designed to match median seeing of our survey data and we have used the transformations provided by the ING to go from sloan-gunn magnitudes to Landolt (Johnson-Cousin's). The final completeness magnitudes are  $R_{compl} = 22.0$  mag and  $I_{compl} = 20.5$  mag.

#### 2.4. Spitzer/IRAC and MIPS data

Our Spitzer<sup>5</sup> data were collected in 2005 October 22nd and 2006 March 29th with IRAC, and 2006 March 2nd with MIPS as part of a General Observer cycle 2 program (PID:20339). The two epochs of IRAC imaging were obtained in mapping mode with individual exposures of 12 seconds frame time and three dithers at each map step. The high dynamic range option, which provides additional shorter (0.6 second frametime) exposures interleaved with the longer exposures, was used. Frames from the two epochs were co-added into one single deeper mosaic at each of the four bandpasses using the MOPEX package (Makovoz & Marleau 2005). The region with data in the four IRAC bandpasses covers  $\sim 0.6^\circ \times 1.2^\circ$  and is centered at 05:31:22.77 +12:14:52.35. The mean integration time for the deep mosaics is 62.4 sec. MIPS data were obtained with fast rate scan mode and a total effective integration time per point on the sky of  $\sim 15$  seconds. The mosaic covered an area of  $1^\circ \times 2.4^\circ$  centered around 05:30:23.17 +11:55:52.83. Since there were no visible artifacts in the pipeline mosaic for MIPS 24  $\mu\text{m}$  we used it as our starting point to extract the photometry.

Both source extraction and aperture photometry were done with IRAF. We used apertures of three pixels (3.66 arcsec) radius in the case of IRAC, and the sky was computed using a circular annulus four pixels wide, starting at a radius three pixels away from the center. For the MIPS data at 24  $\mu\text{m}$ , we used a 5.31 pixels (13 arcsec) aperture and a sky annulus from 8.16 pixels (20 arcsec) to 13.06 pixels (32 arcsec). Aperture correction was applied in both cases. Details are summarized in Table 1 and are fully reported in Morales-Calderón (2008).

Since there is some structured nebulosity in the region and in order to verify that our detections are real we have visually inspected the location of every source in a median filtered mosaic (which has part of the diffuse emission filtered). We have also performed a psf fitting to make sure that each detection is consistent with a point source instead of just part of the nebulosity. To do that we used Spitzer/APEX tool within MOPEX to filter our mosaic with a high band pass filter. That removes the majority of the nebulosity. Then we searched that image for point sources and fitted a PSF to them. Thus, when we were able to subtract a psf from the image and the filtered image showed a point source we kept those detections as real.

In some cases, the visual inspection of the filtered image indicated that a 24  $\mu\text{m}$  source might not be real or could be strongly affected by the inhomogeneous extended emission. These values have been flagged with an asterisk in Table 3 and, although some of these detections might be real, the listed values should be used with some caveats.

The LABOCA FOV is not fully covered by the Spitzer/MIPS image at 70  $\mu\text{m}$  (M2 band), which presents stripes with no data

every 3 arcmin all along the north-to-south direction. We extracted the M2 photometry in all the LABOCA detections covered by this filter, and the fluxes are listed in Table 2. For the sources with MIPS M2 emission peaking inside the beam, we measured the flux inside an aperture of 30 arcsec of diameter (the LABOCA beam) centered on the core, and subtracted the background emission assessed in a nearby non-emitting region of the same area. For the sources with extended M2 emission we did not subtract the background as this cannot be easily assessed, and adopted this value as a conservative upper limit. The completeness and limiting magnitudes are:  $[3.6]_{compl}=17.5$  mag,  $[4.5]_{compl}=17.0$  mag,  $[5.8]_{compl}=15.0$  mag,  $[8.0]_{compl}=14.5$  mag,  $[24.0]_{compl}=8.5$  mag; and  $[3.6]_{lim}=18.25$  mag,  $[4.5]_{lim}=17.75$  mag,  $[5.8]_{lim}=15.50$  mag,  $[8.0]_{lim}=14.75$  mag,  $[24.0]_{lim}=9.25$  mag, when selecting objects with magnitudes with errors smaller than 0.15 mag (Table 1).

#### 2.5. Public databases

We have also searched for photometric data in public archives. Among others, we have taken advantage of the tool implemented within Virtual Observatory SED Analyzer (VOSA<sup>6</sup>, Bayo et al. 2008 and Bayo et al. 2018, in prep.), under the Virtual Observatory protocols, and developed by the Spanish node<sup>7</sup>. See details below.

##### 2.5.1. Akari mid- and far-IR data

The Japanese satellite Akari has provided an All-sky catalog in the mid- and far-IR by using two different instruments: IRC and FIS. Updated information can be found at the mission webpage<sup>8</sup>.

In the first case, comprehensive information about IRC can be found in Ishihara et al. (2010), and should be complemented with the mission release notes. Akari has provided fluxes in the S9W and L18W filters down to 50 mJy and 90 mJy –IRC Release We note p. 29– (50 mJy and 120 mJy nominal,  $5\sigma$  detections). The effective beam size is 5.5 and 5.7 arcsec, respectively and sources within 7 arcsec of each other are considered the same. Regarding the accuracy of the pointing (IRC Release Note p. 19), the latest value is  $0.765 \pm 0.574$  arcsec. Moreover, 95% of the Akari/IRC detections are closer than 2arcsec to the 2MASS counterparts (75% are closer than 1 arcsec).

In the case of the FIS instrument (Kawada et al. 2007), there are four different wide channels, namely N60 (65  $\mu\text{m}$ ), WIDE-S (90  $\mu\text{m}$ ), WIDE-L (140  $\mu\text{m}$ ), and N160 (160  $\mu\text{m}$ ). The  $5\sigma$  limiting fluxes in survey mode are 2.4, 0.55, 1.4 and 6.3 Jy. Effective size of the point spread function of AKARI FIS in FWHM is estimated to be  $37 \pm 1$  arcsec,  $39 \pm 1$  arcsec,  $58 \pm 3$  arcsec, and  $61 \pm 4$  arcsec at N60, WIDE-S, WIDE-L, and N160. Finally, the pointing accuracy is 3.8 arcsec in RA ( $\sim$  cross-scan) and 4.8 arcsec in DEC ( $\sim$  inscan), as stated in the FIS Release Note p. 27.

##### 2.5.2. WISE mid-IR photometry

We have also made use of the Wide-field Infrared Survey Explorer (WISE; Wright et al. 2010) and its latest version (All-WISE Data Release, November 13 2013, Cutri et al. 2013). WISE has mapped the sky at 3.4, 4.6, 12, and 22  $\mu\text{m}$  (W1, W2, W3, W4) with an angular resolution of 6.1, 6.4, 6.5 & 12.0 arcsec (FWHM psf) in the four bands, achieving  $5\sigma$  sensitivities better

<sup>5</sup> This work is based in part on observations made with the Spitzer Space Telescope, which is operated by the Jet Propulsion Laboratory, California Institute of Technology under a contract with NASA.

<sup>6</sup> <http://svo2.cab.inta-csic.es/svo/theory/vosa4>

<sup>7</sup> <http://svo.cab.inta-csic.es/main/index.php>

<sup>8</sup> <http://www.ir.isas.jaxa.jp/AKARI/Publications/guideline.html#REFS>

than 0.08, 0.11, 1 and 6 mJy in unconfused regions for point sources. The All-Sky Release includes all data taken during the WISE full cryogenic mission phase (7 January 2010 to 6 August 2010) and its postcryogenic phase (Mainzer et al. 2011). In addition, we ignored values with no errors, and also removed some data after a visual inspection, based on the significant source confusion.

### 2.5.3. Optical data from Dolan & Mathieu

We used the published data from Dolan & Mathieu (1999, 2002), which includes optical photometry in three bands down to completeness and detection limits, in the B30 area, of  $V_{\text{compl}}=18.5$ ,  $R_{\text{compl}}=17.5$ ,  $I_{\text{compl}}=17.0$  mag; and  $V_{\text{lim}}=21.0$ ,  $R_{\text{lim}}=21.0$  and  $I_{\text{lim}}=19.0$  mag. The data were calibrated with standards stars from Landolt (1992) and, therefore, the  $R$  and  $I$  photometry is tied to the Cousins system (Cousins 1976, also called as Kron-Cousins) and the  $V$  to the Johnson (1963) (see also Landolt 1973).

We note that several objects spectroscopically studied by Dolan & Mathieu (1999) are located within the APEX/LABOCA FOV, namely: DM114, 115, 118, 121, 125, 127, 131, 135, 136, 142, 143, 149, 152, 158, 164, 169, and 172. They are characterized by radial velocity compatible with membership to the Lambda Orionis star forming region and a lithium detection, a clear indication of youth for late spectral type stars. Only two among this group are close to our APEX/LABOCA sources, namely DM115 –inside LB33– and DM142 –within LB20– (see subsections A.3 and A.2, respectively). The others are not detected at  $870 \mu\text{m}$  with APEX/LABOCA.

### 2.5.4. IRAS data

Two of our APEX/LABOCA detections have been identified with IRAS sources, namely B30-LB19 (IRAS05286+1203) and B30-LB32 (IRAS05293+1207), using a 25 arcsec radius search. The fluxes are listed in Table 2.

### 2.5.5. 2MASS near-IR photometry

The All-Sky 2MASS catalog (Cutri et al. 2003; Skrutskie et al. 2006) has completeness and limiting magnitudes, in the central region of the B30 dark cloud, of  $J_{\text{compl}}\sim 16.65$  mag,  $H_{\text{compl}}\sim 15.95$  mag,  $K_{\text{scompl}}\sim 15.45$  mag; and  $J_{\text{lim}}\sim 18.95$  mag,  $H_{\text{lim}}\sim 18.05$  mag,  $K_{\text{slim}}\sim 17.45$  mag. They have been used, among other things, to calibrate and complement our deep near-IR data.

### 2.5.6. Absorption map based on 2MASS

We have followed the approach in Cambresy et al. (1997) to derive an extinction map of the B30 sky area via an adaptive-step star count method. We used as base for the method the 2MASS all-sky point-source catalog (Skrutskie et al. 2006) as in López Martí et al. (2013). This technique, based in local density of stars as compared to an unobscured field at the same galactic latitude (in our case we use Collinder 69 as comparison field given its low and homogeneous extinction properties), provides an average resolution of  $1.5'$  across a region centered at 05:29:58.50 +12:01:52.0 with 1.5 degree radius. The results, for each APEX/LABOCA detection, are listed in Table 2 and the conversion from  $A_J$  to  $A_V$  follows Fitzpatrick (1999).

## 2.6. Cross-correlation and identifications

We have carried out a careful cross-correlation of the data taking into account both the errors in the pointing, which are not negligible in the case of APEX/LABOCA, and the beam size. The relatively wide beam sizes are very important when cross-matching detected sources at other wavelengths for Akari/FIS, Spitzer/MIPS, Wise (particularly W3 and W4) and APEX/LABOCA, and still significant for WISE W1 and W2, Akari/IRC, and Spitzer/IRAC.

The beam size of APEX/LABOCA has an angular size of  $\sim 27.6$  arcsec, so multiple identifications with optical, near- and mid-IR sources are possible. Since the grid pixel is about 4 arcsec, when searching for possible counterparts, we have assumed a 5 arcsec angular distance as the optimal counterpart search radius (at least for the non-extended sources). We note that some stars could have moved from their birth site, so the position of YSO could differ from the center of the submillimeter emission. Jørgensen et al. (2008) have studied the correlation between MIPS and SCUBA data in Perseus and Ophiuchus and concluded that no significant dispersion has taken place if the formation is recent. In any case, we cannot completely rule out the possibility of a real offset due to a drift. In addition, we have visually inspected all possible cross-matches and in some cases rejected the WISE W3 and W4 due to confusion, as stated before. The results, including all possible identifications and the magnitudes at each filter, are listed in Table 3 and Table 4 –near- and mid-IR photometry, Table 5 –optical plus 2MASS, and Table 6 –Akari data.

## 2.7. Classification of the LABOCA submm sources and the counterparts

We have cross-correlated the data from LABOCA with our catalogs of optical/IR sources. Based on the availability of data at  $70 \mu\text{m}$  as a primary indicator and  $24 \mu\text{m}$  as a secondary, we have classified the cross-matches into three groups, as listed in Table 2:

- Group A.- Sources detected at  $70 \mu\text{m}$ . Depending whether they also have been detected at  $24 \mu\text{m}$  they would belong to subgroup A1 or A2 (with or without measured flux at  $24 \mu\text{m}$ , respectively).
- Group B.- Undetected sources at  $70 \mu\text{m}$  (i.e., upper limits with Spitzer/MIPS M2). As in the previous case, we have differentiate whether they also have been detected at  $24 \mu\text{m}$ : subgroups B1 and B2 correspond to those with or without measured flux at  $24 \mu\text{m}$
- Group C.- LABOCA sources outside the MIPS M2 FOV (i.e., no information at  $70 \mu\text{m}$ , see subsection 2.4). Some have been detected at  $24 \mu\text{m}$  (subgroup C1) whereas others only display upper limits (subgroup C2).

This classification appears in Table 2. We have also included information regarding whether we classify the submm source as YSO (regardless of whether it is stellar or substellar), there are counterparts with IR excesses within the beam or the source seems to be a starless core; whether there is a potential substellar candidate (sometimes more than one) within the whole APEX/LABOCA beam; and whether there is a counterpart within 5 arcsec from the APEX/LABOCA emission peak (and whether it could be a brown dwarf). A detailed discussion can be found in Appendix A.

### 3. Properties of the submm APEX/LABOCA sources

#### 3.1. Individual submm sources and a estimate of the emitting mass

We show the 870  $\mu\text{m}$  LABOCA emission of the B30 dark cloud, together with the detected submm sources, in Fig. 1a. On top of the image we display the  $H\alpha$  nebular emission (Virginia Tech Spectral line Survey with 6 arcmin resolution, Finkbeiner 2003). Most of the detected sources are located in a “valley” in between the  $H\alpha$  peaks. Fig. 1b correspond to a Spitzer/MIPS1 image at 24  $\mu\text{m}$  in colorscale, where the submm LABOCA sources have been overplotted (see subsection 2.1 for details). The 24  $\mu\text{m}$  image traces the hot dust at the border of the pillar facing the star  $\lambda$  Ori, where the ionization front from the O-type star is interacting with B30. Another bright region at 24  $\mu\text{m}$  is found about 4 arcmin to the north of this sharp edge, where several point-like sources surrounded by extended emission are located.

Our LABOCA map at 870  $\mu\text{m}$ , tracing mainly the emission of cold dust, reveals tens of cores, some of them showing extensions and substructure, which follow the filaments seen in the MIPS image at 24  $\mu\text{m}$ , and which are mainly distributed in two parts of the cloud. The first group of cores lie slightly north of the edge of the HII region, and are arranged in filaments elongated in the east-west direction, while the second group matches well the 24  $\mu\text{m}$  bright emission 4' north of the cloud border and follow a rather north-south direction.

We identified a total of 34 cores above the 4- $\sigma$  level (see their labels in Fig. 1), and their flux and envelope mass (see below) are provided in Table 2. Near the edge of the HII region, sources B30-LB21 to B30-LB24, and B30-LB29 to B30-LB31 follow remarkably well the 24  $\mu\text{m}$  emission tracing the border of the pillar. In this region the two strongest sources are B30-LB19, which is associated with a 24  $\mu\text{m}$  point source, and B30-LB27, which is more extended and fainter in the infrared. A ridge of faint sources (B30-LB20, B30-LB25, B30-LB26) joins B30-LB19 and B30-LB27. The other group of submillimeter sources located farther to the north are also forming filamentary structures. For example, sources B30-LB05 to B30-LB07 are arranged in one single north-south filament, and sources B30-LB08, B30-LB09 and B30-LB12, are forming a chain of cores along the southeast-northwest direction. Finally, sources B30-LB02 to B30-LB04, still 4' farther to the north, seem to be the continuation of the B30-LB05/B30-LB07 filament. The chain of cores B30-LB02/B30-LB07 is dark in the infrared, and are associated with only very weak 24  $\mu\text{m}$  emission, contrary to the filamentary structure of cores B30-LB08/B30-LB12, which is associated with bright 24  $\mu\text{m}$  emission.

We estimated the envelope masses in the following way. The total mass  $M$  of gas and dust from thermal continuum emission, assuming that the emission is optically thin, is:

$$M = \frac{S_\nu D^2}{B_\nu(T_d) \kappa_\nu}, \quad (1)$$

where  $S_\nu$  is the flux density at the frequency  $\nu$ ,  $D$  is the distance to the Sun,  $B_\nu(T_d)$  is the Planck function at the dust temperature  $T_d$ , and  $\kappa_\nu$  is the absorption coefficient per unit of total (gas+dust) mass density. Writing Eq. (1) in practical units:

$$\left[ \frac{M}{M_\odot} \right] = 3.25 \times \frac{e^{0.048 \nu/T_d} - 1}{\nu^3 \kappa_\nu} \times \left[ \frac{S_\nu}{\text{Jy}} \right] \left[ \frac{D}{\text{pc}} \right]^2, \quad (2)$$

where  $T_d$  is in K,  $\nu$  is in GHz, and  $\kappa_\nu$  is in  $\text{cm}^2\text{g}^{-1}$ . For the absorption coefficient at 870  $\mu\text{m}$  or 345 GHz we used the interpolated

value from the tables of Ossenkopf & Henning (1994), for the case of thin ice mantles and density of  $10^6 \text{ cm}^{-3}$ :  $0.0175 \text{ cm}^2 \text{ g}^{-1}$ . Since we do not know the evolutionary status of the detected cores, we have adopted an average dust temperature of 15 K for both pre-stellar and protostellar cores (see e.g., Sánchez-Monge et al. 2013).

The total masses estimated from the 870  $\mu\text{m}$  continuum emission range from 0.043 up to 0.166  $M_\odot$  (or 0.279  $M_\odot$  if the extended emission is taken into account). The sources with largest masses, above 0.1  $M_\odot$ , are B30-LB01, B30-LB19, B30-LB27, B30-LB30, and B30-LB32, if we only consider the peak. In addition, when the extended emission is taken into account, this limit is also surpassed by B30-LB06, B30-LB08, B30-LB13, B30-LB21, and B30-LB25. Thus, the submm sources with dust masses below 0.1  $M_\odot$  are: B30-LB02, B30-LB03, B30-LB04, B30-LB05, B30-LB07, B30-LB09, B30-LB10, B30-LB11, B30-LB12, B30-LB14, B30-LB15, B30-LB16, B30-LB17, B30-LB18, B30-LB20, B30-LB22, B30-LB23, B30-LB24, B30-LB26, B30-LB28, B30-LB29, B30-LB31, B30-LB33, and B30-LB34.

#### 3.2. Evolutionary status of the optical/IR counterparts to the submm sources

After the compilation of our photometric catalog of possible counterparts of the APEX/LABOCA sources (Table 2), our first step has been to identify possible infrared excesses based on Spitzer/IRAC data. Figure 3 displays a CCD – panel a – and several color-magnitude diagrams (CMD) –panels b, c, d, and e– for the counterparts identified within the 34 APEX/LABOCA sources. The figure also includes data corresponding to the somewhat older C69 cluster, which also belongs to the same star forming region (5 Myr for C69 versus 1-3 Myr for B30). The data come from Barrado y Navascués et al. (2007), Barrado et al. (2011) and Bayo et al. (2011). We have also added information (plotted on the figure) regarding to members in Taurus (Luhman et al. 2006) and Serpens (Harvey et al. 2007), which is about 1-2 Myr. We have included several extra-galactic samples from Sacchi et al. (2009): we show the AGN1/QSO1/broad lines and AGN2/obscured QSO/narrow lines as well as resolved galaxies and emission line galaxies (which include AGN and star forming galaxies), respectively. We have been able to establish whether our B30 counterparts are likely members or not (see below), and our classifications are indicated in the figure.

Figure 3 clearly shows that a significant number of our counterparts might have circum-(sub)stellar disk or envelopes. Therefore, some might be classified as Class II or Class I objects, or something in-between. There are a number of disk-less objects (Class III), and some of them might even belong to the association, in an analogous situation to what happens in Taurus (simultaneous presence of members in the Class I, II and III phases, see panel a). However, it is also clear, from the comparison with resolved and emission line galaxies and AGN from Sacchi et al. (2009), that our sample can be polluted by a significant number of extra-galactic sources, specially for the faint end (Spitzer/IRAC  $\text{II} \geq 15$  mag). Therefore, in order to select bona-fide candidate members, we have carried out a detailed comparison using our wealth of data. These figures (see e.g., Figure 4) suggest that the pollution by extra-galactic sources should be reduced, since the loci of most of our candidates in the CMDs are not coincident with the population of galaxies. In fact, confirmed members in Serpens from Harvey et al. (2007) are closer to these pollutants. Moreover, the number of extra-galactic sources (Surace et al. 2004, Sacchi et al. 2009)

within the APEX/LABOCA beam should be around 1-2.5 galaxies, and 0.07-0.03 within the central 5 arcsec (i.e., an improbable chance alignment between an extra-galactic center and the submm source).

Both Harvey et al. (2006) and Gutermuth et al. (2008) discuss the nature of Spitzer sources based on CCDs and CMDs built with IRAC and MIPS data, namely [(I2-I3),(I3-I4)], [(I1-I3),(I2-I4)], [I2,(I2-I4)]. We have used their criteria and verified that a small number of our possible counterparts fall in the regions where extra-galactic sources are located. We note that young substellar objects could be located in the same areas in the CCD and CMD (see the case of an excellent proto-brown dwarf in Taurus Barrado et al. 2009; Palau et al. 2012). We have classified these objects as possible extra-galactic, and added the tag G to the membership criteria listed in Table 7.

Moreover, for the handful also having optical photometry in the *I* band, we have checked their position in an optical/near-IR/mid-IR CCD, following Bouy et al. (2009), in order to reveal the presence of quasars. Only two of them appear likely to be quasars, and this information has been added to Table 7. Obviously, additional analysis is required to assess the membership of all these counterparts to the B30 association.

### 3.3. Membership of the optical/IR counterparts to the submm sources

Several additional CMDs, which combine near- and mid-IR photometry, can be found in Fig. 4. This figure is similar to Fig. 3, but in it we have included several BT-Settl isochrones from the Lyon group (Allard et al. 2012) namely those corresponding to ages of 3 and 20 Myr, in order to establish whether the counterparts are young or old. Without taking into account the interstellar and inter association reddening (as well as that produced by the object itself), these diagrams suggest the presence of a very large number of very low-mass objects. However, as stated before, we expect a significant rate of pollutants and the reddening effect should be taken into account (it will be dealt with later on).

For each object and CMD, when the photometry is available, we have assigned a qualitative membership tag, namely Y –younger than 20 Myr, Y? –between 20 and 50 Myr, N? –between 50 and 10,000 Myr, and N –older than the 10,000 Myr isochrone. These last two isochrones are not represented in the figure for clarity. We note that the interstellar reddening vector is practically parallel to the isochrones (indicated each panel), so it has not relevant effect in this classification.

Moreover, in order to consider all the photometric information simultaneously, we have derived the effective temperature and bolometric luminosities of all possible counterparts by using VOSA (Bayo et al. 2008). Since the current version of VOSA includes the possibility of adjusting the reddening, we have produced two sets of  $T_{eff}$  and  $L_{bol}$ : i) by fixing  $A_v = 0.322$  mag –an average value for the Lambda Orionis star forming region– and ii) by letting it be variable. We always assumed a distance of 400 pc, solar metallicity ( $[Fe/H]=0.00$ ) and  $logg=3.5$  dex. Results are listed in Table 7. We selected BT-Settl models from Allard et al. (2012) and two Hertzsprung-Russell Diagrams are represented in Fig. 5. A similar exercise to the one carried out with the CMD, regarding membership and qualitative tags, has been executed using the effective temperature and the bolometric luminosity. However, in this case objects located between the 20 and the 10,000 Myr isochrones have been labeled as Y?, whereas objects looking like older than the universe (below the 10,000 Myr isochrone) has been assigned the tag N, since they are ei-

ther extra-galactic or the assumed distance is incorrect (and they cannot be related to the B30 cloud).

All these membership quality tags, when combined with the information regarding the number of photometric points in the SED, the SED shape and the evolutionary status (Class I, II and III, based on the IRAC data), and the possibility of being extra-galactic sources, have been used to produce a final membership classification (Table 7). In the end, we have been able to provide a final membership classification: probable and possible members (tags Y and Y?) and possible and probable non-members (N? and N). They are represented in Figs. 3 and 4, whereas Fig. 5 differentiates probable and possible members with solid and open green circles. We note that for some counterparts, we have not been able to elucidate whether they belong or not to the association due to the lack of enough photometric information. These objects are listed with a “–” tag.

### 3.4. Bolometric luminosity and temperature

By using our massive multi-wavelength database, which includes photometry from 0.5 to 870  $\mu$ m, we have estimated the bolometric temperature and luminosity (see details in Palau et al. 2012). The results are listed in Table 8 and displayed in Figs. 6 and 7, where we have included several samples of young stars and VeLLOs (Chen et al. 1995; Young & Evans 2005; Dunham et al. 2008; Bayo et al. 2011; Tobin et al. 2016). Our Barnard 30 targets appear as green, cyan and red symbols (depending on the figure and the classification, see subsection 2.7), where the size increases with the number of data-points (i.e., being more reliable those with a bigger size). We have only included those objects detected at 24 and/or 70  $\mu$ m. They display significant IR excesses, so the  $T_{bol}$  and  $L_{bol}$  departs from our previous estimate of  $T_{eff}$  and  $L_{bol}$  based on VOSA (the photospheric emission). Our B30 objects have been classified, in most cases, as Class I or Class I/II based on the IRAC data. We note that the flux at 870  $\mu$ m has been assigned in general to the “a” components when there are multiple identifications (see Appendix). Thus, we have studied in detail 15 objects detected at 24  $\mu$ m which are within 11 APEX/LABOCA sources and another eight objects in four different LABOCA beams which display a emission at 70  $\mu$ m but they do not have a detected counterpart at 24  $\mu$ m.

Figures 6 and 7 strongly suggest that we have uncovered a few examples of very young, low-massive objects. They would be objects in the evolutionary stage between Class 0 and Class I in the classification scheme of Lada (1987) and Adams et al. (1987). If we take into account the  $L_{int}$ , as estimated from the flux at 70  $\mu$ m, one object seems to follow fully in the VeLLO category (LB19d, Huélamo et al. 2017). In addition, there is a sample of Class I objects with bolometric luminosities below 0.1  $L_{\odot}$  and  $T_{bol}$  in the range 70-700 K. Unfortunately, some of them have less than ten data-points in the SED and therefore they are not very well characterized. In any case, since there is also another subsample located in the Class II or III are, as defined by Young & Evans (2005) and Dunham et al. (2008), it seems that there is an evolutionary sequence from Class 0/I very low-mass objects, probably substellar, down to the pre-main sequence. This trend persists even if the fluxes at 870  $\mu$ m (and 70  $\mu$ m when available) are included for these counterparts. As a matter of fact, although the  $L_{bol}$  increases,  $T_{bol}$  is shifted toward cooler values and new candidate VeLLOs appear (if, indeed, they are the origin of the submm emission). Regardless of this assumption, what we might be contemplating in the Barnard 30 dark cloud is the unveiling of the brown dwarf population. In next subsection we explore this possibility by having a look at the individual objects. In any case,

the 20 objects clearly detected at 24 and/or 70  $\mu\text{m}$  have been classified as: two WTTs, four CTTs, five YSOs, eight proto-BD candidates and one VeLLO. Another three objects have emission at 24  $\mu\text{m}$  strongly affected by the extended photometry, although they seem to be substellar and they can be classified as proto-BDs candidates.

### 3.5. Starless cores?: LABOCA sources without unambiguous young optical/IR counterparts

In the case of six LABOCA sources, namely B30-LB01, B30-LB06, B30-LB13, B30-LB15, B30-LB16 and B30-LB34, there is not any optical/IR counterpart detected within 5 arcsec. Some include several counterparts detected between 5 and 27 arcsec which have been classified as probable or possible cluster members, but they do not display any obvious excess. In these six cases, we have considered the possibility that these submm sources are starless cores in B30, and we have investigated their nature. We note that all of them lack data at 70  $\mu\text{m}$ , either because there is no positive detection or because the LABOCA source is outside the MIPS M2 FOV.

B30-LB15 and B30-LB16 have envelope masses around 0.05  $M_{\odot}$ . The marginal detection of these sources prevents us from drawing any further conclusions regarding their nature. Each of them contain only one candidate member (counterparts #a in both cases, see Fig. A.8) and their SED (Fig. A.9) are typical of a Class III, disk-less object, although in the case of B30-LB16a it seems substellar. Thus, no convincing optical/IR counterpart can be assigned to these cores.

B30-LB34 has been only detected with APEX/LABOCA. It can be considered as a starless core. We note, however, that it is associated to B30-LB33 (Fig. A.8), a class II star. Thus, if physically associated, they would conform a pair in very different evolutionary stage.

B30-LB01, B30-LB06, and B30-LB13 have relatively large submillimeter flux densities, and thus their estimated envelope masses are among the largest, between 0.108 and 0.260  $M_{\odot}$  (or 0.077 and 0.166  $M_{\odot}$  if we only take the peak intensity for the extended sources). Given that these masses are around the substellar regime ( $\sim 0.072 M_{\odot}$ ), and the known fact that not the entire mass of a starless core ends up to form the star, these are excellent candidates to pre-substellar (pre-BD) cores, that is, cores which will form brown dwarfs in a future but did not form an hydrostatic core yet (e.g., Palau et al. 2012; André et al. 2012). Their submm emission is also extended in these three cases, with sizes of 22, 49 and 23 arcsec, respectively. In order to elucidate their true pre-BD nature, it is necessary to conduct observations of molecular lines, to assess whether these cores are indeed gravitationally bound. If confirmed, they would provide strong evidence favoring the formation of brown-dwarfs in isolation, and thus their formation from the gravoturbulent-fragmentation scenario.

## 4. General discussion and conclusions

The analysis of the LABOCA data of B30 has revealed the detection of 34 submm sources. 15 of them have a clear optical/IR counterpart within 5 arcsec (Table 2), have been classified as a probable or possible cluster members and they display a significant infrared excess. Among them, six have been detected at 24  $\mu\text{m}$  with MIPS M1. Another two are do not have emission at this band but have been detected at 70  $\mu\text{m}$  with MIPS M2. Therefore, we can conclude that the excesses are well established and

the sources are well characterized. Nine out of the 15 might be substellar objects based on the mass of their envelopes and the shape of their SED. Another one would be at the borderline between stars and brown dwarfs. In any case, the final mass would depend on the actual reddening due both to the dark cloud and the object itself (when the submillimeter emission is extended).

Two submm sources in this group are visual binaries, in the sense that there are two optical/IR counterparts which have been classified as probable/possible members, display infrared excesses and are located within the central 5 arcsec of the LABOCA beam. Our current spatial resolution does not allow to assign it to any component. One system, namely B30-LB19, has a primary component (counterpart #a) at the borderline between stars and brown dwarfs, while the more massive component, further away from the center of the submillimeter emission, would be stellar. Even further, but still inside the 27.56 arcsec of the APEX/LABOCA beam, there are several possible/probable members, classified as Class I sources, which could have a substellar nature. Therefore, we may be dealing with a clump which is giving birth to several very low-mass stars and/or brown dwarfs. The other APEX/LABOCA binary, namely B30-LB25, includes counterparts #a and #e.

The second group is composed by those submm sources (13) with no optical/IR counterpart within 5 arcsec but which include sources within the APEX/LABOCA beam displaying excesses (labeled excess in Table 2). All 13 sources contain within the submm beam at least one optical/IR counterpart which can be classified as BD if membership is confirmed. Eight out of 13 have envelope masses below the substellar limit and, in fact, the individual SEDs are characteristic of brown dwarfs, if members. In any case, due to the number of possible and probable members identified within the submm beam, we cannot unambiguously assign the source of the submillimeter emission to any individual object. Nine have been detected at 24  $\mu\text{m}$  (although three of these detections are problematic due to the extended nebulosity and it is possible that some among these three are not real).

Finally, six LABOCA sources might be starless cores, with three of them having masses near the substellar limit and thus are pre-BD core candidates. An additional follow-up of molecular line observations is required to confirm their dynamical status and their nature.

Regarding multiplicity, it seems there is no obvious difference between the submm sources with a counterpart closer than 5 arcsec and without it. The first one contains multiple possible and/or probable members as counterparts within the APEX/LABOCA beam in 13 cases out of the 15 sources. The ratio is 11 to 13 for the second group. However, the six starless cores might be genuinely different, since the ratio is three out of six. However, the low number statistics might be playing a role.

Based on the availability of data at 70 and 24  $\mu\text{m}$ , we have discussed the properties and evolutionary stage of our submm sources in Barnard 30. Overall, the most relevant object is B30-LB19d. With  $L_{int}=0.094 L_{\odot}$ , as estimated from the flux at 70  $\mu\text{m}$ , it is the best Class I BD identified so far in this star forming region. Huélamo et al. (2017) has suggested that it could be associated with a bipolar nebula. Six counterparts, namely B30-LB11a, B30-LB12d, B30-LB22b, B30-LB22j, B30-LB30g and B30-LB31c, have been detected at 24  $\mu\text{m}$  and they have been classified as proto-BD candidates. In addition, three objects associated to B30-LB29 (#a, #b and #f) and the two counterparts related to B30-LB23 (counterparts #a and #c) are very interesting proto-BD candidates, since these two LABOCA sources have been detected at 70  $\mu\text{m}$ . However, the problematic photometry at 24  $\mu\text{m}$  or lack of it poses some significant caveats regarding their evolu-



tionary status. Finally, we have identified four sources at  $24\ \mu\text{m}$  which are located outside the MIPS M2 FoV (LB12a, LB18a, LB32a and LB33a), so there is no information regarding the emission at  $70\ \mu\text{m}$ . They seem to be of stellar nature. B30-LB14, which includes the counterparts #a and #b, and has been detected at  $70\ \mu\text{m}$ , seems to be of stellar nature. We note that Liu et al. (2016) have found Class 0 protostar and a proto-BD candidate West of our study. Our pre- and proto-BD candidates seem to be fainter and/or cooler than this candidate, called G192S, based on the comparison between the SEDs (see their Figure 26).

We can compare our results in B30 with those from two regions with very different properties: Chamaeleon II (Cha II, see de Gregorio-Monsalvo et al. 2016) and the B213-L1495 clouds in Taurus (B213 hereafter Palau et al. 2012; Morata et al. 2015). Unlike B30, these are low-mass star forming regions that lack massive stars, and therefore do not suffer from the strong and ionizing winds associated to hot, massive objects.

In the case of Cha II we followed a similar strategy as in B30, and surveyed a region of  $\sim 34' \times 34'$  with APEX/LABOCA, detecting a total of 15 submm sources (the rms was 4 mJy). Two of them were classified as Class I stellar objects, one appeared to be a proto-BD candidate, and 12 were assigned the status of starless cores. Five (out of the 12) were good pre-BD candidates although kinematic information is needed to assess if they are, indeed, gravitationally bound.

In the case of B213, we have performed a more exhaustive study. We first isolated a sample of 12 proto-BDs based on Spitzer and near-IR data (Barrado et al. 2009). We studied these candidates with different submm, mm and cm continuum observations, together with several gas molecules like CO,  $^{13}\text{CO}$  and  $\text{N}_2\text{H}^+$  data (for details see Palau et al. 2012). As a result, we have confirmed two very good proto-BD candidates and one pre-substellar core candidate. All the sources from these two works focusing on B213 were also observed with the JVLA, and we reported the presence of thermal radiojets in four of them (Morata et al. 2015).

We have also performed a similar detailed study to unveil the nature of all the selected candidates in B30 (Huélamo et al. 2017). One important goal is to understand if the overall properties of the region (e.g., fraction of proto-BD and pre-BD cores) are different due to the presence of the hot star  $\lambda$  Ori when compared with other regions with a different environment.

As a final, general conclusion, the complete characterization of our APEX/LABOCA sources, focusing on those detected at  $24$  and/or  $70\ \mu\text{m}$ , indicates that in our sample of 34 submm sources there are, at least: two WTTs, four CTTs, five YSO, eight proto-BD candidates (with another three dubious cases due to the extended emission at  $24\ \mu\text{m}$ ) and one VeLLO. In addition, we have identified a substantial number of proto-BD and substellar starless cores in the young Barnard 30 dark cloud, located at about 400 pc. They are prime targets for further follow-up and characterization, as we have done in Taurus. In general, high spatial resolution observations (with e.g., ALMA, Huélamo et al. 2017, and other submm and mm arrays), both in the continuum and in specific lines, are necessary to assign the correct counterpart to the submm sources, to confirm these proto-BD and pre-BD core candidates and to reveal their characteristics and formation mechanism.

*Acknowledgements.* We thank the Calar Alto Observatory staff for their excellent work taking the near-IR data under the Service Mode program. A special thanks to Rosario Lorente Balanza for her help with the Akari data. We do appreciate the big role the anonymous referee has played in this paper. Although we did not always agree, we thank her/him for the significant contribution. We also thank Almudena Alonso-Herrero for her help with the MIPS photometry. This re-

search has been funded by the Spanish grants AYA 2014-55840-P, and AYA2014-57369-C3-3-P, ESP2015-65712-C5-1-R, and ESP2017-87676-C5-1-R. AP and MTR acknowledge financial support from UNAM-DGAPA-PAPIIT IA102815 grant, México, and from CATA (PB06) CONICYT, Chile, respectively. AB was financed by proyecto Fondecyt Iniciación 11140572 and the Millennium Science Initiative (Chilean Ministry of Economy), through grant Nucleus P10-022-F. It makes use of VOSA, developed under the Spanish Virtual Observatory project supported from the Spanish MICINN through grant AyA2008-02156, and of the SIMBAD database, operated at CDS, Strasbourg, France. This publication makes use of data products from the Wide-field Infrared Survey Explorer, which is a joint project of the University of California, Los Angeles, and the Jet Propulsion Laboratory/California Institute of Technology, funded by the National Aeronautics and Space Administration. The paper was finished during a stay at ALMA and ESO headquarters in Santiago de Chile by DB and NH, which were supported by ALMA & ESO and by the BBVA foundation, respectively, and another at Universidad de Valparaíso by DB, supported by project Proyecto Fondecyt de Iniciación 11140572 (Chile).

## References

- Adams, F. C., Lada, C. J., & Shu, F. H. 1987, *ApJ*, 312, 788  
Allard, F., Homeier, D., Freytag, B., & Sharp, C. M. 2012, in *EAS Publications Series*, Vol. 57, *EAS Publications Series*, ed. C. Reylé, C. Charbonnel, & M. Schultheis, 3–43  
Allen, L. E., Calvet, N., D'Alessio, P., et al. 2004, *ApJS*, 154, 363  
André, P., Ward-Thompson, D., & Greaves, J. 2012, *Science*, 337, 69  
Baraffe, I., Chabrier, G., Allard, F., & Hauschildt, P. H. 1998, *A&A*, 337, 403  
Barrado, D., Morales-Calderón, M., Palau, A., et al. 2009, *A&A*, 508, 859  
Barrado, D., Stelzer, B., Morales-Calderón, M., et al. 2011, *A&A*, 526, A21+  
Barrado y Navascués, D., Stauffer, J. R., Bouvier, J., Jayawardhana, R., & Cuillandre, J.-C. 2004, *ApJ*, 610, 1064  
Barrado y Navascués, D., Stauffer, J. R., Morales-Calderón, M., et al. 2007, *ApJ*, 664, 481  
Bate, M. R. 2012, *MNRAS*, 419, 3115  
Bate, M. R., Bonnell, I. A., & Bromm, V. 2002, *MNRAS*, 332, L65  
Bayo, A. 2009, PhD dissertations, Universidad Autónoma de Madrid  
Bayo, A., Barrado, D., Stauffer, J., et al. 2011, *A&A*, 536, A63  
Bayo, A., Rodrigo, C., Barrado y Navascués, D., et al. 2008, *A&A*, 492, 277  
Bell, C. P. M., Naylor, T., Mayne, N. J., Jeffries, R. D., & Littlefair, S. P. 2013, *MNRAS*, 434, 806  
Belloche, A., Hennebelle, P., & André, P. 2006a, *A&A*, 453, 145  
Belloche, A., Parise, B., van der Tak, F. F. S., et al. 2006b, *A&A*, 454, L51  
Bonnell, I. A., Clark, P., & Bate, M. R. 2008, *MNRAS*, 389, 1556  
Bouy, H., Huélamo, N., Barrado y Navascués, D., et al. 2009, *A&A*, 504, 199  
Cambresy, L., Epchtein, N., Copet, E., et al. 1997, *A&A*, 324, L5  
Chen, H., Myers, P. C., Ladd, E. F., & Wood, D. O. S. 1995, *ApJ*, 445, 377  
Chen, X., Arce, H. G., Dunham, M. M., et al. 2012, *ApJ*, 751, 89  
Chen, X., Arce, H. G., Zhang, Q., et al. 2010, *ApJ*, 715, 1344  
Connelley, M. S., Reipurth, B., & Tokunaga, A. T. 2008, *AJ*, 135, 2496  
Cousins, A. W. J. 1976, *MmRAS*, 81, 25  
Cunha, K. & Smith, V. V. 1996, *A&A*, 309, 892  
Cutri, R. M., Skrutskie, M. F., van Dyk, S., et al. 2003, 2MASS All Sky Catalog of point sources. (The IRSA 2MASS All-Sky Point Source Catalog, NASA/IPAC Infrared Science Archive. <http://irsa.ipac.caltech.edu/applications/Gator/>)  
Cutri, R. M., Wright, E. L., Conrow, T., et al. 2013, Explanatory Supplement to the AllWISE Data Release Products, Tech. rep.  
de Gregorio-Monsalvo, I., Barrado, D., Bouy, H., et al. 2016, *A&A*, 590, A79  
Devillard, N. 1997, *The Messenger*, 87, 19  
Devillard, N. 1999, in *Astronomical Society of the Pacific Conference Series*, Vol. 172, *Astronomical Data Analysis Software and Systems VIII*, ed. D. M. Mehringer, R. L. Plante, & D. A. Roberts, 333  
di Francesco, J., Evans, II, N. J., Caselli, P., et al. 2007, *Protostars and Planets V*, 17  
Dolan, C. J. & Mathieu, R. D. 1999, *AJ*, 118, 2409  
Dolan, C. J. & Mathieu, R. D. 2001, *AJ*, 121, 2124  
Dolan, C. J. & Mathieu, R. D. 2002, *AJ*, 123, 387  
Drass, H., Haas, M., Chini, R., et al. 2016, *MNRAS*, 461, 1734  
Duerr, R., Imhoff, C. L., & Lada, C. J. 1982, *ApJ*, 261, 135  
Dunham, M. M., Crapsi, A., Evans, II, N. J., et al. 2008, *ApJS*, 179, 249  
Finkbeiner, D. P. 2003, *ApJS*, 146, 407  
Fitzpatrick, E. L. 1999, *PASP*, 111, 63  
Frayser, D. T., Sanders, D. B., Surace, J. A., et al. 2009, *AJ*, 138, 1261  
Gutermuth, R. A., Myers, P. C., Megeath, S. T., et al. 2008, *ApJ*, 674, 336  
Harvey, P., Merín, B., Huard, T. L., et al. 2007, *ApJ*, 663, 1149  
Harvey, P. M., Chapman, N., Lai, S., et al. 2006, *ApJ*, 644, 307  
Hennebelle, P. & Chabrier, G. 2008, *ApJ*, 684, 395

- Hester, J. J., Scowen, P. A., Sankrit, R., et al. 1996, *AJ*, 111, 2349
- Huélamo, N., de Gregorio-Monsalvo, I., Palau, A., et al. 2017, *A&A*, 597, A17
- Irwin, M. & Lewis, J. 2001, *New A Rev.*, 45, 105
- Ishihara, D., Onaka, T., Kataza, H., et al. 2010, *A&A*, 514, A1
- Johnson, H. L. 1963, *Photometric Systems*, ed. K. A. Strand (the University of Chicago Press), 204
- Jørgensen, J. K., Johnstone, D., Kirk, H., et al. 2008, *ApJ*, 683, 822
- Kauffmann, J., Bertoldi, F., Bourke, T. L., et al. 2011, *MNRAS*, 416, 2341
- Kawada, M., Baba, H., Barthel, P. D., et al. 2007, *PASJ*, 59, 389
- Koenig, X., Hillenbrand, L. A., Padgett, D. L., & DeFelippis, D. 2015, *AJ*, 150, 100
- Kovács, A. 2008, in *Society of Photo-Optical Instrumentation Engineers (SPIE) Conference Series*, Vol. 7020, Society of Photo-Optical Instrumentation Engineers (SPIE) Conference Series
- Lada, C. J. 1987, in *IAU Symposium*, Vol. 115, *Star Forming Regions*, ed. M. Peimbert & J. Jugaku, 1–17
- Landolt, A. U. 1973, *AJ*, 78, 959
- Landolt, A. U. 1992, *AJ*, 104, 372
- Larson, R. B. 1969, *MNRAS*, 145, 271
- Lee, C. W., Bourke, T. L., Myers, P. C., et al. 2009, *ApJ*, 693, 1290
- Lee, C. W., Kim, M.-R., Kim, G., et al. 2013, *ApJ*, 777, 50
- Levine, J. L., Steinhauer, A., Elston, R. J., & Lada, E. A. 2006, *ApJ*, 646, 1215
- Liu, T., Zhang, Q., Kim, K.-T., et al. 2016, *ApJS*, 222, 7
- López Martí, B., Jiménez-Esteban, F., Bayo, A., et al. 2013, *A&A*, 556, A144
- Luhman, K. L., Whitney, B. A., Meade, M. R., et al. 2006, *ApJ*, 647, 1180
- Machida, M. N., Inutsuka, S.-i., & Matsumoto, T. 2008, *ApJ*, 676, 1088
- Maddalena, R. J. & Morris, M. 1987, *ApJ*, 323, 179
- Mainzer, A., Bauer, J., Grav, T., et al. 2011, *ApJ*, 731, 53
- Makovoz, D. & Marleau, F. R. 2005, *PASP*, 117, 1113
- Matzner, C. D. & Levin, Y. 2005, *ApJ*, 628, 817
- Morales-Calderón, M. 2008, PhD dissertation, Universidad Autónoma de Madrid
- Morata, O., Palau, A., González, R. F., et al. 2015, *ApJ*, 807, 55
- Murdin, P. & Penston, M. V. 1977, *MNRAS*, 181, 657
- Myers, P. C., Adams, F. C., Chen, H., & Schaff, E. 1998, *ApJ*, 492, 703
- Onishi, T., Mizuno, A., & Fukui, Y. 1999, *PASJ*, 51, 257
- Ossenkopf, V. & Henning, T. 1994, *A&A*, 291, 943
- Padoan, P. & Nordlund, Å. 2004, *ApJ*, 617, 559
- Palau, A., de Gregorio-Monsalvo, I., Morata, O., et al. 2012, *MNRAS*, 424, 2778
- Palau, A., Zapata, L. A., Rodríguez, L. F., et al. 2014, *MNRAS*, 444, 833
- Polychroni, D., Schisano, E., Elia, D., et al. 2013, *ArXiv e-prints* [arXiv:1309.2332]
- Reipurth, B. & Clarke, C. 2001, *AJ*, 122, 432
- Riaz, B., Vorobyov, E., Harsono, D., et al. 2016, *ArXiv e-prints* [arXiv:1610.03093]
- Sacchi, N., La Franca, F., Feruglio, C., et al. 2009, *ApJ*, 703, 1778
- Sánchez-Monge, Á., Palau, A., Fontani, F., et al. 2013, *MNRAS*, 432, 3288
- Scholz, A., Geers, V., Clark, P., Jayawardhana, R., & Muzic, K. 2013, *ApJ*, 775, 138
- Siess, L., Dufour, E., & Forestini, M. 2000, *A&A*, 358, 593
- Skrutskie, M. F. et al. 2006, *AJ*, 131, 1163
- Surace, J. A., Shupe, D. L., Fang, F., et al. 2004, *VizieR Online Data Catalog*, 2255
- Tobin, J. J., Looney, L. W., Li, Z.-Y., et al. 2016, *ApJ*, 818, 73
- Weiß, A., Kovács, A., Coppin, K., et al. 2009, *ApJ*, 707, 1201
- Whitworth, A. P. & Stamatellos, D. 2006, *A&A*, 458, 817
- Whitworth, A. P. & Zinnecker, H. 2004, *A&A*, 427, 299
- Wright, E. L., Eisenhardt, P. R. M., Mainzer, A. K., et al. 2010, *AJ*, 140, 1868
- Young, C. H. & Evans, II, N. J. 2005, *ApJ*, 627, 293
- Young, C. H., Jørgensen, J. K., Shirley, Y. L., et al. 2004, *ApJS*, 154, 396

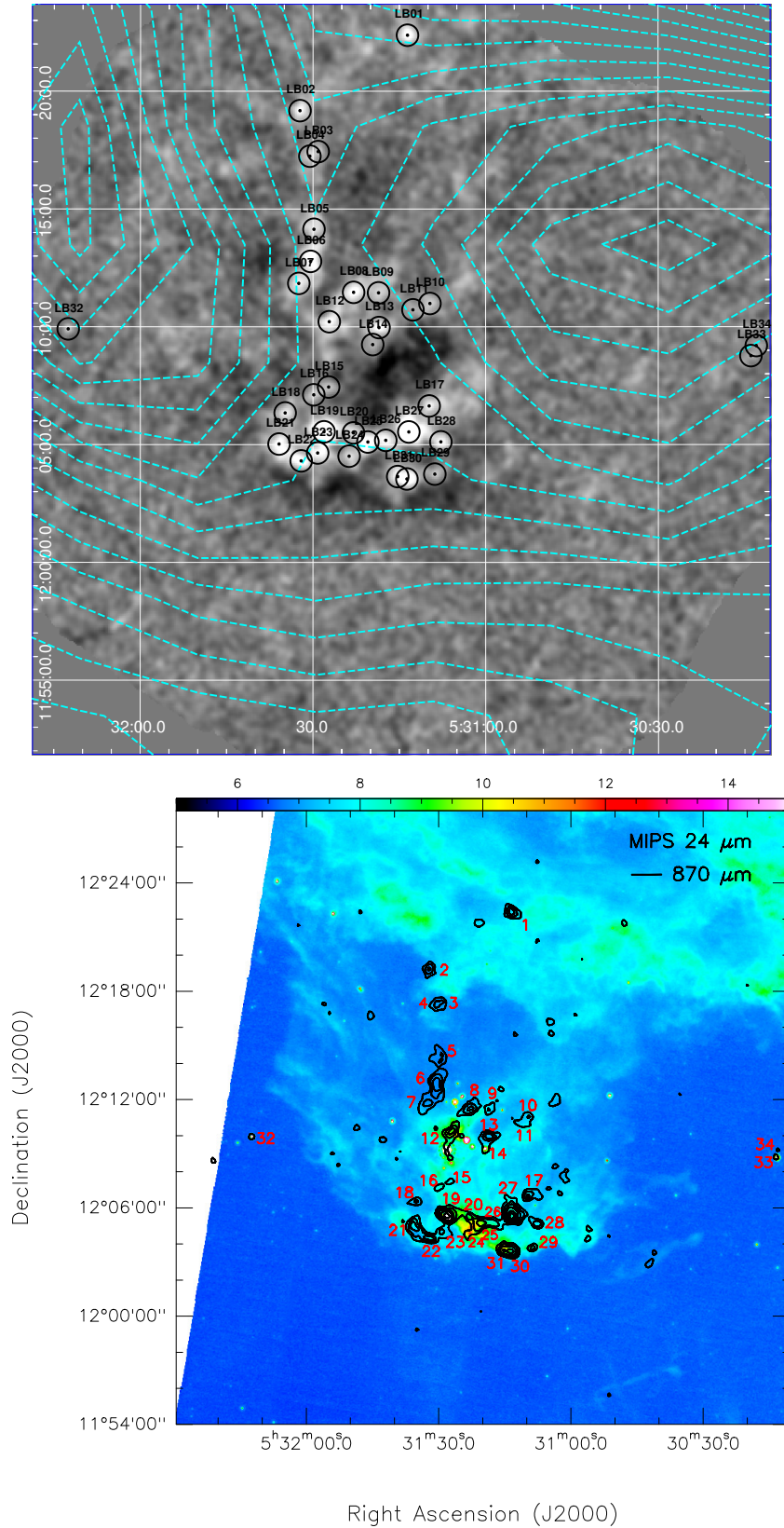


**Fig. 1. Top.-** Our APEX/LABOCA image, with the 34 sources at 870  $\mu\text{m}$ . Black open circles correspond to the LABOCA identified sources, with a 27.6 arcsec beam size. The total size of the map is about 38 arcmin in diameter. The cyan lines represent the  $H\alpha$  emission (Virginia Tech Spectral line Survey with 6 arcmin resolution, Finkbeiner 2003). **Bottom.-** Color scale: MIPS image at 24  $\mu\text{m}$  of B30. Black contours correspond to 3, 5, 7, 9, 12, and 15 times the rms noise of the 870  $\mu\text{m}$  emission (which varies across the image and it increases toward the edge of the map). The 34 submillimeter identified sources are marked with red labels.

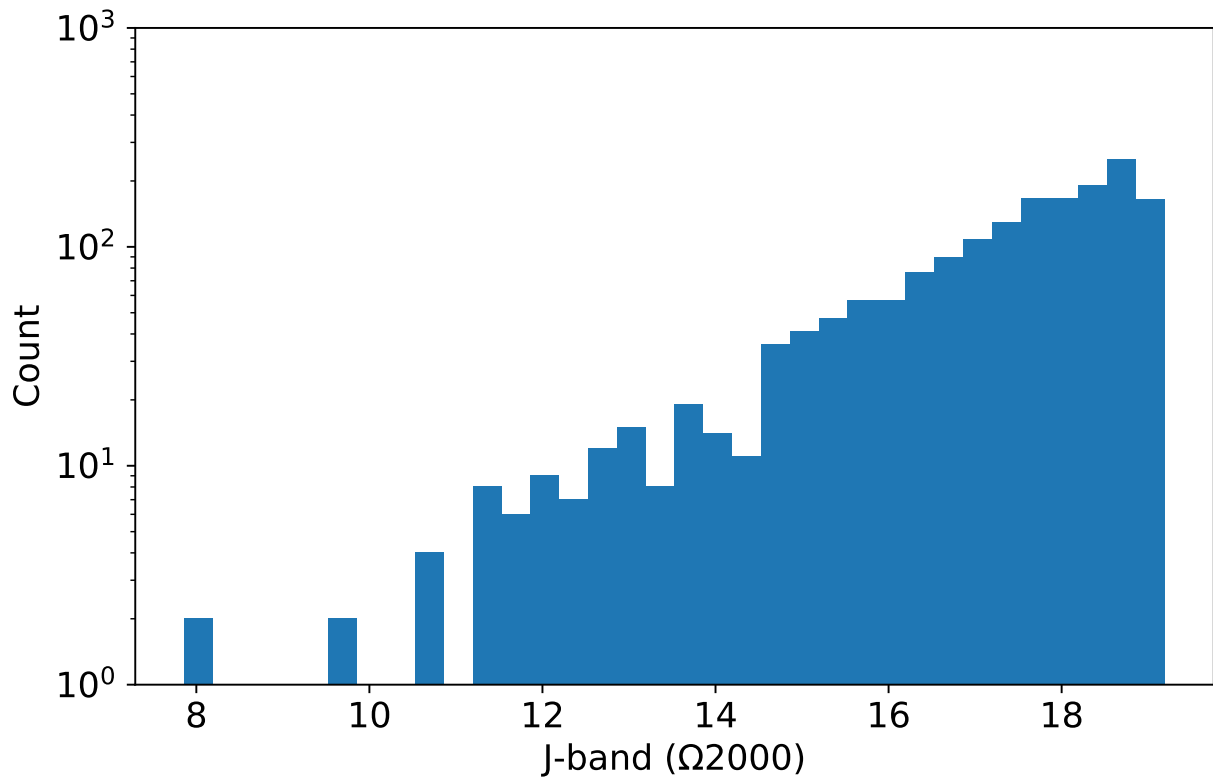


**Fig. 2.** Number of near-IR detections with CAHA/O2000 in the APEX/LABOCA FOV. The bin size has been estimated via the Freedman Diaconis Estimator (resilient to outliers). We estimate that the completeness limit is at  $J_{compl}=18.75$  mag and the detection limit at  $J_{lim}=20.5$  mag.

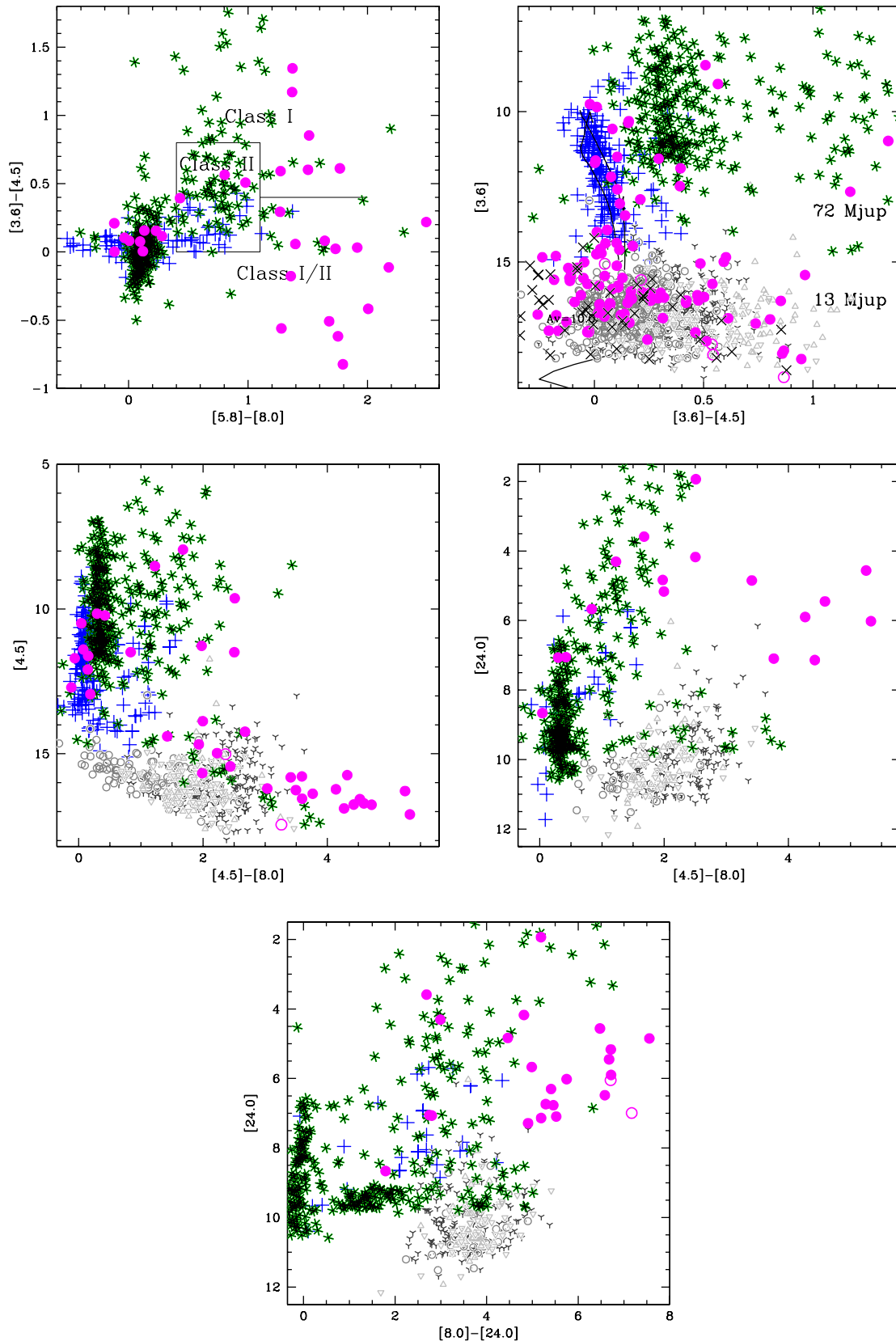


**Fig. 3.** Spitzer/IRAC CCD and CMDs. The first panel (top, left) displays the areas where Class I, II and III objects are located (assuming a stellar or substellar nature). The optical/IR counterparts of the B30 APEX/LABOCA sources are represented as magenta circles (solid for probable and possible members, empty circles for unknown status and a black cross for probable and possible non-members). For comparison, we have added known members of the  $\sim 5$ -8 Myr cluster C69 as plus, blue symbols, which is located in the same star forming region complex ((Dolan & Mathieu 1999; Barrado y Navascués et al. 2004, 2007; Morales-Calderón 2008; Barrado et al. 2011; Bayo et al. 2011)). We have also added confirmed members of Serpens from Harvey et al. (2007), about  $\sim 2$  Myr, as green-black asterisks. Most of our B30 counterparts can be classified as Class I or as transitional objects between Class I and Class II. Other panels include extragalactic sources as light gray symbols and have been extracted from Sacchi et al. (2009): up- and down-ward open triangles correspond to the AGN1 and AGN2, whereas three-point stars represent line galaxies and open circles other galaxies. We also have include BT-settl isochrones (Allard et al. 2012) with 3 and 20 Myr.

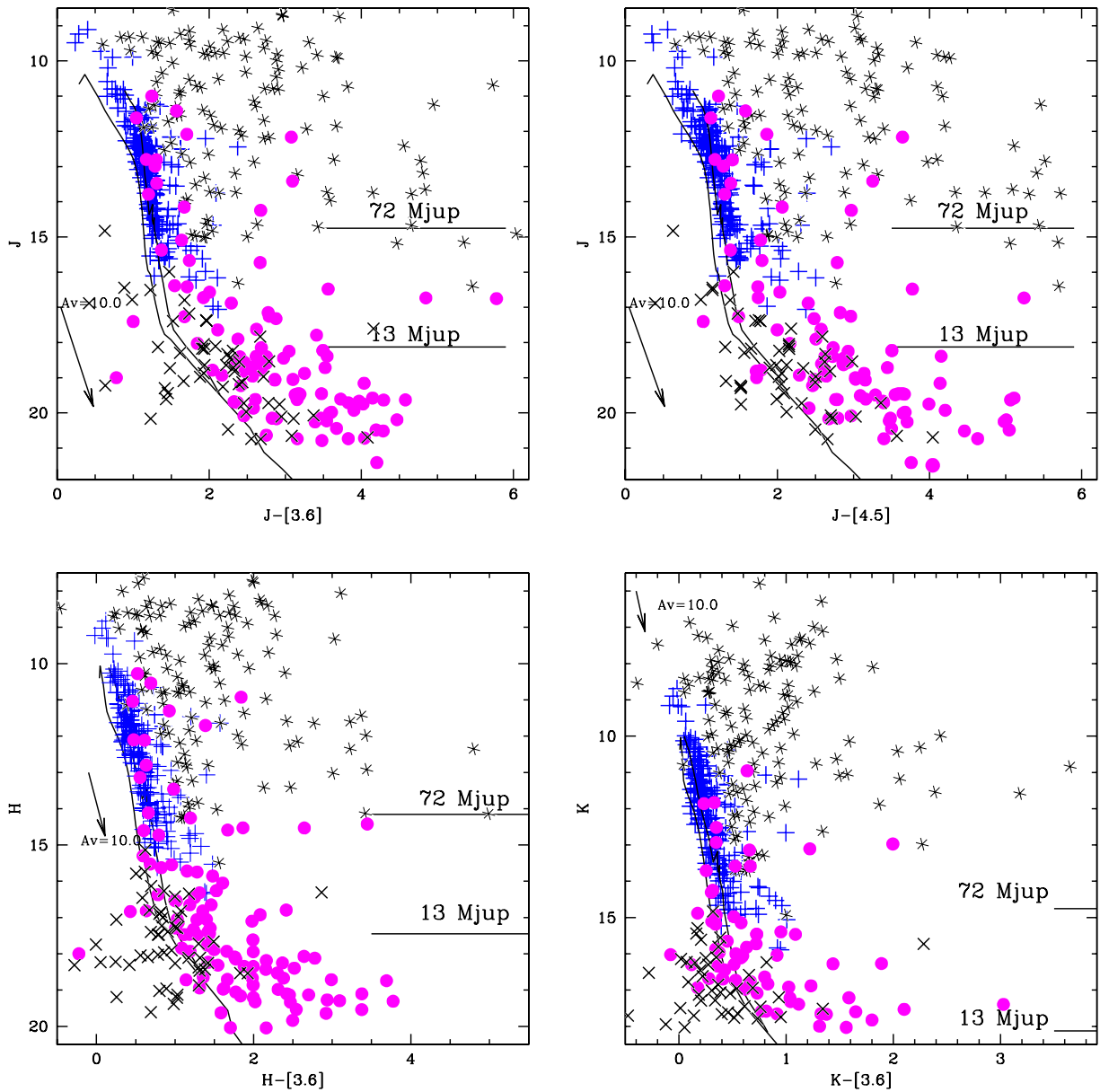


**Fig. 4.** Color-magnitude diagrams for the B30 APEX/LABOCA counterparts. Symbols as in Fig. 3, but in these panels we have included confirmed members of Taurus from Luhman et al. (2006), about 1-2 Myr, as asterisks. As a reference, the locations for 72 and 13  $M_{\text{Jupiter}}$  very low-mass objects at 3 Myr are also included, based on 3 Myr isochrone by (Allard et al. 2012).

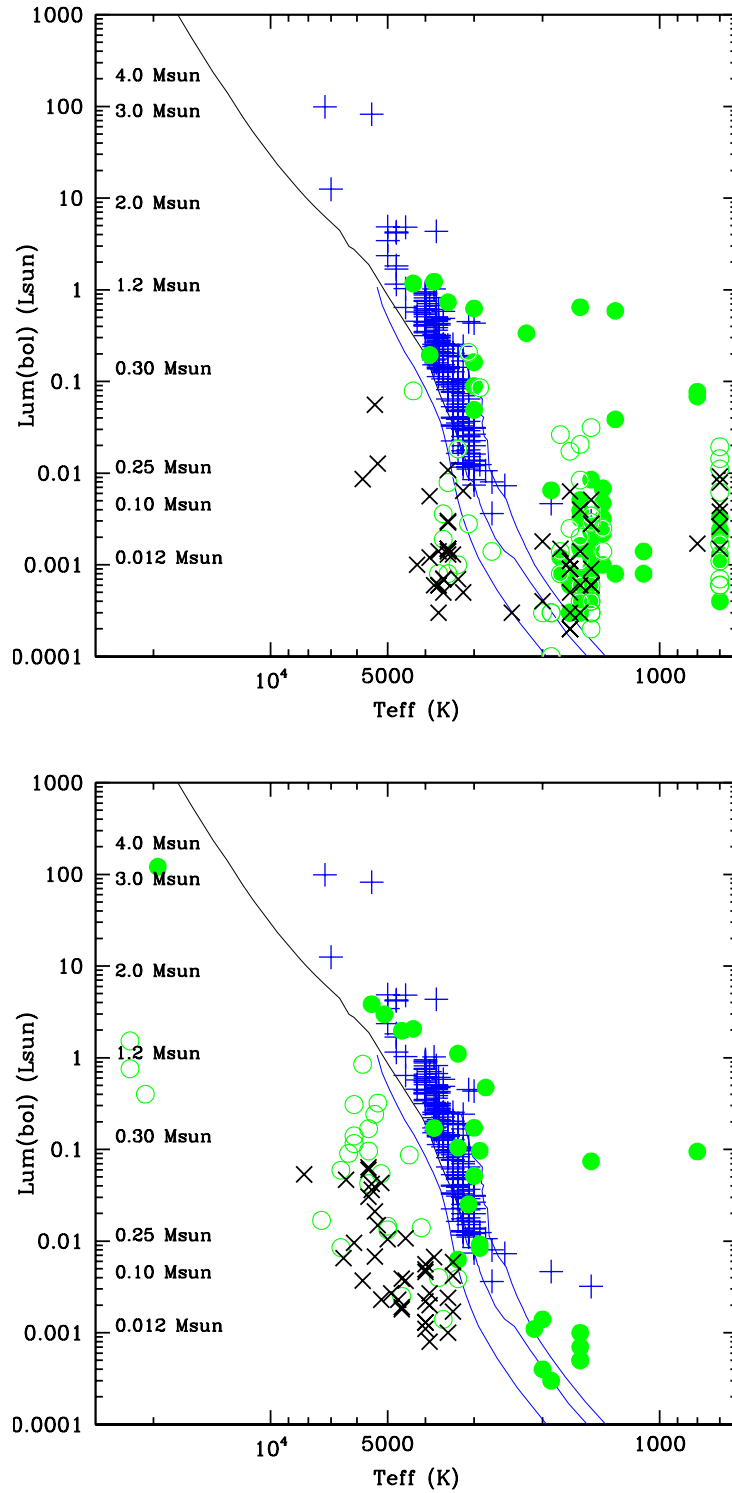


**Fig. 5.** Rejection of possible counterparts based on their location on the HRD. Big, black crosses correspond to possible and probable non-members. Candidate members are shown as open green circles (possible members) and solid green circles (probable members). The bolometric luminosity and the effective temperature were derived using a fixed value of the reddening ( $A_V=0.322$ ) or it was derived during the fitting process (left and right hand-side panels, respectively). Collinder 69 known members, located at similar distance, are displayed as blue plus symbols, and were selected from Dolan & Mathieu (1999), Barrado y Navascués et al. (2007) and Morales-Calderón (2008) and Barrado et al. (2011). Isochrones correspond to a 20 Myr isochrone from Siess et al. (2000) –upper part of the main sequence, in black– and Settl models –blue lines with 1, 20, and 10,000 Myr– from the Lyon group (Allard et al. 2012). We note that some possible members can be found well below the Collinder 69 cluster sequence.

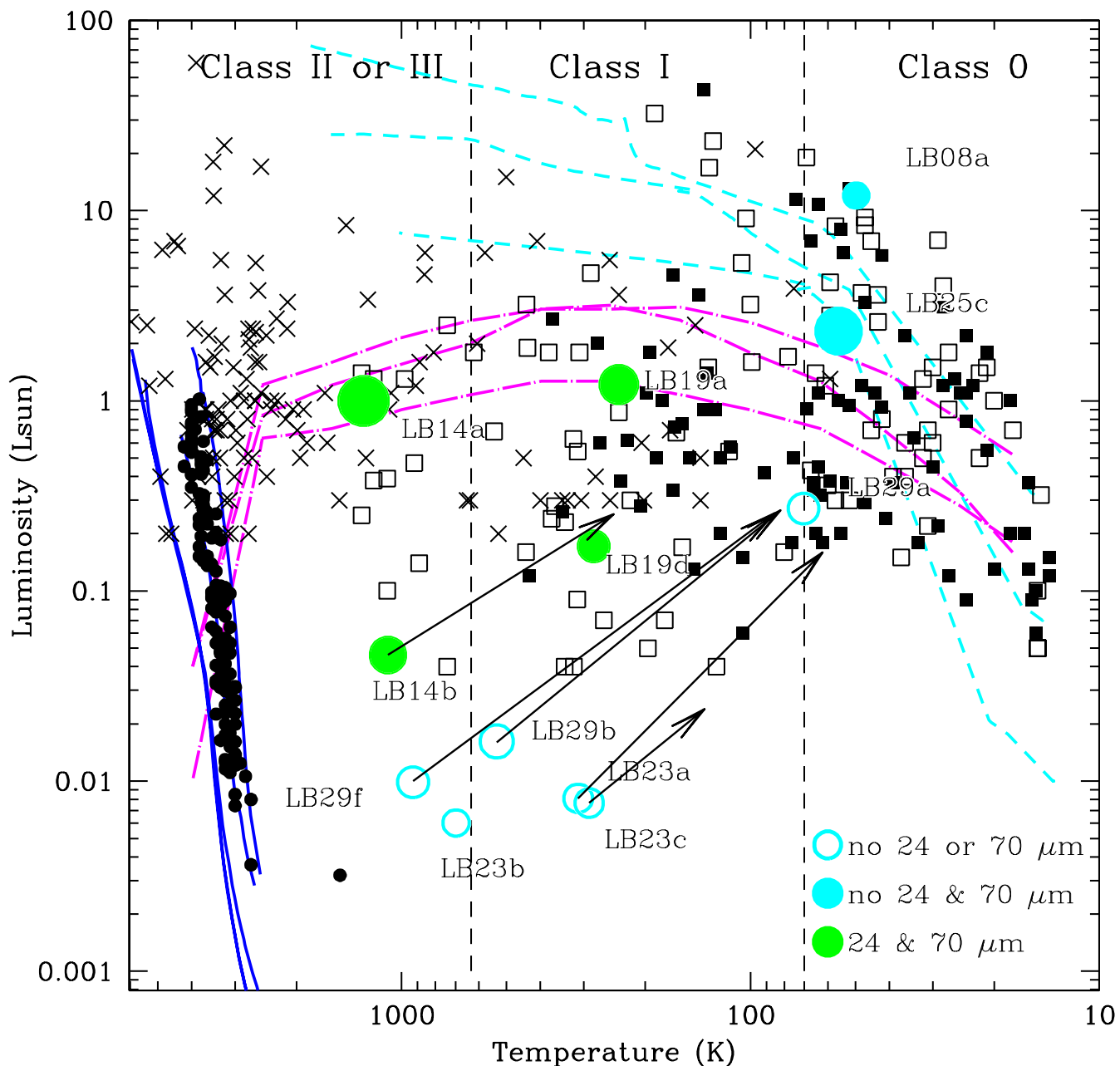


**Fig. 6.**  $L_{bol}$  vs.  $T_{bol}$  after Young & Evans (2005) and Dunham et al. (2008). Sources compiled in these two works, with evidences for being embedded low luminosity sources, are shown as solid black squares. Young members from Tobin et al. (2016) in Perseus are displayed as open squares. The black crosses correspond to Taurus members in Chen et al. (1995), whereas solid, black circles come from Bayo et al. (2011) and the Collinder 69 cluster. The cyan, short-dashed lines show the evolutionary tracks for the three models with different masses (in solar masses) considered by Young & Evans (2005). The magenta, dotted and long-dashed lines show the evolutionary tracks for three models considered by Myers et al. (1998). The blue solid lines correspond to isochrones by Baraffe et al. (1998). The vertical dashed lines show the Class 0–I and Class I–II  $T_{bol}$  boundaries from Chen et al. (1995). The big, labeled circles correspond to several counterparts for our B30 sources detected at  $70\ \mu\text{m}$  (our group A). Green with detections at  $24\ \mu\text{m}$  and cyan undetected at that band. Solid (green or cyan) circles denote counterparts whose properties have been derived with the  $870\ \mu\text{m}$  flux (for counterparts assumed to the primary origin of the submm emission), whereas open symbols represents values estimated without this flux, and the arrows move their location to the values derived when including this value.



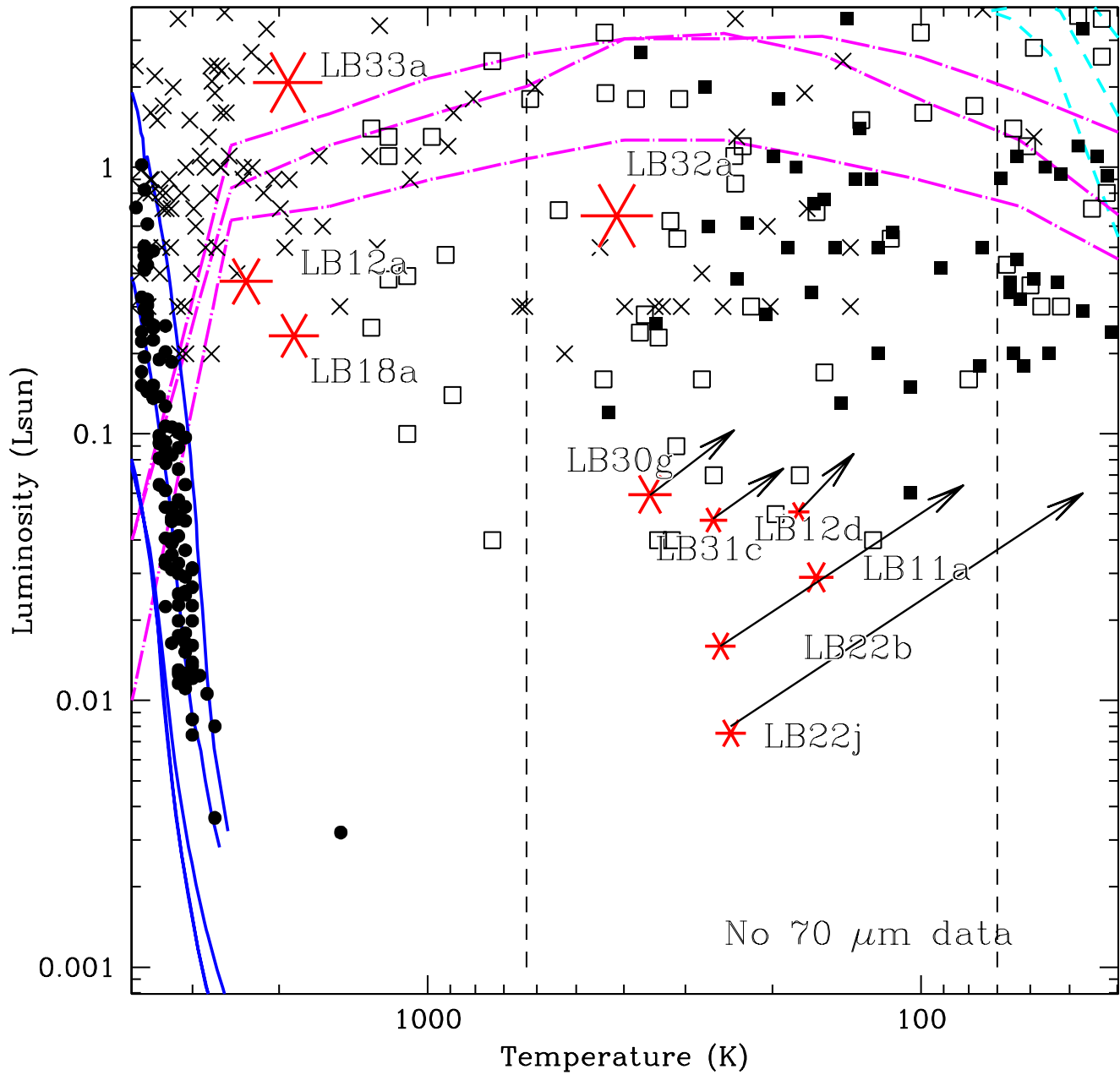


**Fig. 7.** Symbols as in Fig. 6 except for our B30 sources. Sample in group C1 are located outside the area surveyed by MIPS M2 but they have been detected at  $24 \mu\text{m}$ . The red asterisks represent values estimated when the flux at  $870 \mu\text{m}$  has not been included, whereas the end of the arrows signals the values derived with the submm flux.

**Table 1.** Summary of the instruments and photometry: beam size and pointing errors

Instrument	Bands	Beam FWHM /seeing (arcsec)	ErrorPos (arcsec)	Mag(lim)	Flux(lim) (Jy)	ZP <sup>3</sup>
DM	V,Rc,Ic	–	–	21.0,21.0,19.0	–	3952.79, 3002.88, 2520.19
INT/WFC	r,i	–	–	22.88, 21.50	–	–
2MASS	JHKs	–	–	16.8, 16.1, 15.3	–	1636.77, 1115.71, 671.53
Omega2000 <sup>1</sup>	J	–	0.5	20.00	–	1636.77
Omega2000 <sup>2</sup>	JHKs	–	0.5	21.30, 20.40, 18.25	–	1636.77, 1115.71, 671.53
Spitzer/IRAC	3.6, 4.5, 5.8, 8.0	1.66, 1.72, 1.88, 1.98	~1	18.25, 17.75, 15.625, 15.25	–	277.5, 179.5, 116.6, 63.1
Spitzer/MIPS	24, 70	5.8, 18.6	~1	9.0, –	–	7.18, 0.778
WISE	3.4, 4.6, 12, 22	6.1, 6.4, 6.5, 12.0	<1	17.40, 16.05, 11.85, 8.30	–	309.540, 171.787, 31.674, 8.363
Akari/IRC	9, 18	~2.4 <sup>4</sup>	2	–	0.050, 0.120	–
Akari/FIS	65, 90, 140, 160	37, 39, 58, 61	8	–	2.4, 0.55, 1.4, 6.3	–
APEX/LABOCA	870	27.6	3 <sup>5</sup>	–	0.03	–

<sup>1</sup> December 2007.<sup>2</sup> August 2011.<sup>3</sup> Flux (Jy) = ZP×10<sup>-0.4×Mag</sup>.<sup>4</sup> A 4 pixel binning was applied, so the actual beam size is close to 9.5 arcsec.<sup>5</sup> A nominal value of 3 arcsec as quoted in Weiß et al. (2009), but our own calibrations have an pointing error of 1 arcsec. In any case, for our counterpart search we have used 5 arcsec.

**Table 2.** APEX/LABOCA sources in Barnard 30.

B30-ID	RA <sup>1</sup> (2000.0)	DEC <sup>1</sup> (2000.0)	S <sub>v</sub> <sup>2</sup> (870 μm) (mJy)	I <sub>peak</sub> <sup>3</sup> (mJy/beam)	A <sub>v</sub> <sup>4</sup> (mag)	Mass <sup>5</sup>		L(int) <sup>6</sup> (L <sub>⊙</sub> )	Flux 70μm (Jy)	Ang. size <sup>7</sup> (")	rms 870 (mJy)	Gr <sup>8</sup>	Type <sup>9</sup>	BD? <sup>10</sup>	
						All (M <sub>⊙</sub> )	Peak (M <sub>⊙</sub> )							in beam	in 5"
LB01	05 31 13.64	12 22 22.7	182	114	4.109	0.266	0.166	<0.382	<0.89	22	16	B2	starless	–	–
LB02	05 31 32.30	12 19 14.7	68	68	4.141	0.099	0.099	<0.230	<0.52	PL	11	B2	excess	Y	–
LB03 <sup>a</sup>	05 31 29.20	12 17 22.7	39	39	2.471	0.057	0.057	–	–	PL	9	C2	YSO	Y	a <sup>BD</sup>
LB04 <sup>a</sup>	05 31 30.56	12 17 18.7	40	40	2.841	0.059	0.059	–	–	PL	9	C2	excess	Y	–
LB05	05 31 29.47	12 14 30.7	56	35	3.064	0.081	0.051	–	–	PL	36	C2	YSO	Y	a
LB06	05 31 30.83	12 12 46.7	144	527	4.670	0.210	0.077	–	–	PL	49	C2	starless	Y	–
LB07	05 31 32.19	12 11 46.7	36	36	4.415	0.052	0.052	–	–	PL	7	C2	YSO	Y	a <sup>BD</sup>
LB08	05 31 23.19	12 11 26.7	73	46	2.486	0.106	0.066	1.223	3.07	PL	27	A2	YSO	–	a
LB09	05 31 18.55	12 11 26.7	30	30	3.134	0.043	0.043	<0.422	<0.99	PL	7	B2	YSO	Y	a <sup>BD</sup>
LB10	05 31 09.55	12 11 02.7	32	33	1.146	0.046	0.046	–	–	PL	7	C2	YSO	Y	a <sup>BD</sup>
LB11	05 31 10.37	12 10 38.7	32	33	1.844	0.046	0.046	–	–	PL	7	C1	excess	Y	–
LB12	05 31 27.01	12 10 14.7	59	59	2.474	0.087	0.087	–	–	PL	7	C1	excess	Y	–
LB13	05 31 18.55	12 09 58.7	74	59	3.873	0.108	0.086	<0.382	<0.89	PL	23	B2	starless	Y	–
LB14	05 31 19.37	12 09 10.7	35	35	1.984	0.051	0.051	0.276	0.63	PL	7	A1	YSO	Y	a
LB15	05 31 27.28	12 07 26.7	38	38	2.736	0.056	0.056	<0.406	<0.95	PL	7	B2	starless	–	–
LB16	05 31 30.01	12 07 06.7	36	36	3.115	0.053	0.053	–	–	PL	7	C2	starless	Y	–
LB17	05 31 09.82	12 06 42.7	40	40	3.236	0.059	0.059	–	–	PL	7	C2	YSO	Y	a <sup>BD</sup>
LB18	05 31 34.92	12 06 22.7	41	41	2.917	0.059	0.059	–	–	PL	8	C1	excess	Y	–
LB19 <sup>b</sup>	05 31 28.10	12 05 30.7	125	793	2.759	0.182	0.116	0.402	0.94	PL	24	A1	YSO	Y	a, b
LB20 <sup>c</sup>	05 31 22.91	12 05 30.7	33	33	1.775	0.048	0.048	<0.592	<1.42	PL	7	B2*	excess	Y	–
LB21	05 31 36.00	12 05 02.7	74	42	3.897	0.108	0.061	–	–	PL	62	C2*	YSO	Y	a <sup>BD</sup>
LB22 <sup>d</sup>	05 31 31.64	12 04 14.7	60	60	2.710	0.088	0.088	–	–	PL	7	C1	YSO	Y	a <sup>BD</sup>
LB23 <sup>e</sup>	05 31 29.19	12 04 38.7	32	32	3.100	0.046	0.046	0.189	0.42	PL	7	A2	excess	Y	–
LB24	05 31 23.46	12 04 30.7	30	30	2.376	0.044	0.044	<0.604	<1.45	PL	7	B1	excess	Y	–
LB25	05 31 20.46	12 05 06.7	87	52	1.898	0.126	0.076	0.557 <sup>j</sup>	1.33 <sup>j</sup>	PL	34	A2	YSO	Y	a <sup>BD</sup> , e
LB26	05 31 17.73	12 05 06.7	40	40	2.960	0.058	0.058	–	–	PL	7	C2	excess	Y	–
LB27 <sup>f</sup>	05 31 13.37	12 05 30.7	191	103	4.232	0.279	0.150	–	–	PL	29	C2*	excess	Y	–
LB28 <sup>g</sup>	05 31 07.64	12 05 06.7	48	48	3.477	0.071	0.071	<0.573	<1.37	PL	7	B2*	excess	Y	–
LB29	05 31 08.73	12 03 46.7	44	44	3.430	0.064	0.064	0.337	0.78	PL	7	A2*	YSO	Y	a <sup>BD</sup>
LB30	05 31 13.37	12 03 34.7	84	69	2.840	0.123	0.101	–	–	PL	29	C1	excess	Y	–
LB31	05 31 15.28	12 03 38.7	56	56	2.378	0.082	0.082	–	–	PL	7	C1	excess	Y	–
LB32 <sup>h</sup>	05 32 12.56	12 09 54.7	85	85	–	0.123	0.123	–	–	PL	16	C1	YSO	–	a
LB33 <sup>i</sup>	05 30 13.36	12 08 46.7	60	60	0.714	0.087	0.087	–	–	PL	16	C1	YSO	–	a
LB34 <sup>i</sup>	05 30 13.36	12 08 58.7	44	44	0.123	0.064	0.064	–	–	PL	16	C2	starless	–	–

<sup>1</sup> Position of the maximum emission of the cores. The coordinates have an error of approximately 1 arcsec (pointing rms, but each APEX/LABOCA cell has a 4 arcsec size).

<sup>2</sup> APEX/LABOCA flux density at 870 μm computed above 3σ emission. The absolute uncertainty in the flux scale is 8%.

<sup>3</sup> APEX/LABOCA peak intensity at 870 μm (maximum of the emission). For point-like sources, the value is equal to the previous column.

<sup>4</sup> Values derived from the extinction map, with a resolution of 1.5 arcmin, three times larger the LABOCA beam-size.

<sup>5</sup> Envelope masses derived using the 870 μm flux densities and assuming a dust temperature of 15 K (Sánchez-Monge et al. 2013), and a dust (and gas) mass opacity coefficient of 0.0175 cm<sup>2</sup> g<sup>-1</sup> (obtained by interpolating the tabulated values of Ossenkopf & Henning 1994, see subsec. 3.1). The uncertainty in the masses due to the dust temperature and opacity law is estimated to be a factor of 4.

<sup>6</sup> Internal luminosity of the core, based on MIPS flux at 70 μm, after Dunham et al. (2008).

<sup>7</sup> Deconvolved size after fitting a Gaussian to the cores. The averaged of the major and minor axis is represented. "PL" stands for point-like source.

<sup>8</sup> Gr = Groups based on the detection at 70 and 24 μm and presence of counterparts, as discussed in subsection 2.7: A1 = Detection at 70 and 24 μm; A2 = detection at 70 and upper limit at 24 μm; B1 = upper limit at 70 μm and detection at 24 μm; B2 = upper limit both at 70 and 24 μm; C1 = no data at 70 μm and detection at 24 μm; C2 = no data at 70 μm and upper limit at 24 μm.

<sup>9</sup> Tentative classification:

YSO = Young Stellar Object, with a optical and/or near-IR sources within 5 arcsec of APEX/LABOCA central coordinate. Our tentative interpretation is that most of them are proto-stars or proto-BDs. Excess = Optical and/or near-IR sources with excesses within the APEX/LABOCA beam but farther than 5 arcsec. The submm source cannot be assigned unambiguously to any counterpart so its nature remains unknown. Starless = Possible starless core, since there is neither counterparts closer than 5 arcsec nor an optical/IR source farther away with excess.

<sup>10</sup> Presence of brown dwarf candidates: the first column indicates whether there is a BD candidate within APEX/LABOCA beam, whereas the second column indicates whether there is a optical/IR counterpart within 5 arcsec from APEX/LABOCA peak (the letter for the identification and the "BD" super-index for the substellar candidates).

<sup>a</sup> B30-LB03 and B30-LB04 very close to each other, see subsection A.1.

<sup>b</sup> IRAS05286+1203, RA=82.8671, DEC=+12.0899, [12]=7.79e-01±0.0779 Jy, [25]=1.91e+00±0.2101 Jy, [60]=9.35e+00±1.7765 Jy, [100]=7.04e+01±14.784 Jy. LB30-LB19d has a MIPS 2 flux at 70 μm of 0.200 Jy, which translate to L(int)=0.094 L<sub>⊙</sub> (i.e., a VeLLO). Note that within the LABOCA beam there is a APEX/SABOCA source detected at 350 μm (B30-SB08, Huélamo et al. 2017)).

<sup>c</sup> B30-LB20 contains a APEX/SABOCA at 350 μm (B30-SB09, Huélamo et al. 2017)).

<sup>d</sup> There are two APEX/SABOCA sources within the B30-LB22 beam (B30-SB03 and B30-SB04, Huélamo et al. 2017).

<sup>e</sup> There are two APEX/SABOCA sources within the B30-LB23 beam (B30-SB05 and B30-SB06, Huélamo et al. 2017).

<sup>f</sup> B30-LB27 contains a APEX/SABOCA at 350 μm (B30-SB12, Huélamo et al. 2017)).

<sup>g</sup> B30-LB28 contains a APEX/SABOCA at 350 μm (B30-SB16, Huélamo et al. 2017)).

<sup>h</sup> IRAS05293+1207, RA=83.0450, DEC=+12.1629, [12]<2.50e-01 Jy, [25]<2.71e-01 Jy, [60]=1.15e+00±0.1725 Jy, [100]<2.66e+01 Jy.

<sup>i</sup> B30-LB33 and B30-LB34 very close to each other, see subsection A.1.

<sup>j</sup> The MIPS M2 flux probably corresponds to the counterpart identified as LB25c.

\* Extended emission at 24 μm.

Table 3. Photometric data for all counterparts.

B30-ID	RA(ind) (deg)	DEC(ind) (deg)	J	eJ	H CAHA/ $\Omega_{\text{Mega}2000}$	eH	K	eK	I1	eI1	I2	eI2	I3	eI3	I4	eI4	M1	eM1
LB01_a	82.8103943	12.3745267	12.990	0.070	-	-	-	-	11.704	0.003	11.702	0.004	11.647	0.012	11.766	0.041	-	-
LB01_b	82.8095387	12.3746628	14.301	0.070	-	-	-	-	15.599	0.044	15.386	0.053	-	-	-	-	-	-
LB01_c	82.8108063	12.3768333	-	-	-	-	-	-	17.945	0.197	17.078	0.166	-	-	-	-	-	-
LB02_a	82.8820496	12.3225374	-	-	-	-	-	-	17.736	0.159	17.198	0.133	-	-	-	-	-	-
LB02_b	82.8837585	12.3257999	-	-	-	-	-	-	18.079	0.193	17.536	0.193	-	-	-	-	-	-
LB02_c	82.888237	12.3213615	-	-	-	-	-	-	14.990	0.017	14.398	0.019	14.245	0.104	12.973	0.118	-	-
LB02_d	82.8833542	12.3129959	-	-	-	-	-	-	17.083	0.104	17.088	0.133	-	-	-	-	-	-
LB03_a	82.8715635	12.2891899	19.454	0.061	17.397	0.027	16.342	0.067	15.978	0.028	15.811	0.047	-	-	-	-	-	-
LB03_b	82.878997	12.288692	20.442	0.122	18.314	0.057	17.582	0.142	16.768	0.059	16.943	0.147	-	-	-	-	-	-
LB03_c	82.8828009	12.2905016	16.88	0.007	15.547	0.005	14.936	0.019	14.590	0.011	14.476	0.02	14.403	0.082	-	-	-	-
LB03_d	82.8781682	12.2934734	19.223	0.053	17.627	0.031	17.072	-	-	-	-	-	-	-	-	-	-	-
LB03_e	82.8704761	12.2850072	20.167	0.098	19.055	0.098	-	-	17.282	0.078	17.491	0.193	-	-	-	-	-	-
LB03_f	82.8752735	12.2819404	20.485	0.113	18.671	0.073	17.667	0.144	16.291	0.054	15.438	0.044	14.509	0.109	12.998	0.084	-	-
LB03_g	82.8685852	12.2881695	17.364	0.011	16.266	0.010	15.612	0.036	15.406	0.02	15.608	0.039	15.452	0.227	-	-	-	-
LB03_h	82.877498	12.2929915	18.23	0.021	16.261	0.010	15.460	0.030	14.735	0.013	14.726	0.021	14.892	0.123	-	-	-	-
LB04_a	82.877498	12.2929915	18.23	0.021	16.261	0.010	15.460	0.030	14.735	0.013	14.726	0.021	14.892	0.123	-	-	-	-
LB05_a	82.872252	12.2411915	11.619	0.004	11.038	0.002	-	-	10.578	0.002	10.496	0.002	10.459	0.006	10.454	0.014	-	-
LB05_b	82.8752217	12.2423194	15.729	0.003	14.257	0.002	13.585	0.006	13.060	0.007	12.944	0.009	13.036	0.041	12.757	0.069	-	-
LB05_c	82.8747836	12.247714	18.822	0.042	17.471	0.028	16.971	0.090	16.354	0.049	16.202	0.071	-	-	-	-	-	-
LB05_d	82.8662881	12.2437099	19.612	0.069	18.232	0.054	17.704	0.160	18.180	0.28	17.621	0.272	-	-	-	-	-	-
LB05_e	82.8728663	12.2481522	20.736	0.142	19.210	0.164	-	-	18.184	0.339	-	-	-	-	-	-	-	-
LB06_a	82.8729098	12.2138781	16.482	0.005	14.589	0.002	13.585	0.006	12.919	0.004	12.709	0.006	12.708	0.021	12.828	0.051	-	-
LB06_b	82.8817291	12.2117243	-	-	-	-	-	-	18.825	0.442	17.958	0.381	-	-	-	-	-	-
LB06_c	82.8716738	12.216362	19.451	0.058	17.462	0.026	16.682	0.077	16.278	0.048	15.857	0.068	-	-	-	-	-	-
LB06_d	82.8820695	12.2186419	20.695	0.137	18.540	0.066	17.092	0.107	16.614	0.063	16.653	0.126	-	-	-	-	-	-
LB07_a	82.8845502	12.1965247	-	-	19.641	0.140	-	-	16.719	0.067	16.582	0.098	-	-	-	-	-	-
LB07_b	82.8816234	12.1965027	20.743	0.177	18.959	0.098	17.945	0.200	18.068	0.241	18.086	0.417	-	-	-	-	-	-
LB07_c	82.8828726	12.1992986	-	-	19.626	0.138	-	-	18.041	0.251	17.181	0.18	-	-	-	-	-	-
LB07_d	82.8825019	12.1927908	20.652	0.136	18.871	0.114	17.706	0.173	17.567	0.145	17.083	0.161	-	-	-	-	-	-
LB07_e	82.875824	12.1930475	18.954	0.088	17.883	0.050	-	-	16.386	0.055	16.314	0.087	-	-	14.127	0.278	-	-
LB07_f	82.8885421	12.1999506	-	-	19.088	0.162	-	-	-	-	-	-	-	-	-	-	-	-
LB07_g	82.8901372	12.1990874	20.072	0.129	18.531	0.066	17.461	0.130	16.700	0.084	17.37	0.215	-	-	-	-	-	-
LB07_h	82.8783659	12.2009678	-	-	19.383	0.137	-	-	18.399	0.265	-	-	-	-	-	-	-	-
LB07_i	82.8767882	12.1977526	-	-	20.036	0.192	-	-	18.331	0.299	-	-	-	-	-	-	-	-
LB08_a	82.8479608	12.1911092	18.926	0.081	17.844	0.055	16.934	0.121	16.759	0.077	16.638	0.111	-	-	-	-	-	-
LB08_b	82.8490389	12.195165	18.546	0.028	16.995	0.018	16.224	0.058	16.151	0.043	15.925	0.064	-	-	-	-	-	-
LB08_c	82.8478087	12.1849561	18.534	0.028	16.822	0.016	16.095	0.052	15.747	0.029	15.551	0.038	-	-	-	-	-	-
LB08_d	82.8487087	12.1976932	-	-	17.744	0.068	-	-	17.752	0.227	-	-	-	-	-	-	-	-
LB08_e	82.8450846	12.1841564	20.469	0.129	19.025	0.093	17.671	0.210	18.223	0.379	17.972	0.442	-	-	-	-	-	-
LB08_f	82.8393117	12.1900185	21.077	0.148	19.086	0.091	-	-	-	-	-	-	-	-	-	-	-	-
LB08_g	82.8410187	12.1867886	-	-	-	-	-	-	-	-	-	-	-	-	14.163	0.718	-	-
LB08_h	82.8538342	12.1925179	20.161	0.098	18.431	0.060	17.785	0.139	17.051	0.109	17.447	0.275	-	-	-	-	-	-

\* MIPS photometry might be affected by the inhomogeneous extended emission by the nebulosity.

Table 3. Photometric data for all counterparts.

B30-ID	RA(ind) (deg)	DEC(ind) (deg)	J	eJ	H		K	eK	I1	eI1	I2	eI2	I3	eI3	I4	eI4	M1	eM1
					CAHA/Omega2000	eH												
LB09_a	82.8274595	12.1912422	20.151	0.144	18.666	0.084	17.995	0.208	16.683	0.096	16.666	0.106	-	-	-	-	-	-
LB09_b	82.8286146	12.192915	-	-	19.534	0.136	-	-	16.991	0.16	17.119	0.229	-	-	-	-	-	-
LB09_c	82.8233122	12.1910026	18.713	0.040	16.650	0.016	15.821	0.047	15.190	0.018	15.268	0.033	14.921	0.207	-	-	-	-
LB09_d	82.8244826	12.1877228	20.103	0.119	18.466	0.063	17.613	0.140	17.154	0.101	17.073	0.139	-	-	-	-	-	-
LB09_e	82.831573	12.1865735	18.631	0.031	17.047	0.019	16.445	0.066	16.018	0.038	15.763	0.054	-	-	-	-	-	-
LB09_f	82.8338717	12.1928557	19.755	0.085	18.253	0.053	17.444	0.129	16.833	0.129	18.235	0.749	-	-	-	-	-	-
LB09_g	82.8307994	12.1940775	21.412	0.155	19.205	0.110	-	-	17.209	0.232	17.654	0.371	-	-	-	-	-	-
LB09_h	82.8265858	12.1960763	-	-	19.125	0.137	-	-	18.093	0.269	18.296	0.561	-	-	-	-	-	-
LB10_a	82.7909414	12.1845672	18.028	0.018	16.817	0.016	16.300	0.063	16.183	0.052	15.865	0.048	15.057	0.213	-	-	-	-
LB10_b	82.7897077	12.1863344	18.976	0.040	17.959	0.041	17.647	0.155	17.098	0.104	16.959	0.146	-	-	-	-	-	-
LB10_c	82.7899993	12.1816228	18.592	0.044	17.289	0.032	16.642	0.103	15.842	0.036	15.733	0.049	-	-	-	-	-	-
LB10_d	82.7906454	12.1805146	17.392	0.011	16.455	0.011	16.119	0.054	15.870	0.038	15.614	0.045	-	-	-	-	-	-
LB10_e	82.7929654	12.1829769	19.509	0.061	18.089	0.045	17.654	0.150	16.329	0.051	16.429	0.08	-	-	-	-	-	-
LB10_f	82.7940554	12.1827567	18.104	0.020	16.844	0.016	16.297	0.064	16.023	0.042	15.952	0.056	-	-	-	-	-	-
LB10_g	82.7954744	12.181736	18.606	0.030	17.290	0.024	16.694	0.093	16.284	0.049	16.027	0.063	-	-	-	-	-	-
LB10_h	82.7929218	12.1881804	15.374	0.002	14.604	0.002	14.305	0.011	14.003	0.008	13.992	0.012	14.331	0.129	13.683	0.16	-	-
LB10_i	82.7957761	12.1864233	18.396	0.041	17.059	0.026	16.294	0.075	15.780	0.036	15.671	0.047	-	-	-	-	-	-
LB10_j	82.792862	12.1905084	19.298	0.052	18.302	0.054	-	-	17.883	0.216	17.781	0.317	-	-	-	-	-	-
LB10_k	82.7826309	12.1854864	16.386	0.005	15.526	0.001	15.183	0.025	14.841	0.02	15.08	0.027	-	-	-	-	-	-
LB10_l	82.7873969	12.1780491	20.164	0.144	19.190	0.101	-	-	18.934	0.719	-	-	-	-	-	-	-	-
LB10_m	82.7873969	12.1780491	20.083	0.125	18.940	0.095	-	-	17.628	0.262	17.115	0.152	-	-	-	-	-	-
LB11_a	82.7921273	12.1737653	20.491	0.111	19.470	0.142	-	-	-	-	-	-	-	-	-	6.527	0.079	-
LB11_b	82.7991141	12.1765574	20.634	0.125	20.044	0.161	-	-	17.884	0.378	-	-	-	-	-	-	-	-
LB11_c	82.7959332	12.1745673	20.132	0.146	19.430	0.136	-	-	-	-	-	-	-	12.307	0.194	-	-	-
LB11_d	82.7977769	12.1732308	19.098	0.063	18.090	0.047	-	-	-	-	-	-	-	-	-	-	-	-
LB11_e	82.7945144	12.170888	20.785	0.139	19.323	0.147	-	-	17.436	0.276	17.777	0.384	-	-	-	-	-	-
LB11_f	82.7871577	12.1760213	19.434	0.074	18.221	0.053	18.031	0.135	17.978	0.299	17.349	0.213	-	-	-	-	-	-
LB12_a	82.8622399	12.1723873	12.083	0.006	11.305	0.003	-	-	10.378	0.002	10.223	0.002	10.031	0.007	9.802	0.038	7.719*	0.431*
LB12_b	82.860249	12.1732605	-	-	-	-	17.395	0.130	14.367	0.027	14.266	0.04	-	-	-	-	-	-
LB12_c	82.8616483	12.1773707	-	-	18.861	0.134	-	-	16.867	0.137	16.255	0.094	14.53	0.174	12.761	0.164	-	-
LB12_d	82.858020	12.166592	-	-	-	-	-	-	15.783	0.158	15.762	0.19	12.333	0.187	-	-	5.409	0.062
LB12_e	82.8602536	12.1663629	-	-	19.307	0.167	-	-	15.532	0.074	15.583	0.128	12.05	0.081	-	-	-	-
LB12_f	82.8658218	12.169281	-	-	-	-	-	-	-	-	-	-	-	-	12.759	0.273	6.049*	0.061*
LB12_g	82.8675273	12.1702059	19.159	0.057	17.102	0.022	16.038	0.050	15.123	0.034	15.021	0.054	13.631	0.215	-	-	-	-
LB12_h	82.8669147	12.1677647	19.555	0.144	18.462	0.136	-	-	-	-	-	-	14.003	0.268	12.552	0.184	-	-
LB12_i	82.8647003	12.1651821	-	-	-	-	-	-	-	-	-	-	-	-	13.248	0.607	-	-
LB12_j	82.8687731	12.1739057	19.489	0.061	17.768	0.037	17.083	0.099	16.354	0.083	16.202	0.1	-	-	13.168	0.456	-	-
LB12_k	82.8610365	12.1758133	-	-	19.539	0.120	-	-	16.163	0.079	15.661	0.104	-	-	-	-	-	-
LB12_l	82.86409	12.1714582	-	-	-	-	-	-	14.845	0.038	-	-	-	-	-	-	-	-
LB13_a	82.8314832	12.1614693	13.477	0.001	12.801	0.001	12.516	0.003	12.168	0.004	12.092	0.005	12.043	0.024	11.947	0.078	-	-
LB13_b	82.8248788	12.1638624	20.735	0.122	18.718	0.107	-	-	17.578	0.207	17.336	0.257	-	-	-	-	-	-

\* MIPS photometry might be affected by the inhomogeneous extended emission by the nebulosity.

Table 3. Photometric data for all counterparts.

B30-ID	RA(ind) (deg)	DEC(ind) (deg)	J	eJ	H CAHA/Omega2000	eH	K	eK	I1	eI1	I2	eI2	I3	eI3	I4	eI4	M1	eM1
LB14_a	82.8310571	12.1542772	12.164	0.001	10.926	0.002	—	—	9.085	0.001	8.52	0.002	8.099	0.002	7.295	0.001	4.305	0.011
LB14_b	82.8313354	12.1495811	16.734	0.006	14.531	0.002	13.107	0.004	11.886	0.004	11.492	0.004	11.086	0.013	10.656	0.028	5.67	0.027
LB14_c	82.8355319	12.1547291	12.808	0.001	12.115	0.001	11.833	0.002	11.504	0.005	11.4	0.005	11.291	0.013	11.326	0.044	—	—
LB14_d	82.8285637	12.1530748	19.63	0.078	18.742	0.074	—	—	15.051	0.058	14.566	0.049	—	—	—	—	—	—
LB14_e	82.8256866	12.1508073	18.729	0.032	18.028	0.043	17.761	0.139	17.245	0.216	16.39	0.134	—	—	—	—	—	—
LB14_f	82.8350675	12.1520706	20.248	0.099	18.907	0.079	—	—	17.245	0.216	16.39	0.134	—	—	—	—	—	—
LB14_g	82.835154	12.1492848	18.715	0.035	17.228	0.024	16.619	0.085	16.397	0.136	15.268	0.093	—	—	—	—	—	—
LB14_h	82.8313458	12.147645	20.195	0.161	19.104	0.113	—	—	15.727	0.071	16.817	0.273	—	—	—	—	—	—
LB14_j	82.8294198	12.1463334	19.683	0.104	18.971	0.124	—	—	17.358	0.274	15.187	0.071	—	—	—	—	—	—
LB14_k	82.8271388	12.1468297	19.716	0.074	18.694	0.074	16.938	0.094	16.250	0.093	16.028	0.095	—	—	—	—	—	—
LB15_a	82.8675875	12.1263543	12.801	0.001	12.102	0.001	11.861	0.002	11.628	0.003	11.623	0.004	11.59	0.016	11.471	0.072	—	—
LB15_b	82.8619391	12.1178684	18.048	0.021	16.795	0.017	16.141	0.062	16.121	0.064	15.898	0.072	—	—	—	—	—	—
LB15_c	82.8632264	12.1307359	19.225	0.056	18.314	0.059	—	—	18.593	0.521	17.714	0.318	—	—	—	—	—	—
LB15_d	82.8631076	12.1172072	20.566	0.111	19.200	0.109	—	—	18.593	0.521	17.714	0.318	—	—	—	—	—	—
LB16_a	82.8742455	12.1128436	18.25	0.023	16.449	0.012	15.651	0.037	15.201	0.025	15.321	0.035	15.34	0.341	—	—	—	—
LB16_b	82.8797155	12.112797	18.33	0.025	16.895	0.017	16.243	0.057	16.094	0.066	15.699	0.058	—	—	—	—	—	—
LB16_c	82.881731	12.1191153	17.835	0.016	16.344	0.011	15.552	0.033	15.166	0.02	15.246	0.037	15.451	0.357	—	—	—	—
LB16_d	82.8767443	12.1161898	—	—	19.610	0.132	—	—	18.916	0.446	—	—	—	—	—	—	—	—
LB16_e	82.87578313	12.1217787	21.49	0.216	19.626	0.128	—	—	18.916	0.446	17.449	0.273	15.302	0.225	14.188	0.324	—	—
LB16_f	82.8718226	12.1202306	—	—	—	—	—	—	—	—	—	—	—	—	—	—	—	—
LB17_a	82.7896196	12.1125454	18.561	0.037	17.142	0.022	16.023	0.078	16.101	0.042	15.63	0.038	15.115	0.309	—	—	—	—
LB17_b	82.7895729	12.1169664	17.903	0.018	16.543	0.013	15.869	0.044	15.526	0.028	15.398	0.033	15.944	0.595	—	—	—	—
LB17_c	82.7956702	12.1080471	20.13	0.106	18.705	0.105	—	—	17.064	0.163	17.518	0.256	14.185	0.152	—	—	—	—
LB17_d	82.7934952	12.1105013	—	—	—	—	—	—	17.064	0.163	17.518	0.256	14.312	0.135	—	—	—	—
LB17_e	82.7967072	12.1139727	—	—	—	—	—	—	17.064	0.163	17.518	0.256	15.916	0.482	—	—	—	—
LB17_f	82.7934146	12.116857	19.865	0.130	18.644	0.085	—	—	17.285	0.239	17.451	0.241	—	—	—	—	—	—
LB17_g	82.7840129	12.110386	18.641	0.031	17.399	0.026	17.012	0.098	16.705	0.079	16.521	0.07	—	—	—	—	—	—
LB18_a	82.893931	12.1086094	13.415	0.001	11.707	0.001	10.956	0.001	10.320	0.002	10.163	0.002	10.0	0.004	9.868	0.009	7.188	0.058
LB18_b	82.8941585	12.1112154	19.578	0.063	18.072	0.044	17.532	0.135	15.431	0.065	14.467	0.04	—	—	—	—	—	—
LB18_c	82.900058	12.1082994	20.226	0.171	19.103	0.103	—	—	16.682	0.121	—	—	—	—	—	—	—	—
LB18_d	82.8994244	12.1055759	20.216	0.136	19.129	0.130	—	—	16.682	0.121	—	—	—	—	—	—	—	—
LB18_e	82.8907647	12.1071047	19.926	0.082	18.186	0.048	17.825	0.146	16.024	0.05	15.721	0.054	—	—	—	—	—	—
LB18_f	82.8979923	12.0998372	19.721	0.076	18.268	0.053	17.667	0.148	17.268	0.095	17.404	0.168	—	—	—	—	—	—
LB18_g	82.8914648	12.1000721	19.716	0.069	18.112	0.048	17.126	0.106	16.939	0.083	16.357	0.07	—	—	—	—	—	—
LB18_h	82.8959583	12.1037709	—	—	18.707	0.128	—	—	17.041	0.128	16.303	0.089	—	—	—	—	—	—
LB19_a	82.8658453	12.0919505	16.753	0.010	14.422	0.003	12.972	0.004	10.976	0.003	9.631	0.003	8.492	0.003	7.12	0.003	1.933	0.0020
LB19_b	82.8676553	12.0917727	14.151	0.001	13.462	0.001	13.138	0.004	12.480	0.015	12.089	0.025	10.276	0.018	—	—	—	—
LB19_c	82.8686592	12.0905224	13.786	0.001	13.138	0.001	12.931	0.004	12.664	0.008	12.48	0.009	12.457	0.036	—	—	—	—
LB19_d	82.8733996	12.0925052	—	—	14.528	0.056	—	—	12.664	0.008	11.493	0.004	10.358	0.009	8.989	0.012	4.173	0.016
LB19_e	82.8614809	12.0885397	18.39	0.025	16.923	0.018	16.277	0.059	14.840	0.019	14.238	0.018	13.064	0.056	11.562	0.043	—	—
LB19_f	82.8678788	12.0866633	—	—	—	—	16.921	0.137	15.897	0.126	15.815	0.122	14.046	0.258	12.404	0.236	—	—
LB19_g	82.8612144	12.0926726	—	—	16.266	0.045	—	—	—	—	—	—	—	—	—	—	—	—
LB19_h	82.8668776	12.0875591	—	—	17.736	0.094	—	—	—	—	16.228	0.153	14.046	0.171	12.089	0.162	—	—

\* MIPS photometry might be affected by the inhomogeneous extended emission by the nebulosity.

**Table 3.** Photometric data for all counterparts.

B30-ID	RA(ind) (deg)	DEC(ind) (deg)	J	eJ	H	eH	K	eK	I1	eI1	I2	eI2	I3	eI3	I4	eI4	M1	eM1	CAHA/Omega2000	
																			H	eH
LB20_a	82.8508555	12.0902626	15.091	0.002	14.115	0.002	13.708	0.007	13.454	0.015	13.314	0.01	13.315	0.079	-	-	-	-	-	-
LB20_b	82.8513261	12.0917094	19.635	0.118	18.120	0.083	-	-	15.342	0.103	-	-	-	-	-	-	-	-	-	-
LB20_c	82.8402513	12.0966039	10.999	0.003	10.276	0.002	-	-	9.754	0.002	9.775	0.004	9.645	0.005	-	-	-	-	-	-
LB20_d	82.8394462	12.0955432	11.419	0.003	10.541	0.002	-	-	9.849	0.003	9.839	0.004	9.719	0.006	-	-	6.918*	0.122*	-	-
LB20_e	82.8394127	12.0930814	17.152	0.022	15.856	0.007	15.464	0.030	14.377	0.028	14.327	0.038	14.628	0.356	-	-	-	-	-	-
LB20_f	82.8468218	12.096629	19.127	0.046	17.474	0.028	16.778	0.085	16.691	0.135	16.629	0.125	-	-	-	-	-	-	-	-
LB20_g	82.8439374	12.0959187	20.719	0.120	19.133	0.101	-	-	16.678	0.266	-	-	-	-	-	-	-	-	-	-
LB20_h	82.844606	12.0966218	-	-	19.836	0.120	-	-	17.339	0.317	16.877	0.392	-	-	-	-	-	-	-	-
LB20_i	82.8430989	12.0983201	19.748	0.071	18.714	0.069	-	-	15.725	0.09	15.757	0.123	-	-	-	-	-	-	-	-
LB20_j	82.8529105	12.0926289	-	-	18.981	0.140	-	-	16.669	0.217	16.623	0.168	-	-	-	-	-	-	-	-
LB21_a	82.8988495	12.0846224	-	-	-	-	-	-	-	-	-	-	13.954	0.157	12.193	0.144	7.287*	0.176*	-	-
LB21_b	82.899437	12.0812626	-	-	-	-	-	-	-	-	-	-	-	-	12.652	0.196	-	-	-	-
LB21_c	82.90199	12.081975	19.045	0.045	-	-	17.218	0.126	16.182	0.068	16.018	0.067	-	-	-	-	-	-	-	-
LB21_d	82.8997765	12.0891346	19.0	0.041	17.998	0.041	17.645	0.131	18.222	0.36	17.275	0.165	-	-	-	-	-	-	-	-
LB21_e	82.906055	12.0828322	19.184	0.052	18.113	0.047	17.743	0.136	16.794	0.236	17.133	0.281	-	-	-	-	-	-	-	-
LB21_f	82.8998506	12.0914761	20.152	0.154	19.159	0.118	-	-	17.326	0.21	17.359	0.247	-	-	-	-	-	-	-	-
LB21_g	82.8943406	12.0873348	19.483	0.110	18.350	0.090	-	-	16.354	0.075	15.935	0.055	-	-	-	-	-	-	-	-
LB21_h	82.8972397	12.0861282	-	-	-	-	-	-	-	-	-	-	13.022	0.183	-	-	-	-	-	-
LB21_i	82.8977103	12.0892541	-	-	-	-	-	-	-	-	-	-	-	-	-	-	-	-	-	-
LB22_a	82.8822765	12.0712583	18.406	0.051	17.051	0.040	16.883	0.116	15.651	0.092	-	-	13.351	0.152	-	-	6.749	0.079	-	-
LB22_b	82.879810	12.070272	-	-	-	-	-	-	-	-	-	-	-	-	-	-	-	-	-	-
LB22_c	82.8842633	12.0692825	19.712	0.107	18.251	0.08	-	-	15.884	0.095	16.317	0.145	-	-	-	-	-	-	-	-
LB22_d	82.8865316	12.0684093	17.175	0.009	16.135	0.009	15.806	0.043	15.438	0.047	15.697	0.074	-	-	-	-	-	-	-	-
LB22_e	82.883323	12.069021	18.237	0.033	16.969	0.020	16.581	0.075	15.927	0.107	16.212	0.141	-	-	-	-	-	-	-	-
LB22_f	82.8850515	12.0706474	18.13	0.021	17.057	0.019	16.524	0.073	16.805	0.243	16.817	0.231	-	-	-	-	-	-	-	-
LB22_g	82.886582	12.0713157	19.621	0.085	18.347	0.065	18.028	0.189	16.467	0.107	16.835	0.198	-	-	-	-	-	-	-	-
LB22_h	82.876306	12.0709514	20.012	0.112	19.131	0.103	-	-	16.431	0.117	16.36	0.15	13.569	0.113	-	-	-	-	-	-
LB22_i	82.879455	12.0659626	18.889	0.047	18.129	0.053	17.810	0.189	-	-	-	-	-	-	-	-	-	-	-	-
LB22_j	82.8845747	12.0683098	-	-	19.272	0.161	-	-	16.336	0.127	16.753	0.186	14.334	0.203	12.328	0.115	7.137*	0.169*	-	-
LB23_a	82.8733007	12.0754017	18.785	0.066	17.931	0.063	17.657	0.144	16.742	0.123	17.002	0.199	14.456	0.177	-	-	-	-	-	-
LB23_b	82.8740083	12.0797718	18.445	0.029	16.821	0.017	15.999	0.050	15.468	0.03	15.576	0.06	15.117	0.211	-	-	-	-	-	-
LB23_c	82.8761053	12.0778312	20.255	0.156	19.332	0.114	-	-	16.864	0.133	16.551	0.124	-	-	12.957	0.169	-	-	-	-
LB23_d	82.8687196	12.0718283	16.507	0.005	15.787	0.007	15.445	0.034	15.282	0.049	15.36	0.055	-	-	-	-	-	-	-	-
LB23_e	82.8684924	12.0782548	19.974	0.115	18.047	0.065	17.497	0.160	17.485	0.242	17.854	0.378	-	-	-	-	-	-	-	-
LB23_f	82.8684686	12.0757307	18.968	0.044	17.285	0.025	16.455	0.074	16.256	0.056	16.465	0.106	-	-	-	-	-	-	-	-
LB23_g	82.8733448	12.0814827	19.98	0.133	18.145	0.082	-	-	16.372	0.068	16.302	0.098	-	-	-	-	-	-	-	-
LB23_h	82.8712059	12.0724084	17.79	0.015	16.794	0.016	16.269	0.060	16.379	0.015	-	-	-	-	-	-	-	-	-	-
LB23_i	82.87796	12.080151	19.853	0.128	18.801	0.120	-	-	-	-	-	-	-	-	-	-	-	-	-	-
LB24_a	82.8498907	12.0748369	19.003	0.085	18.156	0.087	17.169	0.167	-	-	15.98	0.214	-	-	-	-	-	-	-	-
LB24_b	82.8529587	12.0784426	-	-	-	-	-	-	-	-	-	-	-	-	-	-	-	-	-	-
LB24_c	82.8439484	12.0800447	-	-	-	-	-	-	-	-	16.311	0.243	-	-	-	-	-	-	-	-
LB24_d	82.844633	12.075634	-	-	-	-	-	-	15.352	0.168	15.766	0.169	12.453	0.131	10.755	0.115	5.081*	0.047*	-	-
LB24_e	82.8468915	12.072453	17.642	0.014	16.528	0.013	16.109	0.054	15.531	0.088	15.646	0.089	13.181	0.17	-	-	4.804	0.048	-	-
LB24_f	82.8432544	12.0696761	18.872	0.036	17.900	0.040	17.282	0.113	16.945	0.124	16.816	0.148	-	-	-	-	-	-	-	-
LB24_g	82.8469663	12.08225	18.877	0.036	17.616	0.031	17.211	0.112	15.625	0.058	15.738	0.074	13.595	0.163	11.417	0.078	-	-	-	-

\*MIPS photometry might be affected by the inhomogeneous extended emission by the nebulosity.

Table 3. Photometric data for all counterparts.

B30-ID	RA(ind) (deg)	DEC(ind) (deg)	J	eJ	H CAHA/ $\Omega_{\text{M}}\alpha_{2000}$	eH	K	eK	I1	eI1	I2	eI2	I3	eI3	I4	eI4	M1	eM1
LB25_a	82.8354366	12.0851035	19.067	0.057	17.483	0.033	16.733	0.116	16.205	0.164	15.913	0.111	14.657	0.235	12.743	0.204	—	—
LB25_b	82.8303947	12.080038	16.418	0.005	15.301	0.004	14.882	0.019	14.708	0.022	14.676	0.022	13.274	0.131	11.878	0.132	—	—
LB25_c	82.8416812	12.0856044	15.671	0.003	14.726	0.003	14.248	0.012	13.933	0.029	13.875	0.019	13.274	0.131	11.878	0.132	—	—
LB25_d	82.8393083	12.0822474	18.642	0.064	17.719	0.062	16.959	0.150	16.420	0.404	16.658	0.377	14.595	0.237	12.047	0.214	—	—
LB25_e	82.8342835	12.0861197	20.514	0.188	18.529	0.112	—	—	16.227	0.189	16.056	0.105	13.462	0.201	—	—	—	—
LB25_f	82.8397243	12.0872619	—	—	19.294	0.108	—	—	16.200	0.132	16.76	0.173	13.326	0.173	12.047	0.214	—	—
LB26_a	82.8254809	12.0871155	18.147	0.023	16.650	0.016	16.056	0.050	15.462	0.034	15.415	0.038	14.74	0.164	—	—	—	—
LB26_b	82.82662	12.0823778	18.817	0.035	17.391	0.026	16.850	0.093	16.483	0.122	16.126	0.085	14.595	0.237	—	—	—	—
LB26_c	82.8216294	12.0792754	18.172	0.021	17.267	0.023	17.198	0.115	16.266	0.086	16.519	0.122	14.595	0.237	—	—	—	—
LB27_a	82.8100128	12.0964232	17.254	0.010	15.746	0.007	14.978	0.022	14.466	0.022	14.291	0.02	13.972	0.177	—	—	—	—
LB27_b	82.8064117	12.0876884	—	—	—	—	—	—	—	—	16.888	0.176	14.217	0.177	12.618	0.182	5.899*	0.045*
LB27_c	82.8052597	12.0901575	—	—	—	—	—	—	—	—	—	—	14.645	0.252	—	—	—	—
LB27_d	82.8040515	12.0845908	17.605	0.014	16.310	0.011	15.728	0.039	13.445	0.012	15.427	0.069	—	—	—	—	—	—
LB27_e	82.8021317	12.0896969	—	—	—	—	—	—	17.315	0.281	17.343	0.266	—	—	—	—	—	—
LB27_f	82.8020477	12.0958843	—	—	—	—	—	—	—	—	—	—	13.96	0.152	—	—	6.729*	0.148*
LB28_a	82.7841035	12.0847157	18.783	0.051	17.334	0.028	16.766	0.088	16.100	0.103	16.162	0.099	—	—	—	—	—	—
LB28_b	82.784874	12.0824242	—	—	—	—	—	—	—	—	—	—	13.96	0.141	12.028	0.127	6.737*	0.102*
LB28_c	82.7759399	12.0832968	—	—	—	—	—	—	—	—	—	—	—	—	12.227	0.149	6.769*	0.086*
LB28_d	82.7767727	12.085662	18.404	0.054	17.441	0.045	16.831	0.125	16.002	0.09	15.783	0.065	14.684	0.226	12.192	0.1	—	—
LB29_a	82.7869358	12.0624632	18.816	0.056	17.931	0.057	17.390	0.123	16.273	0.136	17.096	0.203	13.561	0.157	11.767	0.15	6.019*	0.09*
LB29_b	82.7845362	12.0612638	17.265	0.015	16.372	0.013	15.965	0.049	15.590	0.049	15.775	0.064	14.924	0.285	—	—	6.212*	0.174*
LB29_c	82.784803	12.067079	15.99	0.003	15.135	0.004	14.833	0.019	14.515	0.018	14.568	0.019	14.454	0.148	—	—	—	—
LB29_d	82.7912491	12.0631026	19.255	0.089	18.378	0.100	—	—	17.077	0.255	17.733	0.328	—	—	—	—	5.881*	0.064*
LB29_e	82.7846915	12.0644042	18.295	0.031	17.471	0.029	17.065	0.111	16.678	0.129	16.733	0.137	15.025	0.395	—	—	—	—
LB29_f	82.7910175	12.0668983	17.404	0.012	16.835	0.017	16.682	0.084	16.404	0.129	16.381	0.106	14.348	0.184	12.616	0.148	7.095*	0.129*
LB29_g	82.7809669	12.0645025	20.733	0.184	—	—	—	—	16.905	0.222	16.101	0.097	—	—	—	—	—	—
LB29_h	82.7803662	12.0659296	19.704	0.099	18.956	0.125	—	—	17.334	0.471	—	—	—	—	—	—	—	—
LB29_i	82.7808674	12.0589337	19.467	0.064	18.429	0.063	17.315	0.173	16.274	0.205	15.798	0.099	—	—	—	—	—	—
LB29_j	82.787634	12.0558409	16.786	0.008	—	—	—	—	15.8	0.083	15.796	0.066	—	—	—	—	—	—
LB30_a	82.8030423	12.0608531	16.725	0.006	15.626	0.006	15.108	0.023	14.801	0.027	14.978	0.031	14.11	0.207	12.752	0.232	—	—
LB30_b	82.801508	12.0605056	19.225	0.005	18.232	0.052	17.580	0.127	16.809	0.236	16.763	0.158	—	—	—	—	—	—
LB30_c	82.8016933	12.0635964	19.049	0.049	17.944	0.047	17.598	0.119	15.949	0.082	16.567	0.127	13.796	0.144	12.043	0.133	—	—
LB30_d	82.8019218	12.064775	20.633	0.113	19.762	0.126	—	—	—	—	—	—	—	—	—	—	—	—
LB30_e	82.808399	12.0577028	17.627	0.018	16.318	0.012	15.726	0.048	15.006	0.089	15.053	0.078	13.582	0.343	—	—	—	—
LB30_f	82.80728	12.061461	20.225	0.096	18.704	0.072	17.883	0.147	14.444	0.042	16.754	0.283	—	—	—	—	—	—
LB30_g	82.8103715	12.0592594	17.321	0.011	16.050	0.008	15.395	0.032	14.444	0.042	14.84	0.039	13.659	0.249	—	—	4.992	0.064
LB31_a	82.8140335	12.0624819	—	—	—	—	—	—	16.207	0.123	16.715	0.171	13.805	0.127	12.126	0.123	5.45*	0.064*
LB31_b	82.8175493	12.0635955	17.383	0.011	16.417	0.012	16.236	0.057	15.418	0.063	15.674	0.076	13.951	0.193	—	—	—	—
LB31_c	82.8158798	12.0589838	—	—	—	—	—	—	15.786	0.072	—	—	—	—	—	—	5.964	0.148
LB31_g	82.8131356	12.0558984	16.794	0.007	15.736	0.007	15.294	0.029	15.120	0.118	15.415	0.111	—	—	—	—	—	—
LB31_h	82.8147323	12.0538983	16.569	0.006	15.718	0.008	15.145	0.031	14.565	0.024	14.538	0.029	13.996	0.228	—	—	—	—
LB31_d	82.8149427	12.0656361	18.504	0.028	17.727	0.034	16.925	0.134	—	—	—	—	—	—	—	—	—	—
LB31_e	82.8187075	12.0627859	19.607	0.082	18.397	0.085	—	—	15.879	0.102	16.447	0.123	—	—	—	—	—	—
LB31_f	82.8188762	12.0560849	18.444	0.026	17.664	0.034	17.514	0.125	16.172	0.272	—	—	—	—	—	—	—	—
LB32_a	83.0513535	12.1654158	14.244	0.080	—	—	—	—	11.568	0.003	11.274	0.004	10.564	0.005	9.296	0.003	4.833	0.004
LB32_b	83.0526962	12.1675291	14.825	0.080	—	—	—	—	14.197	0.013	14.198	0.018	14.142	0.077	—	—	—	—
LB32_c	83.0493698	12.1644573	16.441	0.080	—	—	—	—	15.559	0.025	15.294	0.048	—	—	—	—	—	—
LB32_d	83.0553741	12.1640244	16.882	0.081	—	—	—	—	16.462	0.051	16.49	0.092	—	—	—	—	—	—
LB32_e	83.0466461	12.1649246	19.667	0.212	—	—	—	—	15.698	0.025	16.28	0.068	—	—	—	—	—	—
LB32_f	83.0588531	12.1689034	19.619	0.204	—	—	—	—	17.013	0.07	16.853	0.117	—	—	—	—	—	—
LB33_a	82.5546799	12.1460333	—	—	—	—	—	—	8.459	0.001	7.951	0.001	7.251	0.002	6.273	0.001	3.586	0.001

\* MIPS photometry might be affected by the inhomogeneous extended emission by the nebulosity.



**Table 4.** Photometric data for all counterparts, WISE data, release 2013.

B30-ID	RA(ind) (deg)	DEC(ind) (deg)	Dist (arcsec)	WISE ID	W1 <sup>1</sup>	eW1 <sup>1</sup>	W2 <sup>1</sup>	eW2 <sup>1</sup>	W3 <sup>1</sup>	eW3 <sup>1</sup>	W4 <sup>1</sup>	eW4 <sup>1</sup>	Cont <sup>2</sup>	Ext <sup>3</sup>	Qflag <sup>4</sup>
LB01_a	82.8103943	12.3743267	0.532	J053114.45+122227.6	11.725	0.024	11.698	0.023	>11.55	—	>8.299	—	0000	0	AAUU
LB02_d	82.8833542	12.3129959	0.355	J053132.02+121846.6	15.092	0.045	14.208	0.056	>11.47	—	>8.62	—	0000	0	AAUU
LB03_c	82.8828009	12.2905016	0.252	J053131.87+121725.5	14.769	0.042	14.743	0.071	>11.407	—	>8.283	—	0000	0	AAUU
LB03_g	82.8685852	12.2881695	0.113	J053128.45+121717.3	15.736	0.073	15.756	0.168	>12.019	—	>8.501	—	0h00	0	ABUU
LB03_i	82.877498	12.2929915	0.617	J053130.63+121735.1	15.06	0.041	15.037	0.091	>11.864	—	>8.87	—	0000	0	AAUU
LB05_a	82.872252	12.2411915	0.044	J053129.34+121428.2	10.653	0.023	10.539	0.021	10.706	0.124	>8.914	—	0000	0	AAUU
LB06_a	82.8729098	12.2138781	0.056	J053129.49+121249.9	13.035	0.025	12.703	0.026	>12.423	—	>8.955	—	0000	0	AAUU
LB06_d	82.8820695	12.2186419	1.716	J053131.79+121308.0	16.088	0.07	16.092	0.198	>11.959	—	>8.877	—	0000	0	ABUU
LB09_c	82.8233122	12.1910026	0.25	J053117.58+121237.3	14.995	0.044	14.512	0.06	(9.893)	(0.111)	(7.461)	(0.183)	dddd	0	AAAB
LB09_e	82.831573	12.1865735	1.117	J053119.64+121111.2	15.085	0.046	14.577	0.067	(8.601)	(0.064)	(6.404)	(0.071)	dddd	1	AAAA
LB10_a	82.7909414	12.1845672	0.375	J053109.82+121104.8	15.608	0.071	16.357	0.34	>12.027	—	>8.549	—	0000	0	ABUU
LB10_d	82.7906454	12.1805146	1.672	J053109.69+121051.2	15.448	0.064	16.37	0.298	>10.751	—	>8.241	—	0000	0	ABUU
LB10_h	82.7929218	12.1881804	0.156	J053110.29+121117.4	14.04	0.032	14.232	0.061	>12.254	—	>8.6	—	0000	0	AAUU
LB10_k	82.7826309	12.1854864	0.335	J053107.82+121107.4	14.639	0.041	14.617	0.068	9.495	0.083	7.275	0.323	0000	0	AAAB
LB12_a	82.8622399	12.1723873	0.099	J053126.93+121020.4	10.591	0.023	10.215	0.02	8.11	0.075	5.388	0.075	hhdh	1	AAAA
LB13_a	82.8314832	12.1614693	0.094	J053119.55+120941.2	12.376	0.025	12.112	0.023	>10.261	—	>7.201	—	hhdh	0	AAUU
LB14_a	82.8310571	12.1542772	0.276	J053120.51+120915.3	9.41	0.023	8.694	0.019	6.426	0.025	(4.563)	(0.048)	0hhh	0	AAAA
LB14_b	82.8355319	12.1547291	0.046	J053119.45+120858.6	12.209	0.025	11.492	0.021	9.407	0.234	6.204	0.178	hhdh	1	AAAB
LB15_a	82.8675875	12.1263543	0.351	J053128.22+120735.2	11.586	0.028	11.266	0.022	10.049	0.421	6.48	0.22	hhhh	1	AACB
LB16_a	82.8742455	12.1128436	0.683	J053129.84+120645.6	14.974	0.046	15.161	0.12	9.522	0.341	7.053	0.152	00hh	0	ABBB
LB16_b	82.8797155	12.112797	0.875	J053131.08+120646.5	15.417	0.068	16.376	0.353	>11.589	—	8.409	0.507	0hDH	0	AACB
LB16_c	82.881731	12.1191153	0.131	J053131.61+120708.6	14.966	0.068	14.845	0.09	9.47	0.062	>8.777	—	00hH	0	ABBU
LB17_a	82.7896196	12.1125454	0.876	J053109.56+120645.4	(15.622)	(0.086)	(16.126)	(0.23)	(10.496)	(0.379)	(7.414)	(0.185)	00hd	0	AAAB
LB17_b	82.7895729	12.1169664	0.288	J053109.51+120701.0	15.257	0.066	15.584	0.145	10.417	0.35	7.424	0.163	0000	0	ABBB
LB17_d	82.7934952	12.1105013	1.544	J053110.34+120637.0	16.044	0.084	16.114	0.222	10.104	0.217	7.146	0.15	0000	0	ABBB
LB18_a	82.893931	12.1086094	0.346	J053134.54+120631.3	10.521	0.023	10.157	0.02	10.248	0.131	>8.569	—	0000	0	AAUU
LB19_a	82.8658453	12.0919505	0.218	J053127.81+120530.9	11.185	0.024	9.415	0.02	5.269	0.017	2.039	0.017	0000	1	AAAA
LB19_d	82.8733996	12.0925052	0.159	J053129.61+120532.8	13.104	0.027	11.872	0.023	7.57	0.035	4.453	0.053	0hdd	1	AAAA
LB19_h	82.8668776	12.0875591	0.608	J053128.05+120514.6	14.65	0.071	14.64	0.103	8.878	0.123	4.351	0.04	0hdd	1	AABA

<sup>1</sup> Values in parenthesis have not been used.<sup>2</sup> Contamination and confusion flag, one per band. 0 for OK, any other value indicate a problem. See source catalog for details (Cutri et al. 2013).<sup>3</sup> Extended source flag. 0 for OK, any other value indicate a problem. See source catalog for details.<sup>4</sup> Photometric quality flag. A, B, C for S/N >10, in the range 3-10 and <3. U stand for upper limit.

**Table 4.** Photometric data for all counterparts, WISE data, release 2013.

B30-ID	RA(ind) (deg)	DEC(ind) (deg)	Dist (arcsec)	WISE ID	W1 <sup>1</sup>	eW1 <sup>1</sup>	W2 <sup>1</sup>	eW2 <sup>1</sup>	W3 <sup>1</sup>	eW3 <sup>1</sup>	W4 <sup>1</sup>	eW4 <sup>1</sup>	Cont <sup>2</sup>	Ext <sup>3</sup>	Qflag <sup>4</sup>
LB20_a	82.8508555	12.0902626	0.147	J053124.19+120525.0	13.14	0.063	13.0	0.055	8.34	0.233	6.103	0.348	00dh	0	AABB
LB20_c	82.8402513	12.0966039	0.251	J053121.66+120547.5	9.854	0.037	9.866	0.038	9.261	0.253	>8.081	–	hit0h	0	AABU
LB20_d	82.8394462	12.0955432	0.23	J053121.47+120543.7	10.136	0.044	10.085	0.044	8.984	0.197	6.766	0.168	dd0h	0	AABB
LB21_a	82.8988495	12.0846224	1.509	J053135.62+120504.0	15.862	0.098	16.098	0.244	9.623	0.146	6.693	0.215	0000	0	ABBB
LB21_b	82.899437	12.0812626	2.197	J053135.81+120450.4	15.428	0.072	15.144	0.106	>11.119	–	>7.632	–	0000	0	AABU
LB21_c	82.90199	12.081975	0.278	J053136.47+120455.3	15.951	0.129	15.603	0.157	>10.397	–	(7.515)	0.493	d000	0	BBUC
LB21_j	82.8977103	12.0892541	0.862	J053135.40+120521.7	16.246	0.107	16.523	0.347	9.528	0.058	6.924	0.134	0000	0	ABAB
LB22_b	82.879810	12.070272	2.155	J053130.87+120413.6	15.538	0.053	15.573	0.131	9.225	0.202	6.249	0.193	hit0h	0	ABBB
LB22_c	82.8842633	12.0692825	3.469	J053132.00+120410.7	15.068	0.042	15.006	0.079	9.892	0.415	6.434	0.287	hit0d	0	AACB
LB22_d	82.8865516	12.0684093	0.983	J053132.70+120406.3	15.118	0.044	15.053	0.082	>9.323	–	7.129	0.476	hit0d	0	AAUC
LB23_a	82.8733007	12.0754017	1.938	J053129.66+120429.8	16.477	0.123	>17.025	–	>10.929	–	7.616	0.357	000H	0	BUUC
LB23_b	82.8740083	12.0797118	0.372	J053129.76+120447.5	15.412	0.057	15.807	0.176	10.851	0.48	7.43	0.271	00hH	0	ABCB
LB23_c	82.8761053	12.0778312	2.299	J053130.31+120438.0	16.259	0.114	>17.089	–	10.073	0.232	6.774	0.149	000d	0	BUBB
LB23_d	82.8687196	12.0718283	0.696	J053128.52+120418.0	15.497	0.057	>17.053	–	>11.429	–	>8.104	–	0hdH	0	AUUU
LB23_h	82.8712059	12.0724084	0.669	J053129.13+120420.3	15.764	0.059	>16.636	–	>10.208	–	>7.049	–	0h0h	0	AUUU
LB24_f	82.844633	12.075634	0.659	J053122.40+120411.3	14.561	0.04	15.886	0.245	8.705	0.04	5.64	0.09	000d	1	ABAA
LB25_b	82.8303947	12.080038	0.285	J053119.30+120447.8	14.362	0.045	14.719	0.077	10.049	0.312	6.299	0.107	0000	0	ABAA
LB25_c	82.8416812	12.0856044	0.258	J053121.99+120507.9	13.222	0.052	13.078	0.05	7.605	0.087	5.207	0.099	000h	1	AAAA
LB26_a	82.8254809	12.0871155	0.754	J053118.15+120513.2	15.576	0.08	15.729	0.185	>10.754	–	>7.74	–	0000	0	ABUU
LB27_a	82.8100128	12.0964232	0.396	J053114.42+120546.8	14.307	0.04	14.204	0.058	9.94	0.205	6.935	0.151	0000	0	AABB
LB27_b	82.8064117	12.0876884	0.865	J053113.53+120514.8	14.952	0.054	14.959	0.087	10.135	0.425	>6.759	–	0000	0	AACU
LB27_c	82.8052597	12.0901575	2.263	J053113.27+120522.3	15.15	0.061	15.479	0.139	10.078	0.415	7.363	0.348	0000	0	ABCB
LB27_d	82.8040515	12.0845908	1.893	J053112.99+120506.3	15.074	0.055	15.05	0.094	>10.436	–	>8.118	–	0000	0	AAUU
LB27_f	82.8020477	12.0958843	0.956	J053112.49+120544.2	15.127	0.061	15.609	0.16	9.104	0.097	6.487	0.112	0000	0	ABAB
LB28_b	82.784874	12.0824242	1.02	J053108.43+120456.6	15.565	0.08	15.295	0.115	9.446	0.103	7.553	0.2	0000	0	ABAB
LB28_c	82.7759399	12.0832968	1.987	J053106.16+120501.6	15.726	0.104	15.422	0.13	9.528	0.148	7.648	0.245	0000	0	ABBB
LB29_b	82.7845362	12.0612638	0.397	J053108.31+120340.5	14.17	0.034	14.606	0.098	9.186	0.043	6.669	0.299	0000	1	AAAB
LB29_c	82.784803	12.067079	0.546	J053108.35+120400.9	14.388	0.177	14.483	0.171	>10.029	–	>5.85	–	0000	0	BBUU
LB29_d	82.7912491	12.0631026	1.46	J053109.99+120347.6	14.194	0.035	14.819	0.201	8.891	0.032	6.005	0.116	0000	1	ABAB
LB30_a	82.8030423	12.0608531	0.641	J053112.74+120339.6	13.913	0.034	14.364	0.136	9.68	0.078	6.239	0.089	0000	1	ABAA
LB30_g	82.8103715	12.0592594	1.782	J053114.48+120335.1	13.491	0.031	13.617	0.056	7.786	0.024	4.973	0.038	0000	1	AAAA
LB31_b	82.8175493	12.0635955	1.118	J053116.20+120347.8	14.086	0.083	14.231	0.094	8.228	0.04	5.146	0.071	0000	1	AAAA
LB31_c	82.8158798	12.0589838	0.857	J053115.84+120333.0	13.806	0.065	14.235	0.089	8.007	0.033	5.34	0.097	0000	1	AAAA
LB32_a	83.0513535	12.1654158	0.264	J053212.30+120955.6	12.049	0.022	11.299	0.021	8.437	0.025	4.976	0.03	0000	0	AAAA
LB32_d	83.0553741	12.1640244	1.641	J053213.37+120951.5	16.664	0.166	16.737	0.516	>11.366	–	7.272	0.12	0000	0	BCUB
LB32_f	83.0588531	12.1689034	0.594	J053214.08+121007.9	17.336	0.197	>16.426	–	>11.993	–	8.852	0.464	0000	0	BUUC
LB33_a	82.5546799	12.1460333	0.183	J053013.12+120845.8	8.578	0.023	7.594	0.019	4.929	0.014	2.93	0.023	0000	0	AAAA

<sup>1</sup> Values in parenthesis have not been used.<sup>2</sup> Contamination and confusion flag, one per band. 0 for OK, any other value indicate a problem. See source catalog for details (Cutri et al. 2013).<sup>3</sup> Extended source flag. 0 for OK, any other value indicate a problem. See source catalog for details.<sup>4</sup> Photometric quality flag. A, B, C for S/N >10, in the range 3-10 and <3. U stand for upper limit.

Table 5. Optical and near-IR photometry from 2MASS.

B30-ID	RA (deg)	DEC (deg)	V <sup>1</sup>	R <sup>1</sup>	I <sup>1</sup>	i <sup>2</sup>	err_i <sup>2</sup>	i <sup>2</sup>	err_i <sup>2</sup>	J2M	e_J	H2M	e_H	K2M	e_K
LB01_a	82.8103943	12.3743267	15.968	14.963	13.917	15.178	0.035	14.073	0.033	12.891	0.029	12.257	0.035	12.047	0.031
LB03_c	82.8828009	12.2905016	-	-	-	21.672	0.367	19.768	0.167	16.56	0.127	15.423	0.091	14.784	0.105
LB03_g	82.8685852	12.2881695	-	-	-	21.468	0.305	19.761	0.166	16.871	0.167	16.458	0.225	15.819	0.261
LB05_a	82.872252	12.2411915	15.114	14.059	12.835	14.311	0.031	12.884	0.03	11.596	0.02	11.015	0.021	10.775	0.019
LB05_b	82.8752217	12.2423194	-	-	-	20.574	0.14	18.727	0.068	15.685	0.067	14.262	0.042	13.542	0.046
LB06_a	82.8729098	12.2138781	-	-	-	22.248	0.705	20.155	0.293	16.51	0.124	14.522	0.042	13.522	0.037
LB08_b	82.8490389	12.195165	-	-	-	22.667	1.04	20.926	0.613	-	-	-	-	-	-
LB10_a	82.7909414	12.1845672	-	-	-	22.091	0.61	20.213	0.31	-	-	-	-	-	-
LB10_b	82.7897077	12.1863344	-	-	-	22.64	1.014	20.864	0.578	-	-	-	-	-	-
LB10_d	82.7906454	12.1805146	-	-	-	20.544	0.153	19.137	0.113	-	-	-	-	-	-
LB10_f	82.7940554	12.1827567	-	-	-	22.595	0.973	20.52	0.416	-	-	-	-	-	-
LB10_h	82.7929218	12.1881804	19.43	17.961	16.956	18.137	0.311	17.125	0.241	15.239	0.045	14.585	0.051	14.206	0.07
LB10_i	82.795761	12.1864233	-	-	-	23.063	1.503	21.497	1.062	-	-	-	-	-	-
LB10_j	82.792862	12.1905084	-	-	-	22.29	0.733	20.845	0.567	-	-	-	-	-	-
LB10_k	82.7826309	12.1854864	-	-	-	19.316	0.068	18.083	0.05	16.13	0.086	15.375	0.096	15.154	0.154
LB11_d	82.7977769	12.1732308	-	-	-	22.178	0.661	20.745	0.515	-	-	-	-	-	-
LB12_a	82.8622399	12.1723873	-	-	-	17.023	0.113	14.61	0.039	11.956	0.022	11.249	0.02	10.887	0.018
LB13_a	82.8314832	12.1614693	18.602	17.054	15.227	17.699	0.051	15.558	0.03	13.378	0.023	12.766	0.026	12.451	0.023
LB14_a	82.8310571	12.1542772	17.561	16.016	14.486	16.116	0.055	14.584	0.038	11.987	0.022	10.776	0.023	10.091	0.018
LB14_b	82.8313354	12.1495811	-	-	-	21.548	0.37	19.536	0.163	16.645	0.132	14.735	0.059	13.135	0.036
LB14_c	82.8355319	12.1547291	17.782	16.455	14.653	17.154	0.05	15.003	0.03	12.72	0.023	12.096	0.024	11.797	0.02
LB14_e	82.8256866	12.1508073	-	-	-	20.745	0.181	19.911	0.233	-	-	-	-	-	-
LB14_j	82.8302892	12.1454723	-	-	-	20.928	0.212	19.734	0.197	-	-	-	-	-	-
LB15_a	82.8675875	12.1263543	16.162	15.093	13.946	15.093	0.0	13.946	0.0	12.718	0.02	12.006	0.021	11.818	0.021
LB15_b	82.8619391	12.1178684	-	-	-	21.266	0.286	20.188	0.302	-	-	-	-	-	-
LB16_c	82.881731	12.1191153	-	-	-	22.927	1.324	21.079	0.711	17.39	0.255	16.046	0.153	15.547	0.222
LB17_g	82.7840129	12.110386	-	-	-	22.869	1.255	20.835	0.562	-	-	-	-	-	-
LB18_a	82.893931	12.1086094	-	-	-	20.148	0.112	17.533	0.038	13.45	0.026	11.792	0.024	11.027	0.023
LB19_a	82.8658453	12.0919505	-	-	-	95.001	0.0	91.001	0.0	16.319	0.0	14.596	0.08	12.763	0.04
LB19_b	82.8676553	12.0917727	-	-	-	19.325	0.949	16.971	0.209	14.139	0.038	13.407	0.078	12.996	0.075
LB19_c	82.8686592	12.0905224	17.473	16.266	14.906	16.567	0.077	15.236	0.052	13.764	0.04	13.159	0.035	12.921	0.038
LB19_d	82.8733996	12.0925052	-	-	-	95.001	0.0	91.001	0.155	15.903	0.079	14.548	0.054	13.838	0.055
LB19_e	82.8614809	12.0885397	-	-	-	22.447	0.848	21.522	1.089	-	-	-	-	-	-
LB20_a	82.8508555	12.0902626	-	-	-	18.867	0.617	17.491	0.335	15.144	0.057	14.122	0.049	13.682	0.058
LB20_c	82.8402513	12.0966039	13.76	12.809	11.842	13.132	0.03	12.273	0.03	10.946	0.045	10.24	0.049	10.037	0.049
LB20_d	82.8394462	12.0955432	-	-	-	14.485	0.032	13.146	0.031	11.386	0.029	10.519	0.025	10.239	0.027
LB20_e	82.8394127	12.0930814	-	-	-	20.823	0.193	19.423	0.147	16.629	0.217	14.801	0.0	14.81	0.164

<sup>1</sup> Dolan & Mathieu (2001).<sup>2</sup> INT/WFC, this work.

Table 5. Optical and near-IR photometry from 2MASS.

B30-ID	RA (deg)	DEC (deg)	V <sup>1</sup>	R <sup>1</sup>	I <sup>1</sup>	i <sup>2</sup>	err_i <sup>2</sup>	i <sup>2</sup>	err_i <sup>2</sup>	J2M	e_J	H2M	e_H	K2M	e_K
LB21_e	82.906055	12.0828322	-	-	-	22.648	1.022	21.406	0.973	-	-	-	-	-	-
LB22_d	82.886516	12.0684093	-	-	-	21.039	0.234	19.358	0.139	-	-	-	-	-	-
LB22_f	82.885015	12.0706474	-	-	-	23.115	1.577	20.607	0.452	-	-	-	-	-	-
LB22_j	82.879455	12.0659626	-	-	-	21.672	0.415	20.296	0.335	-	-	-	-	-	-
LB23_d	82.8687196	12.0718283	-	-	-	19.246	0.066	18.105	0.05	16.587	0.214	15.539	0.149	16.019	0.0
LB23_h	82.8712059	12.0724084	-	-	-	21.971	0.546	20.002	0.253	-	-	-	-	-	-
LB24_e	82.8468915	12.072453	-	-	-	21.335	0.305	20.023	0.258	-	-	-	-	-	-
LB25_b	82.8303947	12.080038	-	-	-	20.556	0.154	18.78	0.083	16.386	0.175	15.095	0.113	14.672	0.121
LB25_c	82.8416812	12.0856044	-	-	-	19.271	0.902	18.147	0.609	15.655	0.089	14.688	0.07	14.316	0.091
LB26_c	82.8216294	12.0792754	-	-	-	21.311	0.298	20.01	0.255	-	-	-	-	-	-
LB27_a	82.8100128	12.0964232	-	-	-	22.359	0.782	20.624	0.459	16.856	0.0	15.641	0.181	14.63	0.117
LB27_d	82.8040515	12.0845908	-	-	-	22.676	1.049	20.396	0.369	-	-	-	-	-	-
LB29_a	82.7869358	12.0624632	-	-	-	22.46	0.858	20.799	0.543	-	-	-	-	-	-
LB29_c	82.784803	12.067079	-	-	-	18.783	0.57	17.883	0.479	15.99	0.084	15.147	0.071	14.794	0.112
LB29_d	82.7912491	12.0631026	-	-	-	22.406	0.816	21.192	0.792	-	-	-	-	-	-
LB29_e	82.7846915	12.0644042	-	-	-	21.431	0.333	19.985	0.249	-	-	-	-	-	-
LB29_f	82.7910175	12.0668983	-	-	-	19.744	0.085	18.725	0.079	-	-	-	-	-	-
LB29_j	82.787634	12.0558409	-	-	-	18.821	0.058	18.055	0.049	17.078	0.195	16.429	0.223	15.654	0.236
LB30_a	82.8030423	12.0608531	-	-	-	21.18	0.265	19.31	0.133	16.703	0.143	15.399	0.094	15.285	0.176
LB30_c	82.8016933	12.0635964	-	-	-	22.607	0.984	21.543	1.111	-	-	-	-	-	-
LB31_b	82.8175493	12.0635955	-	-	-	20.855	0.199	19.373	0.141	-	-	-	-	-	-
LB30_f	82.80728	12.061461	-	-	-	22.812	1.191	21.714	1.309	-	-	-	-	-	-
LB31_g	82.8131356	12.0558984	-	-	-	20.609	0.161	19.129	0.113	16.827	0.171	15.88	0.157	15.415	0.196
LB31_h	82.8147323	12.0538983	-	-	-	21.231	0.278	18.916	0.093	16.295	0.182	15.855	0.202	15.163	0.195
LB31_d	82.8149427	12.0656361	-	-	-	21.664	0.412	20.103	0.279	-	-	-	-	-	-
LB31_f	82.8188762	12.0560849	-	-	-	20.661	0.168	19.817	0.213	-	-	-	-	-	-
LB32_a	83.0513535	12.1654158	16.228	15.63	15.109	15.679	0.043	15.179	0.05	14.217	0.03	13.427	0.031	12.653	0.028
LB32_b	83.0526962	12.1675291	16.294	15.794	15.307	15.816	0.046	15.408	0.058	14.817	0.041	14.374	0.054	14.257	0.082
LB32_c	83.0493698	12.1644573	-	-	-	17.362	0.152	17.022	0.219	16.514	0.128	15.764	0.143	15.776	0.251
LB32_d	83.0553741	12.1640244	-	-	-	17.859	0.241	17.509	0.34	-	-	-	-	-	-
LB33_a	82.5546799	12.1460333	13.836	13.055	12.282	13.055	0.0	12.282	0.0	10.954	0.022	10.12	0.023	9.557	0.018

<sup>1</sup> Dolan & Mathieu (2001).<sup>2</sup> INT/WFC, this work.

**Table 6.** Akari photometry for our APEX/LABOCA sources.

B30-ID	RA (deg)	DEC (deg)	S09	e_S09	S18	e_S18	S65	e_S65	S90	e_S90	S140	e_S140	S160	e_S160	Name/Akari
08_a	82.8479608	12.1911092	–	–	–	–	5.865	0.923	11.2	0.245	25.0	3.92	29.19	9.29	0531239+121115
14_a	82.8310571	12.1542772	0.095	0.0111	–	–	–	–	–	–	–	–	–	–	0531194+120915
19_a <sup>a</sup>	82.8658453	12.0919505	–	–	0.845	0.0319	–	–	–	–	–	–	–	–	0531278+120531
25_c	82.8416812	12.0856044	–	–	–	–	2.5	1.21	9.587	0.682	11.14	4.37	18.12	10.1	531219+120513
32_a <sup>b</sup>	83.0513535	12.1654158	–	–	–	–	1.201	0.0	1.124	0.0628	2.112	0.399	–	–	0532122+120959
33_a	82.5546799	12.1460333	0.242	0.0152	0.28	0.00562	–	–	–	–	–	–	–	–	0530131+120845

<sup>a</sup> IRAS05286+1203, RA=82.8671, DEC=+12.0899, [12]=7.79e-01±0.0779 Jy, [25]=1.91e+00±0.2101 Jy, [60]=9.35e+00±1.7765 Jy, [100]=7.04e+01±14.784 Jy.  
<sup>b</sup> IRAS05293+1207, RA=83.0450, DEC=+12.1629, [12]<2.50e-01 Jy, [25]<2.71e-01 Jy, [60]=1.15e+00±0.1725 Jy, [100]<2.66e+01 Jy.



**Table 7.** Properties and memberships criteria for all counterparts within the APEX/LABOCA beam (continuation).

B30-ID	RA (deg)	DEC (deg)	Teff (K)	Lbol ( $L_{\odot}$ )		Av (mag)	Teff (K)	eLbol ( $L_{\odot}$ )		Membership <sup>1</sup> HR & CM diagrams	Final <sup>2</sup>	Npoints <sup>3</sup>	Class <sup>4</sup>	IRAC <sup>5</sup> slope	IR excess <sup>6</sup>
				Lbol ( $L_{\odot}$ )	eLbol ( $L_{\odot}$ )			Lbol ( $L_{\odot}$ )	eLbol ( $L_{\odot}$ )						
LB09_a	82.8274595	12.1912422	700	8.0E-4	0.5E-4	-	-	-	-	Y-Y-Y-Y-Y-Y	Y	3 5	-	-	-
LB09_b	82.8286146	12.192915	1500	3.0E-4	0.5E-4	-	-	-	-	Y--Y-Y--	Y?	3 3	-	-	-
LB09_c	82.8233122	12.1910026	1500	0.0034	1.0E-4	-	-	-	-	Y-Y-Y-Y-Y-Y	Y	3 6	-	-	-
LB09_d	82.8244826	12.1877228	1500	7.0E-4	0.5E-4	-	-	-	-	Y-Y-Y-Y-N-N	N?	3 5	-	-	-
LB09_e	82.831573	12.1865735	700	0.0035	1.0E-4	-	-	-	-	Y-Y-Y-Y-Y-Y	Y	3 5	-	-	-
LB09_f	82.8338717	12.1928557	1700	5.0E-4	0.5E-4	7.875	5100	0.0052	1.0E-4	Y-N-Y-N-Y-N	N	5 5	-	-	-
LB09_g	82.8307994	12.1940775	1500	2.0E-4	0.5E-4	9.975	3600	0.0015	1.0E-4	Y-N-Y-Y-Y--	Y?	4 4	-	-	-
LB09_h	82.8265858	12.1960763	2500	3.0E-4	0.5E-4	-	-	-	-	N--N-N--	N	3 3	-	-	-
LB10_a	82.7909414	12.1845672	3700	0.0023	1.0E-4	4.2	4600	0.0078	1.0E-4	N-N-Y-N-Y-N	Y?	4 6	-	-	-
LB10_b	82.7897077	12.1863344	3700	8.0E-4	0.5E-4	-	-	-	-	N-Y-Y-N-Y-Y?	N	3 5	-	-	-
LB10_c	82.789993	12.1816228	700	0.0030	1.0E-4	-	-	-	-	Y-Y-Y-Y-Y-Y	Y	3 5	-	-	-
LB10_d	82.7906454	12.1805146	3500	0.0033	1.0E-4	-	-	-	-	N-Y-N-Y-N-Y?	N	3 7	-	-	-
LB10_e	82.7929654	12.1829769	700	0.0014	1.0E-4	-	-	-	-	Y-Y-Y-Y-Y-Y	Y	3 5	-	-	-
LB10_f	82.7940554	12.1827567	700	0.0046	1.0E-4	-	-	-	-	Y-Y-Y-Y-N-N	N	3 5	-	-	-
LB10_g	82.7954744	12.181736	700	0.0030	1.0E-4	-	-	-	-	Y-Y-Y-Y-Y-Y?	Y	3 5	-	-	-
LB10_h	82.7929218	12.1881804	3100	0.0195	3.0E-4	4.725	7000	0.4199	3.0E-4	Y-N-Y-Y-Y-Y?	Y?	8 14	-	-	-
LB10_i	82.795761	12.1864233	1600	0.0021	1.0E-4	-	-	-	-	Y-Y-Y-Y-Y-Y	Y?	3 7	-	-	-
LB10_j	82.792862	12.1905084	3700	6.0E-4	0.5E-4	-	-	-	-	N-N-N-N--	N	3 4	-	-	-
LB10_k	82.7826309	12.1854864	2100	0.0068	2.0E-4	4.725	6400	0.0597	2.0E-4	Y-N-Y-Y-N-Y-N	Y?	5 10	-	-	-
LB10_l	82.7848876	12.1790492	3700	3.0E-4	0.5E-4	-	-	-	-	N-N-N--	N	3 3	-	-	-
LB10_m	82.7873969	12.1780491	1800	3.0E-4	0.5E-4	-	-	-	-	Y-Y-Y-Y-Y--	Y	3 4	-	-	-
LB11_a	82.7919693	12.1718931	-	-	-	-	-	-	-	Y--Y--Y--	-	-	-	-	-
LB11_b	82.7991141	12.1765574	600	3.0E-4	0.5E-4	-	-	-	-	Y-Y-Y--	Y?	3 3	-	-	-
LB11_c	82.7959332	12.1745673	600	6.0E-4	0.5E-4	-	-	-	-	Y--Y--Y--	Y?	3 3	-	-	-
LB11_d	82.7977769	12.1732308	3600	7.0E-4	0.5E-4	2.625	4600	0.0017	1.0E-4	N-N-N-N--	N	4 4	-	-	-
LB11_e	82.7945144	12.170888	1600	3.0E-4	0.5E-4	-	-	-	-	Y-Y-Y--	Y?	3 3	-	-	-
LB11_f	82.7871577	12.1760213	3700	6.0E-4	0.5E-4	2.1	4000	0.0010	1.0E-4	N-N-Y?N-N-Y?	N	4 5	-	-	-
LB12_a	82.8622399	12.1723873	2200	0.3283	0.0025	6.825	8000	7.911	0.0025	Y-Y-Y-Y-Y--	Y	5 11	III	AAA	Y-T-T-N-N?
LB12_b	82.860249	12.1732605	-	-	-	-	-	-	-	Y--Y--Y--	Y?	-	-	-	-
LB12_c	82.8616483	12.1773707	-	-	-	-	-	-	-	Y--Y--Y--	Y	-	I	T-T-T	N?-N-N-N-G
LB12_d	82.8578644	12.1650391	-	-	-	-	-	-	-	Y--Y--Y--	Y	-	-	-	-
LB12_e	82.8602536	12.1663629	1100	8.0E-4	0.5E-4	-	-	-	-	Y--Y--Y--	Y	3 4	-	-	-
LB12_f	82.8658218	12.169281	-	-	-	-	-	-	-	Y--Y--Y--	-	-	-	-	-
LB12_g	82.8675273	12.1702059	1300	0.0039	1.0E-4	-	-	-	-	Y-Y-Y-Y-Y-Y	Y	3 6	-	-	-
LB12_h	82.8669147	12.1677647	700	0.0012	1.0E-4	-	-	-	-	Y--Y--Y--	Y?	3 4	-	-	-
LB12_i	82.8647003	12.1651821	-	-	-	-	-	-	-	Y--Y--Y--	-	-	-	-	-
LB12_j	82.8687731	12.1739057	1500	0.0012	1.0E-4	-	-	-	-	Y-Y-Y-Y-Y-Y	Y	3 6	-	-	-
LB12_k	82.8610365	12.1758133	-	-	-	-	-	-	-	Y--Y--Y--	Y?	-	-	-	-
LB12_l	82.86409	12.1714582	-	-	-	-	-	-	-	Y--Y--Y--	-	-	-	-	-
LB13_a	82.8314832	12.1614693	2800	0.0997	0.0017	0.0	2900	1.0535	0.0017	Y-Y-Y-Y-Y-Y	Y	9 15	III	NNN	Y?-N-N-N?
LB13_b	82.8248788	12.1638624	1600	3.0E-4	0.5E-4	-	-	-	-	Y-Y-Y-Y-Y?	Y	3 4	-	-	-

<sup>1</sup> Membership criteria based on the location on Herzprung-Russell, optical-IR Color-Color and Color-Magnitude Diagrams: HRD(Av=0.322), HRD(Av variable), (J, J-I), (J, J-I), (J, J-I), (H, H-I), (H, H-I), (K, K-I), (K, K-I), (K, K-I).

<sup>2</sup> Final membership assessment.

<sup>3</sup> Number of photometric points on the SED: Fit and total.

<sup>4</sup> Evolutionary class based on a Spitzer/IRAC (I1 - I2, I3 - I4) CCD.

<sup>5</sup> IRAC slope.

<sup>6</sup> IR excess based on optical, near-IR and Spitzer Color-Color and Color-Magnitude Diagrams: (I1, I1 - I4), (H - K, K - M1), (I1 - I4, I4 - M1), (I2 - I3, I3 - I4), (I1 - I3, I3 - I4), (I2, I2 - I4).

**Table 7.** Properties and memberships criteria for all counterparts within the APEX/LABOCA beam (continuation).

B30-ID	RA (deg)	DEC (deg)	Teff (K)	Lbol ( $L_{\odot}$ )		Av (mag)	Teff (K)	eLbol ( $L_{\odot}$ )		Membership <sup>1</sup> HR & CM diagrams	Final <sup>2</sup>	Npoints <sup>3</sup>	Class <sup>4</sup>	IRAC <sup>5</sup> slope	IR excess <sup>6</sup>
				Lbol ( $L_{\odot}$ )	eLbol ( $L_{\odot}$ )			Lbol ( $L_{\odot}$ )	eLbol ( $L_{\odot}$ )						
LB14_a	82.8310571	12.1542772	1600	0.6658	0.0042	6.3	5500	6.8753	0.0042	Y Y Y Y Y Y --	Y	8 16	II	T T T	Y Y Y N N Y
LB14_b	82.8313354	12.1495811	1100	0.051	3.0E-4	2.1	1700	0.1135	3.0E-4	Y Y Y Y Y Y Y	Y	6 13	II	T T T	Y Y Y N N Y
LB14_c	82.8355319	12.1547291	2900	0.1839	0.0021	0.0	2900	1.923	0.0021	Y Y Y Y Y Y Y	Y	8 15	III	N A N	Y ? - - N N ?
LB14_d	82.8285637	12.1530748	1300	0.0013	1.0E-4	-	-	-	-	Y - Y Y Y - -	Y	3 4	-	-	- - - - -
LB14_e	82.8256866	12.1508073	2900	8.0E-4	0.5E-4	-	-	-	-	N - N Y N Y N Y	N	3 5	-	-	- - - - -
LB14_f	82.8350675	12.1520706	700	7.0E-4	0.5E-4	-	-	-	-	Y - - Y - -	Y ?	3 3	-	-	- - - - -
LB14_g	82.835154	12.1492848	3700	0.0014	1.0E-4	5.25	4200	0.0050	1.0E-4	N N Y Y ? Y ? N N N	N	5 5	-	-	- - - - -
LB14_h	82.8313458	12.147645	1300	8.0E-4	0.5E-4	-	-	-	-	Y - Y Y Y - -	Y	3 4	-	-	- - - - -
LB14_i	82.8294198	12.1463334	1900	4.0E-4	0.5E-4	-	-	-	-	Y - Y - Y - -	Y ?	3 3	-	-	- - - - -
LB14_j	82.8302892	12.1454723	-	-	-	-	-	-	-	- - Y Y - - Y Y	N	-	-	-	- - - - -
LB14_k	82.8271388	12.1468297	-	-	-	-	-	-	-	- - - - -	-	-	-	-	- - - - -
LB15_a	82.8675875	12.1263543	2900	0.2189	0.0088	3.15	6200	1.2524	0.0088	Y N Y Y Y Y Y	Y ?	9 15	III	N N N	Y ? - - N N ?
LB15_b	82.8619391	12.1178684	3600	0.0023	1.0E-4	5.25	4900	0.0112	1.0E-4	N N Y Y ? Y N N	N	5 5	-	-	- - - - -
LB15_c	82.8632264	12.1307359	4200	7.0E-4	0.5E-4	-	-	-	-	N - N N N N - -	N	3 4	-	-	- - - - -
LB15_d	82.8631076	12.1172072	-	-	-	-	-	-	-	- - - - -	-	-	-	-	- - - - -
LB16_a	82.8742455	12.1128436	1500	0.0042	1.0E-4	-	-	-	-	Y - Y Y Y Y N	Y ?	3 9	-	-	- - - - -
LB16_b	82.8797155	12.112797	700	0.0042	1.0E-4	-	-	-	-	Y - Y Y Y Y N Y	N ?	3 6	-	-	- - - - -
LB16_c	82.881731	12.1191153	700	0.0071	2.0E-4	4.725	2000	0.0103	2.0E-4	Y Y Y Y Y Y N	N	5 9	-	-	- - - - -
LB16_d	82.8767443	12.1161898	-	-	-	-	-	-	-	- - - - N - -	N ?	-	-	-	- - - - -
LB16_e	82.87578313	12.1217787	-	-	-	-	-	-	-	- - - Y - -	-	-	-	-	- - - - -
LB16_f	82.8718226	12.1202306	-	-	-	-	-	-	-	- - - - -	-	-	-	-	- - - - -
LB17_a	82.7896196	12.1125454	2000	0.0013	1.0E-4	7.875	5500	0.0171	1.0E-4	Y N Y Y Y N N	Y ?	4 8	-	-	- - - - -
LB17_b	82.7895729	12.1169664	700	0.0059	1.0E-4	-	-	-	-	Y - Y Y Y Y ? Y ?	Y	3 8	-	-	- - - - -
LB17_c	82.7956702	12.1080471	-	-	-	-	-	-	-	- - - - -	-	-	-	-	- - - - -
LB17_d	82.7934952	12.1105013	-	-	-	-	-	-	-	- - - - -	-	-	-	-	- - - - -
LB17_e	82.7967072	12.1139727	-	-	-	-	-	-	-	- - - - -	-	-	-	-	- - - - -
LB17_f	82.7934146	12.116857	2000	3.0E-4	0.5E-4	9.975	14000	0.0887	1.0E-4	Y ? N Y ? Y Y ? - -	Y ?	4 4	-	-	- - - - -
LB17_g	82.7840129	12.110386	700	0.0027	1.0E-4	-	-	-	-	Y - Y N Y ? N N	N	3 5	-	-	- - - - -
LB18_a	82.893931	12.1086094	1500	0.3083	0.0014	7.875	3000	0.5961	0.0014	Y Y Y Y Y Y Y	Y	6 14	III	A A A	Y ? T N N ?
LB18_b	82.8941585	12.1112154	700	0.0014	1.0E-4	-	-	-	-	Y - Y Y Y Y Y	Y	3 5	-	-	- - - - -
LB18_c	82.900058	12.1082994	700	6.0E-4	0.5E-4	-	-	-	-	Y - Y - Y - -	Y ?	3 6	-	-	- - - - -
LB18_d	82.8994244	12.1055759	-	-	-	-	-	-	-	- - - - -	-	-	-	-	- - - - -
LB18_e	82.8907647	12.1071047	700	0.0011	1.0E-4	-	-	-	-	Y - Y Y Y Y Y	Y	3 5	-	-	- - - - -
LB18_f	82.8979923	12.0998372	700	0.0012	1.0E-4	-	-	-	-	Y - Y Y ? Y ? N N N	N ?	3 5	-	-	- - - - -
LB18_g	82.8914648	12.1000721	1500	0.0010	1.0E-4	-	-	-	-	Y - Y Y Y N Y	N ?	3 5	-	-	- - - - -
LB18_h	82.8959583	12.1037709	-	-	-	-	-	-	-	- - - Y - -	Y ?	-	-	-	- - - - -
LB19_a	82.8658453	12.0919505	800	0.0787	2.0E-4	1.05	1200	0.0612	2.0E-4	Y Y Y Y Y Y Y	Y	5 15	I	T T T	N ? Y Y N N Y
LB19_b	82.8676553	12.0917272	2700	0.0505	7.0E-4	4.725	7600	0.7158	7.0E-4	Y N Y Y Y Y Y	Y	5 11	-	-	- - - - -
LB19_c	82.8686592	12.0905224	2800	0.0836	0.0015	3.15	6500	0.3575	0.0015	Y N Y Y Y Y Y	Y ?	8 12	-	-	- - - - -
LB19_d	82.8733996	12.0925052	1600	0.0203	4.0E-4	2.625	3000	0.0815	4.0E-4	Y Y - - Y - -	Y ?	4 13	I	T T T	N ? Y Y N N Y
LB19_e	82.8614809	12.0885397	700	0.0040	1.0E-4	-	-	-	-	Y - Y Y Y Y Y	Y	3 7	I	T T T	N ? - - N N G
LB19_f	82.8678788	12.0866633	-	-	-	-	-	-	-	- - - - - Y Y	Y	-	I/II	T T T	N ? - Y N N G
LB19_g	82.8612144	12.0926726	-	-	-	-	-	-	-	- - - - -	-	-	-	-	- - - - -
LB19_h	82.8668776	12.0875591	-	-	-	-	-	-	-	- - - - - Y - -	Y ?	-	-	-	- - - - -

<sup>1</sup> Membership criteria based on the location on Herzprung-Russell, optical-IR Color-Color and Color-Magnitude Diagrams: HRD(Av=0.322), HRD(Av variable), (J, J - I1), (J, J - I2), (H, H - I1), (H, H - I2), (K, K - I1), (K, K - I2).

<sup>2</sup> Final membership assessment.

<sup>3</sup> Number of photometric points on the SED: Fit and total.

<sup>4</sup> Evolutionary class based on a Spitzer/IRAC (I1 - I2, I3 - I4) CCD.

<sup>5</sup> IRAC slope.

<sup>6</sup> IR excess based on optical, near-IR and Spitzer Color-Color and Color-Magnitude Diagrams: (I1, I1 - I4), (H - K, K - M1), (I1 - I4, I4 - M1), (I2 - I3, I3 - I4), (I1 - I3, I3 - I4), (I2 - I3, I2 - I4), (I2, I2 - I4).



**Table 7.** Properties and memberships criteria for all counterparts within the APEX/LABOCA beam (continuation).

B30-ID	RA (deg)	DEC (deg)	Teff (K)	Lbol ( $L_{\odot}$ )		Av (mag)	Teff (K)	Lbol ( $L_{\odot}$ )		Membership <sup>1</sup> HR & CM diagrams	Final <sup>2</sup>	Npoints <sup>3</sup>	Class <sup>4</sup>	IRAC <sup>5</sup> slope	IR excess <sup>6</sup>
				$A_V=0.322$	$A_V=variable$			$A_V=0.322$	$A_V=variable$						
LB20_a	82.8508555	12.0902626	2000	0.0231	3.0E-4	5.775	6500	0.296	3.0E-4	YNYYYYY	Y?	5	11	-	-
LB20_b	82.8513261	12.0917094	1500	0.0011	1.0E-4	-	-	-	-	Y-Y-Y--	Y?	3	3	-	-
LB20_c	82.8402513	12.0966039	4500	1.3842	0.0229	1.575	5100	2.1228	0.0229	YYYYY--	Y	8	13	-	-
LB20_d	82.8394462	12.0955432	3400	0.7616	0.0054	3.675	5600	3.9349	0.0054	YYYYY--	Y	5	11	-	-
LB20_e	82.8394127	12.0930814	700	0.0123	5.0E-4	3.15	3500	0.0126	5.0E-4	YNYYYYY	Y?	5	9	-	-
LB20_f	82.8468218	12.0966229	2000	8.0E-4	0.5E-4	5.775	4000	0.0040	1.0E-4	YNYYY?N	N	5	5	-	-
LB20_g	82.8439374	12.0959187	1500	4.0E-4	0.5E-4	-	-	-	-	Y-Y-Y--	Y?	3	3	-	-
LB20_h	82.844606	12.0966218	-	-	-	-	-	-	-	---Y--	Y?	-	-	-	-
LB20_i	82.8430989	12.0983201	1500	7.0E-4	0.5E-4	2.625	1900	0.0011	1.0E-4	YYYYY--	Y	4	4	-	-
LB20_j	82.8529105	12.0926289	1600	4.0E-4	0.5E-4	-	-	-	-	Y---Y--	Y?	3	3	-	-
LB21_a	82.8988495	12.0846224	-	-	-	-	-	-	-	-----	-	-	-	-	-
LB21_b	82.899437	12.0812626	-	-	-	-	-	-	-	-----	-	-	-	-	-
LB21_c	82.90199	12.081975	-	-	-	-	-	-	-	-----	-	-	-	-	-
LB21_d	82.8997765	12.0891346	2000	6.0E-4	0.5E-4	-	-	-	-	---Y--	Y?	-	-	-	-
LB21_e	82.906055	12.0828322	1800	6.0E-4	0.5E-4	-	-	-	-	Y-NY?N	Y?	3	8	-	-
LB21_f	82.8998506	12.0914761	1700	3.0E-4	0.5E-4	1.05	1900	4.0E-4	0.5E-4	Y-Y?YNY	N	3	5	-	-
LB21_g	82.8943406	12.0873348	1600	7.0E-4	0.5E-4	-	-	-	-	YYYYY--	Y	4	4	-	-
LB21_h	82.8972397	12.0861282	-	-	-	-	-	-	-	Y-YYY--	Y	3	4	-	-
LB21_i	82.8977103	12.0892541	-	-	-	-	-	-	-	-----	-	-	-	-	-
LB21_j	82.8822765	12.0712583	700	0.0035	1.0E-4	-	-	-	-	---Y-Y-	Y	3	6	-	-
LB21_k	82.8780746	12.0702267	-	-	-	-	-	-	-	-----	-	-	-	-	-
LB22_a	82.8842633	12.0692825	1600	7.0E-4	0.5E-4	5.25	2000	0.0017	1.0E-4	YYYYY--	Y	4	4	-	-
LB22_b	82.8865316	12.0684093	3700	0.0044	1.0E-4	-	-	-	-	N-YNY?N	N	3	8	-	-
LB22_c	82.883323	12.069021	700	0.0040	1.0E-4	-	-	-	-	Y-YYYNY	N?	3	5	-	-
LB22_d	82.8850515	12.0706474	3700	0.0019	1.0E-4	2.625	4400	0.0044	1.0E-4	NNNNNNN	N	5	5	-	-
LB22_e	82.886582	12.0713157	700	0.0011	1.0E-4	-	-	-	-	Y-YYYYY	Y	3	5	-	-
LB22_f	82.876306	12.0709514	1600	4.0E-4	0.5E-4	1.575	1900	8.0E-4	1.0E-4	YYYYY--	Y	4	5	-	-
LB22_g	82.879455	12.0659626	3100	7.0E-4	0.5E-4	-	-	-	-	N-----	N?	3	3	-	-
LB22_h	82.8845747	12.0683098	1500	4.0E-4	0.5E-4	-	-	-	-	Y---Y--	Y	3	5	-	-
LB22_i	82.8733007	12.0754017	3300	8.0E-4	0.5E-4	-	-	-	-	N-Y?YNY	Y?	3	9	-	-
LB22_j	82.8740083	12.0797718	1500	0.0031	1.0E-4	-	-	-	-	Y---Y--	Y?	3	5	-	-
LB23_a	82.8761053	12.0778312	1500	4.0E-4	0.5E-4	2.1	1900	7.0E-4	1.0E-4	Y-YYYNY	Y?	3	9	-	-
LB23_b	82.8687196	12.0718283	2900	0.0060	3.0E-4	6.3	25000	3.1204	3.0E-4	YNY?N	N	6	11	-	-
LB23_c	82.8684924	12.0782548	2000	4.0E-4	0.5E-4	5.775	4000	0.0021	1.0E-4	YNY?N	N	5	5	-	-
LB23_d	82.8684686	12.0757307	2000	0.0010	1.0E-4	6.3	4000	0.0053	1.0E-4	YNY?N	N	5	5	-	-
LB23_e	82.8733448	12.0814827	1600	6.0E-4	0.5E-4	8.925	3100	0.0032	1.0E-4	Y?Y?Y--	Y?	4	4	-	-
LB23_f	82.8712059	12.0724084	1800	0.0023	1.0E-4	-	-	-	-	Y-Y-Y--	Y?	3	4	-	-
LB23_g	82.87796	12.080151	-	-	-	-	-	-	-	-----	-	-	-	-	-
LB23_h	82.8498907	12.0748369	1900	7.0E-4	0.5E-4	-	-	-	-	Y---Y-Y	Y	3	7	-	-
LB24_a	82.8529587	12.0784426	-	-	-	-	-	-	-	-----	-	-	-	-	-
LB24_b	82.8439484	12.0800447	-	-	-	-	-	-	-	-----	-	-	-	-	-
LB24_c	82.8440552	12.0770445	-	-	-	-	-	-	-	-----	-	-	-	-	-
LB24_d	82.8468915	12.072453	1700	0.0031	1.0E-4	-	-	-	-	Y-YYYYY	Y?	3	6	-	-
LB24_e	82.8432544	12.0696761	1800	8.0E-4	0.5E-4	-	-	-	-	Y-Y?Y?N	N?	3	5	-	-
LB24_f	82.8469663	12.08225	700	0.0022	1.0E-4	-	-	-	-	Y-YYYYY	Y	3	7	-	-

<sup>1</sup> Membership criteria based on the location on Herzprung-Russell, optical-IR Color-Color and Color-Magnitude Diagrams: HRD( $A_V=0.322$ ), HRD( $A_V$  variable), ( $J, J-I$ ), ( $J, J-I$ ), ( $J, J-I$ ), ( $H, H-I$ ), ( $H, H-I$ ), ( $K, K-I$ ), ( $K, K-I$ ).

<sup>2</sup> Final membership assessment.

<sup>3</sup> Number of photometric points on the SED: Fit and total.

<sup>4</sup> Evolutionary class based on a Spitzer/IRAC ( $I1-I2, I3-I4$ ) CCD.

<sup>5</sup> IRAC slope.

<sup>6</sup> IR excess based on optical, near-IR and Spitzer Color-Color and Color-Magnitude Diagrams: ( $I1-I4$ ), ( $H-K, K-M1$ ), ( $I1-I4, I4-M1$ ), ( $I2-I3, I3-I4$ ), ( $I1-I3, I3-I4$ ), ( $I2, I2-I4$ ).

**Table 7.** Properties and memberships criteria for all counterparts within the APEX/LABOCA beam (continuation).

B30-ID	RA (deg)	DEC (deg)	Teff (K)	Av=0.322		eLbol (L <sub>⊙</sub> )	Av (mag)	Teff (K)	Av=variable		eLbol (L <sub>⊙</sub> )	Membership <sup>1</sup> HR & CM diagrams	Final <sup>2</sup>	Npoints <sup>3</sup>	Class <sup>4</sup>	IRAC <sup>5</sup> slope	IR excess <sup>6</sup>
				Lbol (L <sub>⊙</sub> )	Lbol (L <sub>⊙</sub> )				Lbol (L <sub>⊙</sub> )	eLbol (L <sub>⊙</sub> )							
LB25_a	82.8354366	12.0851035	1500	0.0017	1.0E-4	-	-	-	-	-	Y - Y Y Y Y Y Y	Y	3 8	-	-	-	
LB25_b	82.8303947	12.080038	1700	0.0097	3.0E-4	3.0E-4	5.25	5400	0.0558	3.0E-4	Y N Y Y Y Y N N	Y?	5 12	I/II	TNT	Y - - G G G	
LB25_c	82.8416812	12.0856044	2000	0.0134	3.0E-4	3.0E-4	7.875	22000	7.7318	3.0E-4	Y N Y Y Y Y Y Y	Y?	6 13	I/II	TTT	N? - - N G G	
LB25_d	82.8393083	12.0822474	1900	0.0010	1.0E-4	-	-	-	-	-	Y - Y Y Y Y Y Y	N?	3 5	-	-	-	
LB25_e	82.8342835	12.0861197	1500	6.0E-4	0.5E-4	-	-	-	-	-	Y - Y Y Y Y - Y	Y?	3 5	-	-T-	-	
LB25_f	82.8397243	12.0872619	1500	4.0E-4	0.5E-4	-	-	-	-	-	Y - - - Y Y - Y?	Y?	3 5	I/II	TTT	N? - - N N G	
LB26_a	82.8254809	12.0871155	700	0.0051	1.0E-4	-	-	-	-	-	Y - Y Y Y Y Y Y	Y?	3 8	-	-T-	-	
LB26_b	82.82662	12.0823778	700	0.0026	1.0E-4	-	-	-	-	-	Y - Y Y Y Y Y Y	N?	3 5	-	-	-	
LB26_c	82.8216294	12.0792754	4100	0.0019	1.0E-4	-	-	-	-	-	N - Y Y Y N Y Y?	N	3 6	-	-	-	
LB27_a	82.8100128	12.0964232	700	0.012	2.0E-4	2.0E-4	6.825	2700	0.0207	2.0E-4	Y Y Y Y Y Y Y Y	Y	5 11	-	NAN	Y? - - - -	
LB27_b	82.8064117	12.0876884	-	-	-	-	-	-	-	-	-	-	-	-	-	-	N - G
LB27_c	82.8052597	12.0901575	-	-	-	-	-	-	-	-	-	-	-	-	-	-	-
LB27_d	82.8040515	12.0845908	700	0.0074	1.0E-4	-	-	-	-	-	Y - Y Y Y Y Y N	N	3 7	-	-	-	-
LB27_e	82.8021317	12.0896969	-	-	-	-	-	-	-	-	-	-	-	-	-	-	-
LB27_f	82.8020477	12.0958843	-	-	-	-	-	-	-	-	-	-	-	-	-	-	-
LB28_a	82.7841035	12.0847157	700	0.0028	1.0E-4	-	-	-	-	-	Y - Y Y Y Y Y Y	Y	3 5	-	-	-	-
LB28_b	82.784874	12.0824242	-	-	-	-	-	-	-	-	-	-	-	-	-	-	-
LB28_c	82.7759399	12.0832968	-	-	-	-	-	-	-	-	-	-	-	-	-	-	-
LB28_d	82.7767727	12.085662	1800	0.0013	1.0E-4	-	-	-	-	-	Y - Y Y Y Y Y Y	Y	3 7	I/II	TTT	N? - - N G -	
LB29_a	82.7869358	12.0624632	2000	7.0E-4	0.5E-4	-	-	-	-	-	Y - Y Y Y N Y N	Y?	3 12	I/II	TTT	-	
LB29_b	82.7845362	12.0612638	2100	0.0030	1.0E-4	-	-	-	-	-	Y - Y Y N Y Y N	Y?	3 9	-	-T-	-	
LB29_c	82.784803	12.067079	3300	0.0109	2.0E-4	2.0E-4	3.675	5700	0.0501	2.0E-4	N? N Y Y Y N Y N	N	5 11	-	-	-	-
LB29_d	82.7912491	12.0631026	3200	6.0E-4	0.5E-4	1.0E-4	7.35	14000	0.0708	1.0E-4	N N Y Y N Y - -	N	4 9	-	-	-	-
LB29_e	82.7846915	12.0644042	2200	0.0011	1.0E-4	-	-	-	-	-	Y - Y? Y? N N N N	N	3 6	-	-T-	-	-
LB29_f	82.7910175	12.0668983	5100	0.0048	1.0E-4	-	-	-	-	-	N - N N N N N N	Y?	3 8	I/II	TTT	N? - Y N N G	
LB29_g	82.7809669	12.0645025	700	4.0E-4	0.5E-4	-	-	-	-	-	Y - Y - Y - - -	Y	3 7	-	-	-	-
LB29_h	82.7808674	12.0589337	2200	3.0E-4	0.5E-4	-	-	-	-	-	N? - Y - Y - - -	Y?	3 3	-	-	-	-
LB29_i	82.7808674	12.0589337	1700	6.0E-4	0.5E-4	-	-	-	-	-	Y - Y Y Y Y Y Y	Y	3 3	-	-	-	-
LB29_j	82.787634	12.0558409	4400	0.0069	2.0E-4	2.0E-4	4.2	13500	0.2458	2.0E-4	N N N N - - - -	N	6 6	-	-T	N? - - - - G	
LB30_a	82.8030423	12.0608531	1700	0.0071	2.0E-4	2.0E-4	7.35	7000	0.1219	2.0E-4	Y N Y Y Y Y? Y? N	Y?	6 12	I/II	TTT	N? - - N G G	
LB30_b	82.801508	12.0605056	1800	6.0E-4	0.5E-4	-	-	-	-	-	Y - Y Y Y Y Y Y	Y	3 5	-	-	-	-
LB30_c	82.8016933	12.0635964	1800	7.0E-4	0.5E-4	-	-	-	-	-	Y - Y Y Y Y Y Y	Y?	3 7	I/II	TTT	N? - - N N G	
LB30_d	82.8019218	12.064775	-	-	-	-	-	-	-	-	-	-	-	-	-	-	-
LB30_e	82.8103715	12.0592594	700	0.0096	1.0E-4	-	-	-	-	-	Y - Y Y Y Y Y Y	Y	3 9	-	-T-	-	-
LB30_f	82.8175493	12.0635955	3700	0.0035	1.0E-4	-	-	-	-	-	N - Y Y Y? Y Y	N	3 8	-	-T-	-	-
LB30_g	82.8158798	12.0589838	-	-	-	-	-	-	-	-	-	-	-	-	-	-	-
LB30_h	82.8140335	12.0624819	-	-	-	-	-	-	-	-	-	-	-	-	-	-	-
LB30_i	82.808399	12.0577028	700	0.0074	1.0E-4	-	-	-	-	-	Y - Y Y Y Y Y Y	Y	3 6	-	-T-	N? - - N N G	
LB30_j	82.80728	12.061461	1500	6.0E-4	0.5E-4	-	-	-	-	-	Y - Y - Y - Y - -	Y	3 4	-	-	-	-
LB31_a	82.8131356	12.0558984	1800	0.0055	3.0E-4	3.0E-4	6.3	6400	0.0709	3.0E-4	Y - - Y - Y - Y	Y	3 4	-	-	-	-
LB31_b	82.8147323	12.0538983	2100	0.0056	4.0E-4	4.0E-4	6.825	9200	0.2404	4.0E-4	Y N Y Y Y Y Y Y	Y	6 9	-	-T-	-	-
LB31_c	82.8149427	12.0656361	2200	9.0E-4	0.5E-4	-	-	-	-	-	Y - - - - - - -	Y?	3 3	-	-	-	-
LB31_d	82.8187075	12.0627859	1600	7.0E-4	0.5E-4	1.0E-4	0.0	1900	0.0010	1.0E-4	Y Y Y Y Y Y - -	Y	4 4	-	-	-	-
LB31_e	82.8188762	12.0560849	4400	0.0016	1.0E-4	-	-	-	-	-	N - Y - Y - Y - -	N	3 4	-	-	-	-
LB32_a	83.0513535	12.1654158	4300	0.082	0.0021	0.0021	0.525	4100	0.0848	0.0021	N N Y Y - - - -	Y?	7 16	I/II	TTT	N? Y Y N N -	
LB32_b	83.0526962	12.1675291	5400	0.0574	0.0017	0.0017	0.525	5700	0.0668	0.0017	N N N N - - - -	N	10 10	-	-N-	-	-
LB32_c	83.0493698	12.1644573	4800	0.0104	3.0E-4	3.0E-4	0.0	4600	0.0090	3.0E-4	N N N N - - - -	N	4 6	-	-	-	-
LB32_d	83.0553741	12.1640244	6200	0.0106	1.0E-4	1.0E-4	-	-	-	-	N - N N - - - -	N	3 3	-	-	-	-
LB32_e	83.0466461	12.1649246	1600	9.0E-4	0.5E-4	-	-	-	-	-	Y - Y Y - - - -	Y?	3 3	-	-	-	-
LB32_f	83.0588531	12.1689034	-	-	-	-	-	-	-	-	- Y Y - - - -	Y?	-	-	-	-	-
LB33_a	82.5546799	12.1460333	3900	1.3239	0.0121	0.0121	1.575	4500	2.7174	0.0121	Y Y Y Y - - - -	Y	6 16	II	TTT	N? Y Y N N Y	

<sup>1</sup> Membership criteria based on the location on Herzprung-Russell, optical-IR Color-Color and Color-Magnitude Diagrams: HRD(Av=0.322), HRD(Av variable), (J, J - I), (J, J - I2), (H, H - I2), (K, K - I2), (K, K - I2).

<sup>2</sup> Final membership assessment.

<sup>3</sup> Number of photometric points on the SED: Fit and total.

<sup>4</sup> Evolutionary class based on a Spitzer/IRAC (I1 - I2, I3 - I4) CCD.

<sup>5</sup> IRAC slope.

**Table 8.** Temperatures and luminosities for Barnard 30 objects with significant infrared excesses.

B30-ID	RA2000 (deg)	DEC2000 (deg)	Teff	Lbol	Group <sup>1</sup> APEX	Teff	Lbol	MemF	Tbol	Tbol <sup>2</sup>	Lbol	Lbol <sup>2</sup>	L(int) <sup>3</sup>	Class <sup>4</sup>	Type	Npoint
LB14a	82.8310571	12.1542772	1600	0.6658	A1, YSO	5500	6.8753	Y	–	1284	–	0.998	0.276	II	CTT	20
LB14b	82.8313354	12.1495811	1100	0.0510	A1, YSO	1700	0.1135	Y	1093	246	0.046	0.253	–	II→I	CTT/YSO	14
LB19a <sup>5</sup>	82.8658453	12.0919505	800	0.0787	A1, YSO	1200	0.0612	Y	–	238	–	1.218	0.402	I	YSO	15
LB19d	82.8733996	12.0925052	1600	0.0203	A1, YSO	3000	0.0815	Y?	281	249	0.172	0.199	0.094	I	YSO/VeLLO	12
LB24d	82.8440552	12.0770445	–	–	B1, excess	–	–	Y? <sup>†</sup>	353	88	0.056	≤0.524	≤0.604	I	YSO	12
LB11a	82.7921273	12.1737653	–	–	C1, excess	–	–	Y?	–	163	–	0.029	–	I	YSO/protoBD	7
LB12a	82.8622399	12.1723873	2200	0.3283	C1, excess	8000	7.911	Y	–	2234	–	0.392	–	II	WTT	15
LB12d	82.858020	12.166592	–	–	C1, excess	–	–	Y?	177	136	0.051	0.084	–	I	YSO/protoBD	4
LB18a	82.893931	12.1086094	1500	0.3083	C1, excess	3000	0.5961	Y	–	1753	–	0.249	–	II	WTT	14
LB22b <sup>7</sup>	82.8780746	12.0702267	–	–	C1, YSO	–	–	Y? <sup>†</sup>	255	82	0.016	0.064	–	I	YSO/protoBD	8
LB22j <sup>8</sup>	82.8845747	12.0683098	1500	0.0004	C1, YSO	–	–	Y	243	47	0.008	0.060	–	I→0	YSO/protoBD	6
LB30g	82.8103715	12.0592594	700	0.0096	C1, excess	–	–	Y	354	239	0.059	0.103	–	I	YSO/protoBD	11
LB31c	82.8158798	12.0589838	–	–	C1, excess	–	–	–	264	190	0.048	0.074	–	I	YSO/protoBD	6
LB32a	83.0513535	12.1654158	4300	0.0820	C1, YSO	4100	0.0848	Y?	–	414	–	0.657	–	I	YSO	21
LB33a	82.5546799	12.1460333	3900	1.3239	C1, YSO	4500	2.7174	Y	–	1920	–	2.079	–	II	CTT	20
LB08a	82.8479608	12.1911092	1700	0.0010	A2, YSO	–	–	Y?	–	50	–	12.01	1.223	0	YSO	11
LB23a <sup>6</sup>	82.8733007	12.0754017	3300	0.0008	A2, excess	–	–	Y?	312	62	0.008	0.160	0.189	I→0	YSO/protoBD	11
LB23b	82.8740083	12.0797718	1500	0.0031	A2, excess	–	–	Y?	697	–	0.006	–	–	II	CTT/BD	10
LB23c	82.8761053	12.0778312	1500	0.0004	A2, excess	1900	7.0E-4	Y	290	135	0.008	0.024	–	I	YSO/protoBD	11
LB25c	82.8416812	12.0856044	2000	0.0134	A2, YSO	22000	7.7318	Y?	69	56	1.709	2.325	0.557	0	YSO	20
LB29a	82.7869358	12.0624632	2000	0.0007	A2*, YSO	–	–	Y?	–	(70)*	–	(0.271)*	0.337	I/0	YSO/protoBD*	12
LB29b	82.7845362	12.0612638	2100	0.0030	A2*, YSO	–	–	Y?	(533)*	(82)*	(0.016)*	(0.266)*	–	I	YSO/protoBD*	13
LB29f	82.7910175	12.0668983	5100	0.0048	A2*, YSO	–	–	Y?	(926)*	(85)*	(0.010)*	(0.257)*	–	II→I	YSO/protoBD*	12

<sup>1</sup> Grouping based on the detection at 70 and 24  $\mu\text{m}$  and presence of counterparts, as discussed in subsection 2.7: A1 = Detection at 70 and 24  $\mu\text{m}$ ; A2 = detection at 70 and upper limit at 24  $\mu\text{m}$ ; B1 = upper limit at 70  $\mu\text{m}$  and detection at 24  $\mu\text{m}$ ; C1 = no data at 70  $\mu\text{m}$  and detection at 24  $\mu\text{m}$ . Objects without detected emission at 24 and/or 70  $\mu\text{m}$  are not listed here (B2 and C2). Tentative classification:

YSO = Young Stellar Object, with a optical and/or nearIR sources within 5 arcsec of APEX/LABOCA central coordinate. Our tentative interpretation is that most of them are proto-stars or proto-BDs. Excess = Optical and/or nearIR sources with excesses within the APEX/LABOCA beam but farther than 5 arcsec. The submm source cannot be assigned unambiguously to any counterpart so its nature remains unknown. Starless = Possible starless core, since there is neither counterparts closer than 5 arcsec nor a optical/IR source farther away with excess.

<sup>2</sup> Including the flux at 870  $\mu\text{m}$  from APEX/LaBoca and, if present, MIPS M2.

<sup>3</sup> Internal luminosity, based on MIPS flux at 70  $\mu\text{m}$ , after Dunham et al. (2008).

<sup>4</sup> SED classification based on the  $T_{bol}$  vs.  $L_{bol}$  diagram.

<sup>5</sup> There is a submm source nearby, namely SB08, detected with APEX/SABOCA at 350  $\mu\text{m}$  (Huélamo et al. 2017).

<sup>6</sup> There is a submm source nearby, namely SB05, detected with APEX/SABOCA at 350  $\mu\text{m}$  (Huélamo et al. 2017).

<sup>7</sup> There is a submm source nearby, namely SB04, detected with APEX/SABOCA at 350  $\mu\text{m}$  (Huélamo et al. 2017).

<sup>8</sup> There is a submm source nearby, namely SB03, detected with APEX/SABOCA at 350  $\mu\text{m}$  (Huélamo et al. 2017).

<sup>†</sup> Membership status updated from – (Tab. 7) to Y? based on all the available data and our analysis.

\* Possible detection at MIPS 24  $mum$ , but it real, it might be affected by the inhomogeneous extended emission by the nebulosity.

## Appendix A: Classification of the LABOCA submm sources and the counterparts

### Appendix A.1: Group A: LABOCA sources detected at 70 $\mu\text{m}$

Maps obtained with Spitzer/MIPS M2 might cover only half of the surveyed area due to the loss of one detector. This is our case and we do not have measured fluxes at 70  $\mu\text{m}$  for 20 APEX/LABOCA sources. Of the other 14, only six have been detected at this wavelength and they are discussed in this section. The size of the MIPS M2 beam is about 18.6 arcsec (Frayser et al. 2009), about half of the value of APEX/LABOCA, whereas the MIPS M1 beam is much smaller, 5.8 arcsec. Thus, a visual inspection has been carried out in order to confirm our identifications (Fig. A.1 and Fig. A.3). We note that APEX/LABOCA has a nominal pointing error below  $\sim 2$  arcsec. As stated before, the actual rms of the pointing is about 1 arcsec. Although these optical/IR sources are the most probable counterparts to the submm detections, there are additional young sources within the LABOCA beam that might contribute to (or less probably be responsible of) the measured flux. Thus, we discuss here all sources within the LABOCA beam which have been detected and present mid-IR emission.

#### Appendix A.1.1: Group A1: LABOCA sources detected at 24 $\mu\text{m}$

**B30-LB14.-** B30-LB14a is a Class II object (based on the IRAC data displayed Fig. 3, and in the SED, shown in Fig. A.2), as classified based on IRAC photometry, located within the central 5 arcsec of the LABOCA beam. It is one of the brightest objects in our sample, fully within the stellar domain. The SED has been represented in Fig. A.2. For comparison, we have overplotted in the SED panel the expected emission of a 3 Myr object with  $0.072 M_{\odot}$  without interstellar absorption and with a value of  $A_V = 10$  magnitudes (black solid lines). We note, however, that the interstellar extinction as estimated with the  $A_V$  map from 2MASS data is 2.471 mag (subsect. 2.5.6). The SED allows to derived bolometric temperature and luminosity of 1284 K and  $0.998 L_{\odot}$ . The internal luminosity, as derived from the MIPS M2 flux, is  $0.276 L_{\odot}$ . This source has been detected with ALMA, see details in Huélamo et al. (2017) and it can be classified as a CTT. The envelope mass can be estimated as  $0.051 M_{\odot}$ , based on the flux at 870  $\mu\text{m}$ .

South of the central counterpart is located B30-LB14b (Fig. A.1), also detected at 24  $\mu\text{m}$  (both objects have been detected with WISE W3 and W4 filters at 12 and 22  $\mu\text{m}$ ). The bolometric temperature and luminosity of #b, taken into account the fluxes up to 24  $\mu\text{m}$  (i.e., including MIPS M1), are 1093 K and  $0.046 L_{\odot}$  (i.e., within the substellar domain, in full agreement with the SED analysis with VOSA). Thus, the evolutionary status would correspond to a Class II brown dwarf. However, due to the uncertainty in the assignment of the 70 and 870  $\mu\text{m}$  fluxes, we have repeated the calculation assuming that these fluxes correspond to source #b. Thus, we have derived  $T_{bol}^{70+870}=246$  K and  $L_{bol}^{70+870}=0.253 L_{\odot}$ . Figure 6 displays  $L_{bol}$  versus  $T_{bol}$ . The arrow links both sets of values for B30-LB14b and suggests this counterpart might be a Class I object at the border between stars and brown dwarfs (a very low mass YSO or massive substellar analog).

Other interesting objects within the B30-LB14 beam are #d and #h. Both are very faint and have been detected only at J, H, I1 and I2 and with increasing fluxes. The data for #f and #i are even more scarce. All four are worth further follow-up, since they might be in the substellar domain.

**B30-LB19.-** B30-LB19 can be identified with the source IRAS05286+1203 (RA=82.8671, DEC=+12.0899). This object was included in the work by Connelley et al. (2008), which focused on Class I stellar sources. However, due to the lack of spatial resolution and the large number of objects, we have not included the IRAS data (indicated in Fig. A.2) in any calculation. In any case, the APEX/LABOCA source is also extended with a size of 24 arcsec. The central source, B30-LB19a, is within the 5 arcsec peak and is a probable member. It can also be classified as a very low-mass, Class I member based on the IRAC data and the near-IR photometry (see also Fig. 6). It does not have an optical counterpart and it is at the border line between brown dwarfs and stars. We estimate the mass of the envelope as  $0.116$  or  $0.182 M_{\odot}$ , depending whether we take the peak intensity or all the submm emission – the total flux density, respectively. The bolometric luminosity is  $1.218 L_{\odot}$  with  $T_{bol}=238$  K, whereas the internal luminosity can be estimated as  $0.402 L_{\odot}$  from the flux at 70  $\mu\text{m}$ . This source has been detected with ALMA and by APEX/SABOCA, see details in Huélamo et al. (2017). It can be classified as a YSO. B30-LB19b is also within 5 arcsec of the nominal center of the LABOCA emission. Its photometric data indicate it is a very low-mass stellar object with IR excess.

The MIPS M2 image also contains another source which nicely overlaps in near and mid-IR with B30-LB19d. The SED of this object is consistent with a Class I object with  $T_{bol}=281$  K and  $L_{bol}=0.172 L_{\odot}$ , in agreement with the IRAC data. Adding the 870  $\mu\text{m}$  flux (i.e., estimating an upper limit for the luminosity) would modify these values by about a 10%. We note however that the near-IR images reveal/suggest a high-inclined system with a bipolar nebula (Huélamo

et al. 2017). The  $L_{int}$ , as derived by the 70  $\mu\text{m}$  flux, is  $0.094 L_{\odot}$ . Thus, it seems we are dealing with a bona fide VeLLO in what seems to be a wide multiple system.

Other interesting objects, based on their membership and SED, are #e and #f. Both have been classified as Class I and I/II based on the IRAC data and seem to be substellar. This fact reinforces the idea that we are dealing here with a probable young, multiple system with very low individual masses.

#### Appendix A.1.2: Group A2: LABOCA sources undetected at 24 $\mu\text{m}$

**B30-LB08.-** This source is extended, with an estimated size of 27 arcsec, with elongated contours (Fig. A.3). It has been detected by ALMA (Huélamo et al. 2017). The SED corresponding to #a, as displayed in Fig. A.4, is quite remarkable. A possible member of the association, this object is barely within the central 5 arcsec and seems to be, in principle, substellar, has no excess in IRAC or MIPS/M1 (undetected) and has a very strong excess in the far-IR, as measured with Akari/FIS and MIPS/M2. However, there is an offset with the near-IR source (the M2 center is closer to the #g counterpart), although in part it might be due to the beam size and the positional uncertainty. The alternative is that this contribution comes from another source. The envelope mass is  $0.106 M_{\odot}$  or  $0.066 M_{\odot}$  (total submm flux or the peak intensity, respectively). Based on these data, it would be a substellar transitional object between embedded and Classical T-Tauri stages (a YSO). However, the integrated bolometric luminosity for #a, as derived from the SED and taking into account the far-IR fluxes, is  $12.007 L_{\odot}$ , and  $T_{bol}$  reaches 50 K, although these values should be used with caution, based on the above discussion. The internal luminosity, following the prescription by Dunham et al. (2008) and using the emission at 70  $\mu\text{m}$ , is much smaller,  $L_{int}=1.223 L_{\odot}$ , but still much higher than typical values for VeLLOs. Other counterparts have been classified as non-members and have not been plotted on the figure.

**B30-LB23.-** The dust mass from the submm emission can be estimated as  $0.046 M_{\odot}$  whereas the internal luminosity is  $0.189 L_{\odot}$ . There is no optical or near-IR counterpart within 5 arcsec of the nominal center of the APEX/LABOCA beam. The closest is B30-LB23a and neither it or any other possible counterpart have a detected emission at 24  $\mu\text{m}$  with MIPS. However, another two sources, namely #b and #c, have been detected with WISE W4. In any event, the M2 detection is located between #a and #c and we have computed their bolometric luminosity and temperature with and without including the fluxes at 72 and 870  $\mu\text{m}$ , yielding  $T_{bol}=312$  K and  $L_{bol}=0.008 L_{\odot}$ , or  $T_{bol}^{M2+870}=62$  K and  $L_{bol}^{M2+870}=0.160 L_{\odot}$  for #a;  $T_{bol}=290$  K and  $L_{bol}=0.008 L_{\odot}$ , or  $T_{bol}^{M2+870}=62$  K and  $L_{bol}^{M2+870}=0.161 L_{\odot}$  for #c. With these properties, they would be YSO of possible substellar nature (proto-BDs).

In addition, counterpart #b is characterized by 697 K and  $0.006 L_{\odot}$ , assuming that the W4 measurement is real. These values are represented in Fig. 6. As in the other counterparts, we may be dealing with a proto-BD, in any case a YSO.

Other interesting counterparts, red and faint but not detected at mid-IR, are #g and #h. We note that the MIPS M1 image taken in 2005 has an artifact centered at counterpart #i, as can be easily detected by comparison with the image obtained at the beginning of the mission one year earlier.

**B30-LB25.-** B30-LB25 is extended (34 arcsec) with a total mass of the envelope of  $0.0126 M_{\odot}$  ( $0.076 M_{\odot}$  for the peak emission). It is close to B30-LB20 and B30-LB26 (Fig.1). To avoid ambiguity, the common sources have been assigned to B30-LB25. Another nearby submm source is B30-LB24. The maximum emission in Spitzer/MIPS at 24  $\mu\text{m}$ , but is diffuse, and happens to be in between both APEX/LABOCA sources.

We have assigned the M2 flux to the component B30-LB25c, which is located close to a source detected with the Akari satellite with FIS (Fig. A.3). The integrated fluxes for #c, including the 70  $\mu\text{m}$  value, produce  $T_{bol}=69$  K and  $L_{bol}=1.709 L_{\odot}$ . Adding the flux at 870  $\mu\text{m}$  modifies these values resulting into  $T_{bol}^{70+870}=56$  K and  $L_{bol}^{70+870}=2.325 L_{\odot}$ . The internal luminosity is  $0.557 L_{\odot}$ . In any event, B30-LB25c would be a YSO or Class 0 proto-star (Class I/II from the IRAC CCD, Fig. 6).

At the center of the B30-LB25 submm emission is #a, likely substellar. Moreover, the counterpart #e is within the central 5 arcsec, fainter than #a and seems to be also a Class I object. Thus, it is quite possible we have identified a visual very young brown dwarf binary with an angular separation of 5.5 arcsec which might be (or not) bounded to a more massive component. Although it might be a projection effect, in principle the likelihood is very small and more probable they are coming from the same clump.

In addition, #b resembles a massive BD with an excess at 8  $\mu\text{m}$ . The counterpart #f is interesting, but there is not enough data to characterize it properly, except that the IRAC data indicates it is a class I/II object.

**B30-LB29.-** Counterpart #a is a possible member and has an extended emission with MIPS at 24  $\mu\text{m}$ . It also has been detected at 70  $\mu\text{m}$ . It is within the central 5 arcsec of the submm peak. We note, however, that we might be dealing

with a multiple system or at least with several unevolved BDs which have been born inside the same clump. Its bolometric temperature is 70 K, at the border between Class 0 and Class I (Chen et al. 1995), and the integrated luminosity reaches  $0.271 L_{\odot}$ , whereas the internal luminosity, as derived from Dunham et al. (2008), is  $L_{int}=0.337 L_{\odot}$ . This value is larger than  $L_{bol}$  derived from the integration along the SED. This fact might be due to the way  $L_{int}$  has been estimated. Firstable,  $L_{int}$  is affected by a factor two uncertainty (as derived by the spread in their Figure 4). On the other hand, our fluxes in B30 are below the lower limit in the case of the Taurus members used by Dunham et al. (2008) and this extrapolation might have a consequence on the derived  $L_{int}$ . In any case, as in previous candidates, the mass from the envelope,  $0.064 M_{\odot}$ , is inside the substellar domain. Our tentative classification corresponds to a YSO, perhaps in the substellar domain (a massive proto-BD). On the other hand, B30-LB29 #b and #f have near-IR excesses and can be classified as YSO. Their bolometric temperature and luminosity are 533 K and  $0.016 L_{\odot}$  and 926 K and  $0.010 L_{\odot}$ , respectively. Counterpart #g, faint and detected only at J, I1, and I2, present increasing fluxes at longer wavelengths. Another interesting object is #i, substellar if member. Again, we may be dealing with a multiple system or at least with several unevolved BD, perhaps physically associated.

### Appendix A.2: Group B: LABOCA sources undetected at $70 \mu\text{m}$

#### Appendix A.2.1: Group B1: LABOCA sources with detection at $24 \mu\text{m}$

**B30-LB24.-** The MIPS M1 image (or the contours in the J image, Fig. A.5) indicates that there is an extended emission at  $24 \mu\text{m}$ . Two sources are within it, B30-LB24 #c and #d. None of them is within the central 5 arcsec. The first one is characterized by  $L_{bol} \leq 0.555 L_{\odot}$  and  $T_{bol}=71$  K, whereas the other has  $L_{bol}=0.099 L_{\odot}$  and  $T_{bol}=254$  K ( $\leq 0.531 L_{\odot}$  and 88 K if the upper limit at  $70 \mu\text{m}$  is included). Both look like Class I stellar members (YSO). The mass of the envelope is  $0.044 M_{\odot}$  with  $L_{int} \leq 0.604 L_{bol}$ . Other relevant possible members within the LABOCA beam are #a, #e and #g, especially this last one, whose SED corresponds to a class I or II object, possibly of substellar nature.

#### Appendix A.2.2: Group B2: LABOCA sources undetected at $24 \mu\text{m}$

There are seven LABOCA sources without emission at  $24 \mu\text{m}$  and detection limits at  $70 \mu\text{m}$ , namely B30-LB01, B30-LB02, B30-LB09, B30-LB13, B30-LB15, B30-LB20 and B30-LB28. B30-LB01, B30-LB13 and B30-LB15 do not display any special behavior (apart of the substellar candidate B30-LB13b) and they will not be discussed in this subsection. However, in all these three cases the optical or near-IR counterpart are farther than 5 arcsec from the center of the LABOCA emission and this could indicate they are, in fact, starless cores (subsection 3.5).

**B30-LB02.-** The counterpart #a only has been detected with IRAC I1 and I2, being the flux at  $4.5 \mu\text{m}$  stronger than at  $3.6 \mu\text{m}$ , although close to the detection limits. It is outside the central 5 arcsec. The mass of the submm envelope can be estimated as  $0.099 M_{\odot}$  and the internal luminosity as  $L_{int} < 0.230 L_{bol}$ . Thus, this source is an interesting candidate since, if member, it would be substellar. Counterpart #d has only been detected with IRAC and its colors correspond to a Class I object (Fig. 3), but the SED suggests it is a Class II BD, if membership is confirmed.

**B30-LB09.-** There are several probable and possible members within the B30-LB09 beam (Fig. A.6). All three seem to be substellar (Fig. A.7) and, in fact, #a is located within the submm peak and has not been detected with MIPS either at  $24 \mu\text{m}$  or at  $70 \mu\text{m}$ . The upper limit at  $70 \mu\text{m}$  an internal luminosity of  $L_{int} \leq 0.422 L_{bol}$ . Therefore, we have identified it as the origin of the LABOCA emission and it is another excellent brown dwarf candidate with a significant submm emission and an envelope mass of  $0.043 M_{\odot}$  (subsection 3.1). We note, however, that the near-IR slope in the SED is not rising. Apart from the central source, there are two probable members within the B30-LB09 beam, namely #c and #e (Fig. A.6). Both seem to be substellar.

**B30-LB20.-** This LABOCA source has two interesting counterparts, identified as #a and #d. Both are far from the submm peak (Fig. A.6). Moreover, they have been detected with WISE W3 and W4, but only #d has a possible, extended flux with MIPS M1. Most likely, both are class II stars. The total mass of the envelope is  $0.048 M_{\odot}$  and the internal luminosity is  $L_{int} \leq 0.592 L_{\odot}$ .

In addition, there are another two interesting objects, namely #b and #g, which could be substellar. They only have three data-points in the SED, but the shape suggests they might be Class II or even Class I. We note that B30-LB20c is DM142, but it does not show any IR excess. Moreover, Huélamo et al. (2017)

have detected a  $350 \mu\text{m}$  source with APEX/SABOCA within the LABOCA beam, but it does not have any optical or IR counterpart.

**B30-LB28.-** The envelope mass for this submm source is  $0.071 M_{\odot}$ . Although the WISE fluxes measured for components #b and #c are uncertain, both have dubious emission at  $24 \mu\text{m}$  and their SED indicates they are Class I or even Class 0 (the shortest wavelength they display correspond to WISE W1). Thus, they are potential proto-BD candidates but additional data are required. In any case, there is no optical or IR source within the central 5 arcsec and the LABOCA source is elongated in the north-east direction, toward the very intense submm source B30-LB27.

Counterpart #d has been classified as I/II from the IRAC CCD (Fig. 3) and the complete SED agrees with this classification. If member, it would be substellar. This is the case of #a, but contrary to #d, there is no IR excesses. We note, however, that there is submm emission as seen by APEX/SABOCA at  $350 \mu\text{m}$  (Huélamo et al. 2017). However, because the shape of the SED (Fig. A.7), we believe that they are unrelated although we cannot discard completely that B30-LB28a has a submm excess.

### Appendix A.3: Group C: LABOCA sources with no data at $70 \mu\text{m}$

#### Appendix A.3.1: Group C1: LABOCA sources detected at $24 \mu\text{m}$

**B30-LB11.-** The counterpart #a, detected with MIPS M1, is quite distant from the peak of the submm emission (Fig. A.8). The integrated properties are  $T_{bol}=145$  K,  $L_{bol}=0.028 L_{bol}$  and an envelope mass of  $0.046 M_{\odot}$ . Thus, it seems it could be a Class I object in the substellar domain (a proto-BD candidate).

Moreover, counterpart #c displays an interesting SED with a significant flux at  $8 \mu\text{m}$ . If member, it would also be substellar. Other interesting sources are #b and #e, since there are also red and faint.

**B30-LB12.-** From the flux at  $870 \mu\text{m}$  we derive an envelope mass of  $0.087 M_{\odot}$ . Counterparts #a and #d have been detected at  $24 \mu\text{m}$ . The first one is the probable origin of the submm emission, since it is almost within the central 5 arcsec, and has  $L_{bol}=0.418 L_{\odot}$  and  $T_{bol}=2108$  K. The IRAC data indicate it is a class III star and the SED shows that the excess is only at  $24 \mu\text{m}$  (i.e., a WTT).

More interesting is #d, with  $L_{bol}=0.058 L_{\odot}$  and  $T_{bol}=174$  K. If the  $870 \mu\text{m}$  flux is considered, the values change to  $L_{bol}^{870}=0.094 L_{\odot}$  and  $T_{bol}^{870}=138$  K, although it is at the edge of the submm beam. In any case, its properties make it a substellar Class I object (proto-BD candidate).

Other interesting possible or probable members are #c, #g and #j, specially the first one, very faint and classified as Class I based on the IRAC colors. In other words, another proto-BD candidate.

**B30-LB18.-** Counterpart #a is not within the submm peak. It is a class III star (possibly a WTT) with  $L_{bol}=0.249 L_{bol}$ ,  $T_{bol}=1748$  K and an excess only at  $24 \mu\text{m}$ , being the mass for the dust envelope, as estimated with the flux at  $870 \mu\text{m}$ ,  $0.059 M_{\odot}$ .

The counterparts #b and #c might be of substellar nature. The first one, close to #a, presents increasing fluxes up to I2, suggesting it might be a class I BD associated to #a (i.e., a proto-BD candidate y physical association to a more evolved low-mass star).

**B30-LB22.-** Counterpart #a is located very close to the nominal center of the submm, it is a probable member and has a peculiar SED (although with only four points, Fig. A.9), indicating it is a Class I source of the substellar nature, with an envelope mass of  $0.088 M_{\odot}$ . However, although #a is not detected at  $24 \mu\text{m}$ , there is a SABOCA source at  $350 \mu\text{m}$  (Huélamo et al. 2017). In addition, there is a source at this wavelength west of it, halfway toward component #b, which seems to the origin of it.

In the case of the counterpart B30-LB22b, Without taking into account the  $870 \mu\text{m}$  flux, we derive  $L_{bol}=0.016 L_{\odot}$  and  $T_{bol}=255$  K. When including the flux at  $870 \mu\text{m}$  the estimates are  $L_{bol}^{870}=0.064 L_{\odot}$  and  $T_{bol}^{870}=82$  K. In either case, a Class I YSO of possible substellar nature. Counterpart #j is also detected at  $24 \mu\text{m}$  and has 243 K and  $0.008 L_{\odot}$ , possibly a Class I BD (proto-BD candidate).

The LABOCA source includes another possible embedded object, namely #h. Finally, there are other two probable members: #c and #g. In addition, there is some overlap with B30-LB23 (Fig. 1), but there are not common optical or IR sources. B30-LB22f is also a submm source at  $350 \mu\text{m}$  (Huélamo et al. 2017), but it does not seem to belong to the association and might be extra-galactic.

**B30-LB30.-** The submm emission is extended and the derived mass for the envelop is  $0.123 M_{\odot}$  ( $0.101 M_{\odot}$  at peak intensity). There is no counterpart within the submm peak, but nearby there are two objects detected either with MIPS M1 (#g) or W4 (#a). We have derived  $0.059 L_{\odot}$  and  $354$  K for B30-LB30g without taking into account the  $870 \mu\text{m}$  flux. With it, the bolometric luminosity and temperature for each of them would be  $L_{bol}^{870}=0.103 L_{\odot}$  and  $T_{bol}^{870}=239$  K. In any case, it seems we are dealing with very low-mass Class I object (YSO), perhaps of the substellar nature. Counterpart #b lacks excess and might be substellar. Finally, #c has been classified, based on the IR data, as class I/II BD (Fig. 3).

**B30-LB31.-** This LABOCA source has also been detected by ALMA (Huélamo et al. 2017). The mass of the envelope is  $0.082 M_{\odot}$ . Counterpart #a is almost within the 5 arcsec beam of the submm source and presents a possible extended emission at  $24 \mu\text{m}$ .

In addition, LB30-LB31c has been detected at  $24 \mu\text{m}$  and its properties are  $L_{\text{bol}}=0.048 L_{\odot}$  and  $T_{\text{bol}}=264 \text{ K}$ . Adding up the  $870 \mu\text{m}$  would change these values to  $L_{\text{bol}}^{870}=0.074 L_{\odot}$  and  $T_{\text{bol}}^{870}=190 \text{ K}$ . Then, it is possible Class I proto-BD candidate. Other relevant objects, because their faintest and red SEDs, are #h, #e and, especially because of the increased fluxes toward longer wavelength, #d.

**B30-LB32.-** LB32a can be identified with the source IRAS 05293+1207 (RA=83.0450, DEC=+12.1629). It was only detected at  $60 \mu\text{m}$  and the flux,  $[60]=1.15e+00\pm 0.1725 \text{ Jy}$ , agrees very well with the current SED (Fig. A.9) and the fluxes detected with Akari/FIS. It is outside the M2 FOV but it is detected with MIPS/M1. The integrated bolometric luminosity is  $0.657 L_{\odot}$  with  $T_{\text{bol}}=414 \text{ K}$ , and the mass of the envelope is  $0.123 M_{\odot}$ . In any event, we are dealing with a Class I stellar member of the association (a YSO), although the small dip observed at  $4.5 \mu\text{m}$  might indicate it has already started to lose part of the envelope.

**B30-LB33 and LB34.-** This double peak submm source is located at the Western border of our LABOCA map and outside the clustering of submm sources (or the dust structure seen with IRAC). The individual values for the masses of each envelope are  $0.087 M_{\odot}$  and  $0.064 M_{\odot}$ , respectively. There is only one optical and near-IR counterpart located closer to B30-LB33 (counterpart #a, Fig. A.8), both identified previously by Dolan & Mathieu (1999, 2002) and by Duerr et al. (1982). It is GY Ori, identified by those works as DM115 and DIL19, respectively. There is no MIPS/M2 data but it has been detected at  $24 \mu\text{m}$ . Thus, B30-LB33a has  $T_{\text{bol}}=1920 \text{ K}$  and  $L_{\text{bol}}=2.079 L_{\odot}$ . We have classified B30-LB33a as a Class II stellar member.

## Appendix A.3.2: Group C2: LABOCA sources undetected at $24 \mu\text{m}$

**B30-LB03 and LB04.-** The sources B30-LB03 and B30-LB04 are very close to each other, as shown in Fig. A.10. While B30-LB04 does not show any counterpart within 5 arcsec, B30-LB03 shows one source, a YSO.

The SED of central source of B30-LB03, #a for short, together with the previous analysis based on CC and CM diagrams, indicates its is a possible member with substellar nature, but without IR excesses up to  $3.6 \mu\text{m}$ . Some excess might be at  $4.5 \mu\text{m}$ , although it is unclear. The center of the LABOCA source is outside the MIPS/M2 images (due to the malfunctioning of one of the detectors), but the counterpart #a is not detectable at  $24 \mu\text{m}$ . Thus, it is not completely clear whether this object is the origin of the submm emission. In any case, the mass of the envelope can be estimated as  $0.057 M_{\odot}$  (subsection 3.1), well below the stellar/substellar limit.

Source #b, located close to the B30-LB04 peak, is a probable substellar member without any detectable excess. The mass of the envelope is  $0.059 M_{\odot}$ .

In addition, we have classified as cluster candidates #d and #c –possible, and #e, #i, and #f –probable members. This last one is a very red object with a steep slope which can be classified as a Class I source based on the IRAC CCD. Therefore, we are dealing with a very low luminosity object (in the optical to mid-IR range, lower than the characteristic luminosity of Class II or III brown dwarfs) and a quite extended emission in the submm, which might not be directly associated to it, although the visual inspection indicates that B30-LB03f is in the middle of a filament like asymmetric structure about  $60 \times 30 \text{ arcsec}$ .

### B30-LB05.-

This is an extended submm source with an estimated size, after deconvolving with a Gaussian to take into account the core, of 36 arcsec. The mass of the envelope can be estimated as  $0.081 M_{\odot}$  (full beam) or  $0.051 M_{\odot}$  (peak).

B30-LB05a is located within 5 arcsec of the submm peak intensity and it is not detected at  $24 \mu\text{m}$ , as measured with Spitzer/MIPS, but it is outside the M2 FOV. This source seems to be the origin of the submm excess. We note, however, that #a is a Class III star based on its IRAC data.

In addition, B30-LB05c, at  $\sim 25 \text{ arcsec}$  from the main source (Fig. A.10), seems to be a bona-fide, substellar member. We note that both optical/IR counterparts (#a and #c) are within the APEX/LABOCA beam.

**B30-LB07.-** Counterpart #a, located close to the center, might be the origin of the submm emission (Fig. A.10). The SED suggests it is a substellar object, if it is indeed a member of B30 (its membership status is Y?, although it is based on only three data-points). The total mass of the submm envelope (subsection 3.1) is  $0.052 M_{\odot}$ , which provides a stronger hint regarding its proto-BD status. However, there is no information regarding emission at  $70 \mu\text{m}$  and it lacks emission at  $24 \mu\text{m}$ , which casts some doubts about the actual connection between the near-IR and the submm sources.

B30-LB07e is also an interesting object, since it is a probable member whose luminosity indicates it is substellar. Other interesting sources are #c and #i, which have a relatively flat spectrum and have been classified as possible members. In addition, B30-LB07f has been detected in only two bands, so no membership status has been assigned, but its SED slope is positive.

**B30-LB10.-** As can be seen in Fig. 1, B30-LB11 is located southeast of B30-LB10 and overlaps with it. All sources in the common area have been assigned to B30-LB10. It has been detected by ALMA (Huélamo et al. 2017). The source #a is just at the center, with a weak mid-IR excess as derived with IRAC. There is no M2 flux (outside the FOV) and it is not detected with M1 at  $24 \mu\text{m}$ . It is a possible member and, if membership is confirmed, it would be substellar. The envelope mass has been estimated as  $0.046 M_{\odot}$ .

This submm source includes eight probable (#c, #e, #g and #m) and possible members (#a, #h, #i and #k, see Fig. A.10). Some of them might be substellar, but they display no special feature in the SED.

**B30-LB17.-** Although the closest counterpart to the submm peak is #a, #d shows a significant IR excess, including the emission at  $12 \text{ and } 22 \mu\text{m}$  (WISE W3 and W4, with extended with MIPS M1 and no data for M2), as can be seen in the SED included in Fig. A.9. Both seem to be below the substellar limit. The envelope mass is about half of the limit between stars and brown dwarfs, with a value of  $0.059 M_{\odot}$  (subsection 3.1). Thus, B30-LB17a is a BD candidate and B30-LB17d might be a proto-BD candidate. Figure A.8 includes another interesting substellar candidate: #b is a probable member without IR excess.

**B30-LB21.-** Counterpart #a, located at the submm peak and with a dubious extended emission at  $24 \mu\text{m}$ , is possibly a Class I object. This source is also extended and the Gaussian fit gives an angular size of 62 arcsec, the largest among all our APEX/LABOCA sources. We note that this component is located in the ionizing edge produced by the star  $\lambda \text{ Ori}$  (Fig.1), as projected on the sky, and is also very close to B30-LB22. The mass of the envelope can be estimated as  $0.108 M_{\odot}$  ( $0.061 M_{\odot}$  just for the peak, see detail in subsection 3.1) and based on the SED it might be substellar, making it a candidate as an irradiated brown dwarf embryo, although a more detail analysis is required.

LB21f and B30-LB21g are two probable members of substellar nature. However, they do not show IR excesses. The SED of counterpart #c is similar to #f and #g, except that it has been detected with WISE W4 although the measured flux seems dubious, since might be affected by source confusion. Other possible members are #d and #h.

**B30-LB27.-** No object is within the central 5 arcsec of the LABOCA peak. The brightest counterpart in the optical/near-IR within the B30-LB27 beam is #a, but it seems to be a Class II BD or very low-mass star, if member, detected with WISE W3 and W4 but with no measurement at MIPS M1 ( $L_{\text{bol}}=0.014 L_{\odot}$ ,  $T_{\text{bol}}=988 \text{ K}$ ).

The flux at  $870 \mu\text{m}$  has been assigned to #b, which has a possible extended emission at  $24 \mu\text{m}$ . We note that we have also assigned to this source the SABOCA flux at  $350 \mu\text{m}$ , although it is approximately NW from it (elongated in the same direction, (Huélamo et al. 2017).

There are two other interesting objects: components #c and #f. Both have been detected with WISE W3 and W4 and in the case of #f, there is also a possible detection at  $24 \mu\text{m}$ . Since the mass of the envelope is  $0.279 M_{\odot}$  ( $0.150 M_{\odot}$  at peak intensity) and these three objects have low values of the bolometric temperature and luminosity, regardless the assignment of the submm flux, they look like bona fide BDs candidates.

On the other hand, **B30-LB06**, **B30-LB16**, and **B30-LB26** have not been detected with MIPS and there are no detectable optical nor near-IR sources within the 5 arcsec central peak. Several facts have to be taken into account. B30-LB16 has an envelope mass of  $0.053 M_{\odot}$ . Counterpart #a might also be substellar. There is a counterpart only detected at  $24 \mu\text{m}$  (#f), but it seems to be an artifact and we have not considered it for further discussions. Thus, we believe it is a good candidate to be starless core. In the case of B30-LB06, the counterparts #a and #c seem to be substellar but they lack IR excess. The submm source is extended with masses of  $0.210$  and  $0.077 M_{\odot}$  (whole beam and peak, respectively). Again, it is starless core candidate. A similar situation appears for B30-LB26a, with an envelope mass of  $0.058 M_{\odot}$ . However, this last one might have a small IRAC excess and its submm emission is connected with B30-LB25 (in fact it is elongated into that direction), which has been detected both at  $24$  and at  $70 \mu\text{m}$  (see Fig. A.3 for the finding chart and Fig. A.4 for the SED).

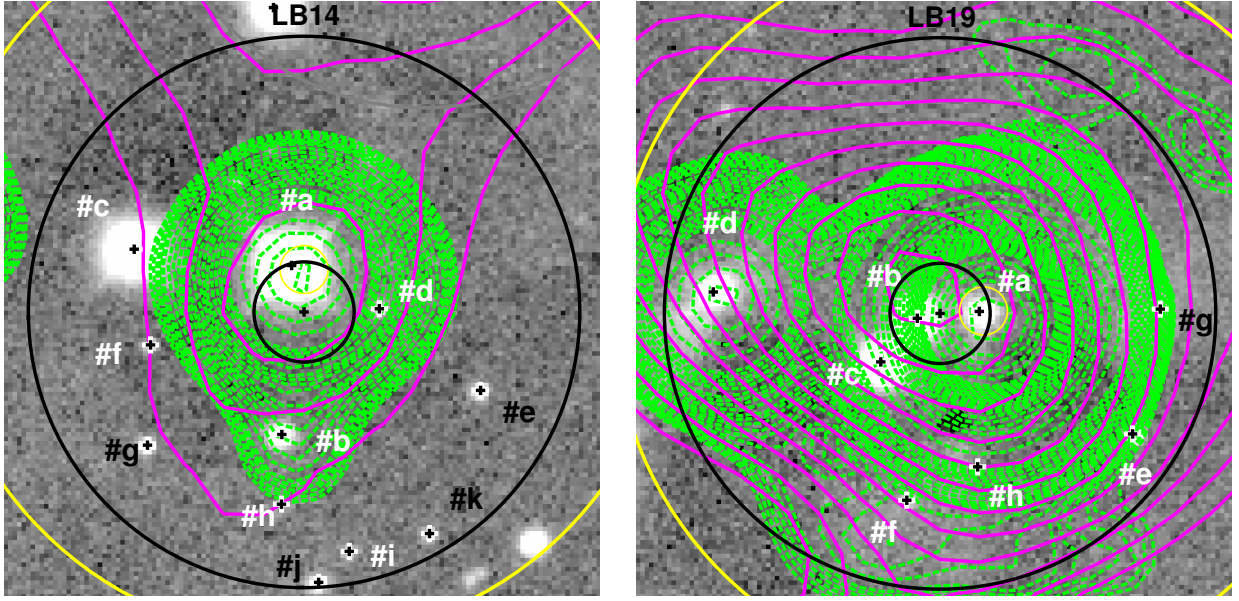


**Fig. A.1.** Finding charts for the relevant sources detected also both at 70 and 24  $\mu\text{m}$  with MIPS (A1 group). The black large and small circles correspond to APEX/LABOCA beam size and the search radius, 27.6 and 5 arcsec respectively, whereas the yellow big and small circles represent the Akari/FIS and Akari/IRC beams. White labels denote possible and probable members of B30, whereas black labels are used for non-members or objects with unknown status. The background images correspond to CAHA/Omega2000 in the  $J$  band. The green, dashed contours come from the Spitzer/MIPS image at 24 micron after removing the diffuse emission by the nebulosity (see subsection 2.4), whereas the magenta levels comes from the APEX/LABOCA and correspond to S/N starting at 2 with increments of 1.

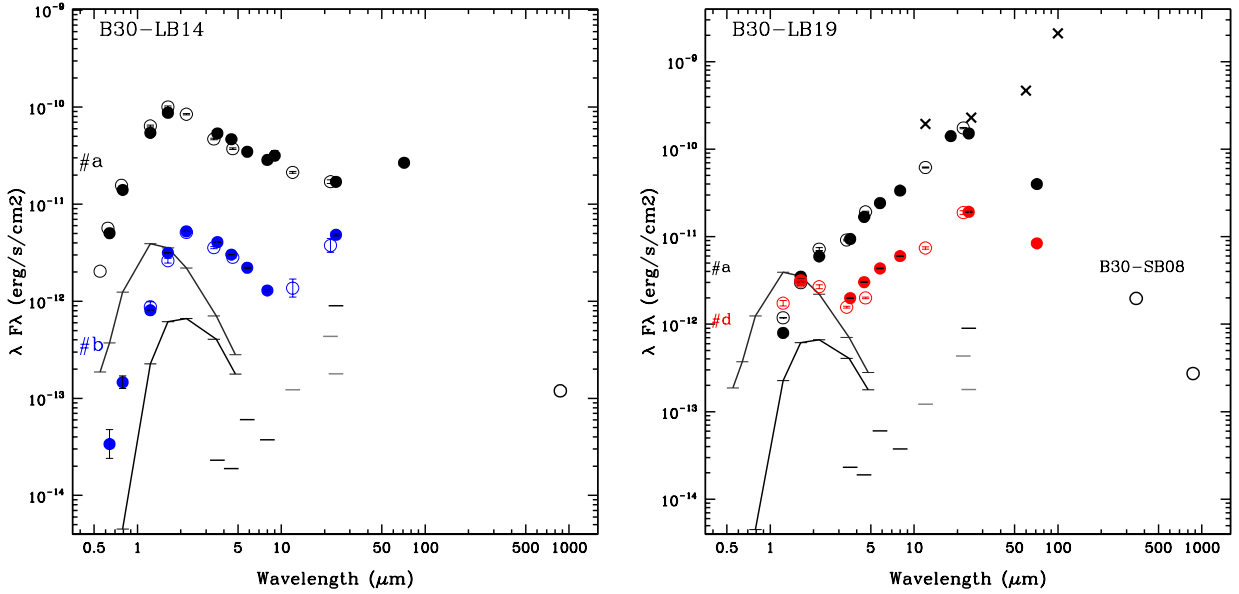


**Fig. A.2.** Spectral energy distribution for the relevant sources detected also both at 70 and 24  $\mu\text{m}$  with MIPS (A1 group). Completeness and detection limits have been included for a Spitzer data, as gray and black line segments, respectively. For comparison, we have overplotted in the SED panel the expected emission of a 3 Myr object with  $0.072 M_{\odot}$  at the distance of B30 –400pc, without interstellar absorption and with a value of  $A_V = 10$  magnitudes (black solid lines).

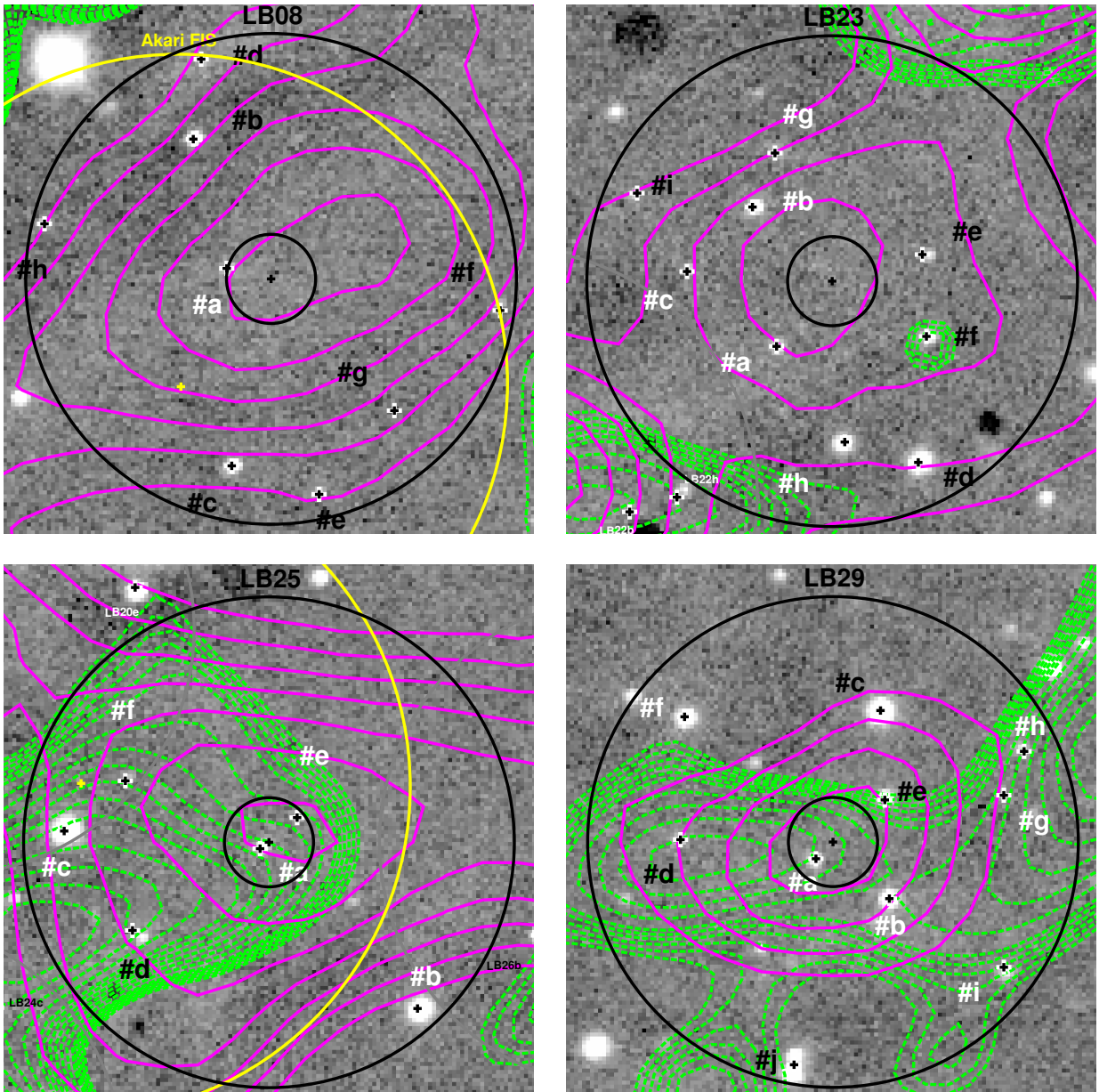


**Fig. A.3.** Finding charts for the relevant sources detected also at 70 and undetected at 24  $\mu\text{m}$  (A2 group). Symbols are in Fig. A.1. We note that the feature displayed at 24  $\mu\text{m}$  for B30-LB23f corresponds to an artifact.



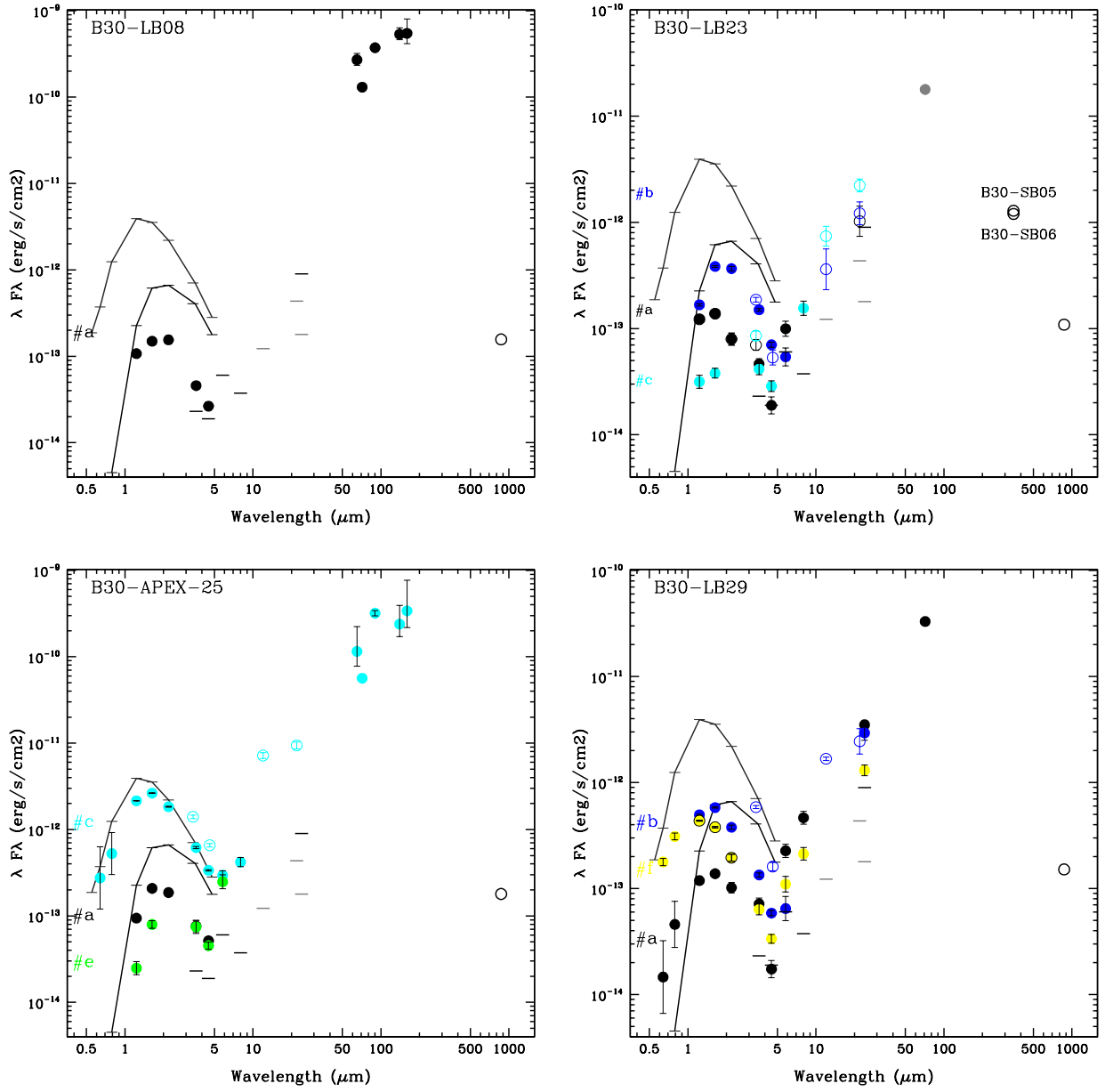


**Fig. A.4.** Spectral energy distribution for the relevant sources with emission at  $70 \mu\text{m}$  but undetected at  $24 \mu\text{m}$  (A2 group). We note that several counterparts for B30-LB29 have a possible extended emission at  $24 \mu\text{m}$ . Symbols as in Fig. A.2.

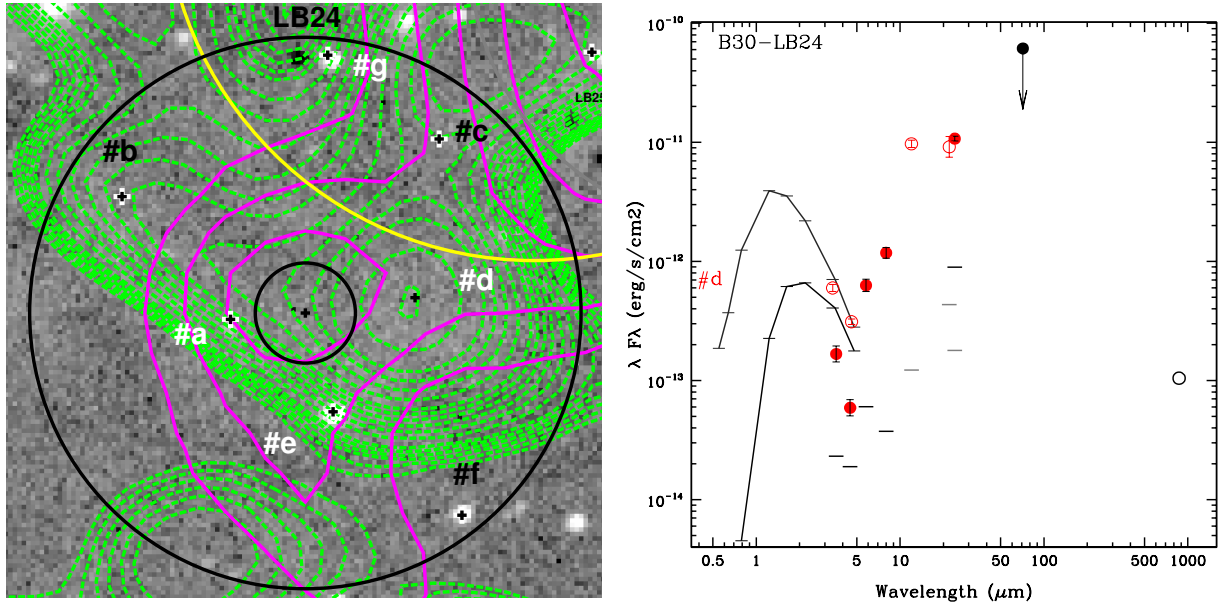


**Fig. A.5.** Finding chart and spectral energy distribution for B30-LB24, the only member within the B1 group (upper limit at 70  $\mu\text{m}$  emission at 24  $\mu\text{m}$ ). Symbols are as in Fig. A.1 and Fig. A.2.

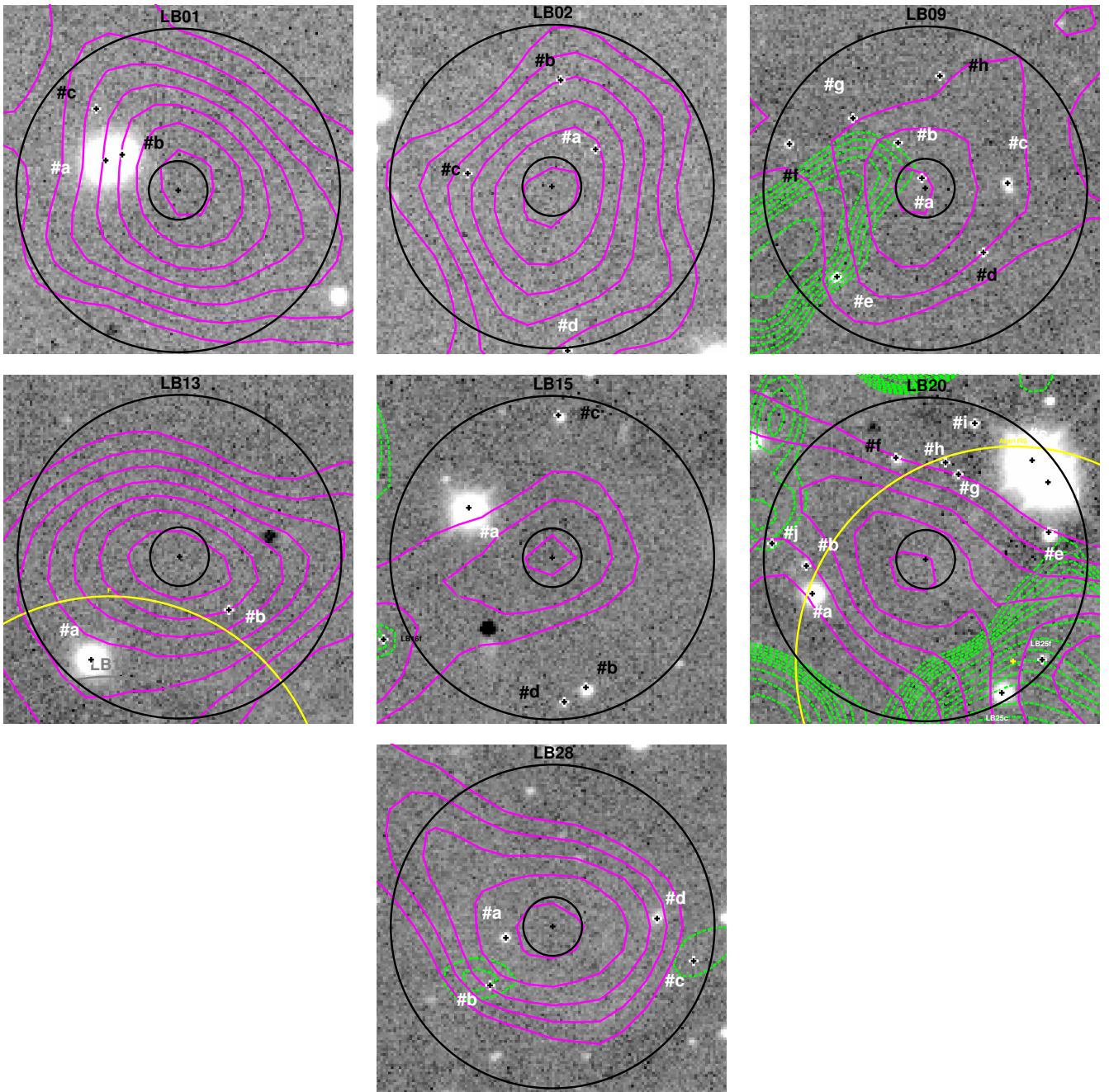


**Fig. A.6.** Finding charts for group B2, undetected both at  $70 \mu\text{m}$  and at  $24 \mu\text{m}$  (upper limits in both cases). Symbols as in Fig. A.1.

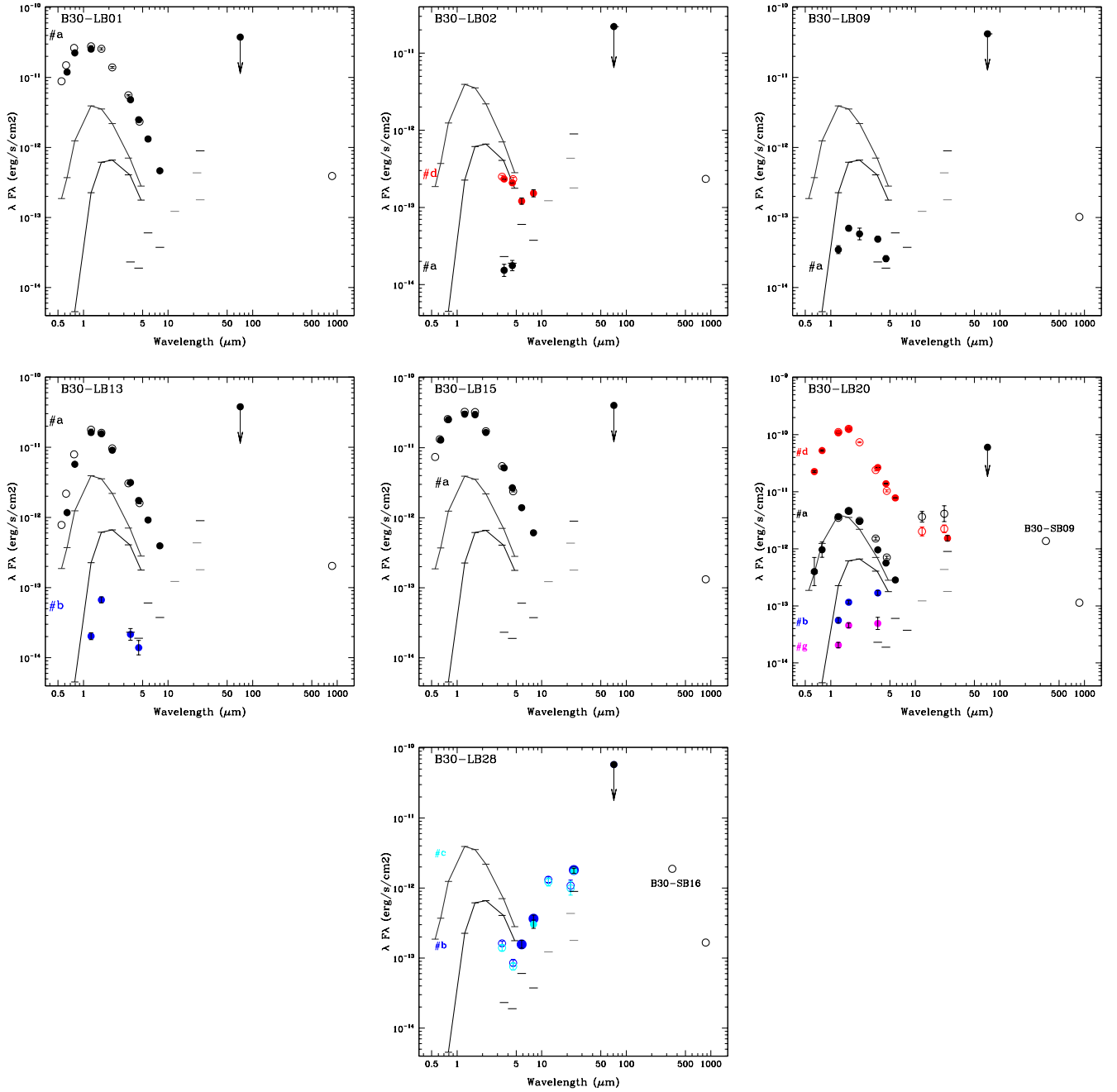


**Fig. A.7.** Spectral energy distribution for group B2 sources undetected at 70 and 24  $\mu\text{m}$  (upper limits). We note that B30-LB20 and B30-LB28 have a possible extended emission at 24  $\mu\text{m}$ . Symbols as in Fig. A.2.

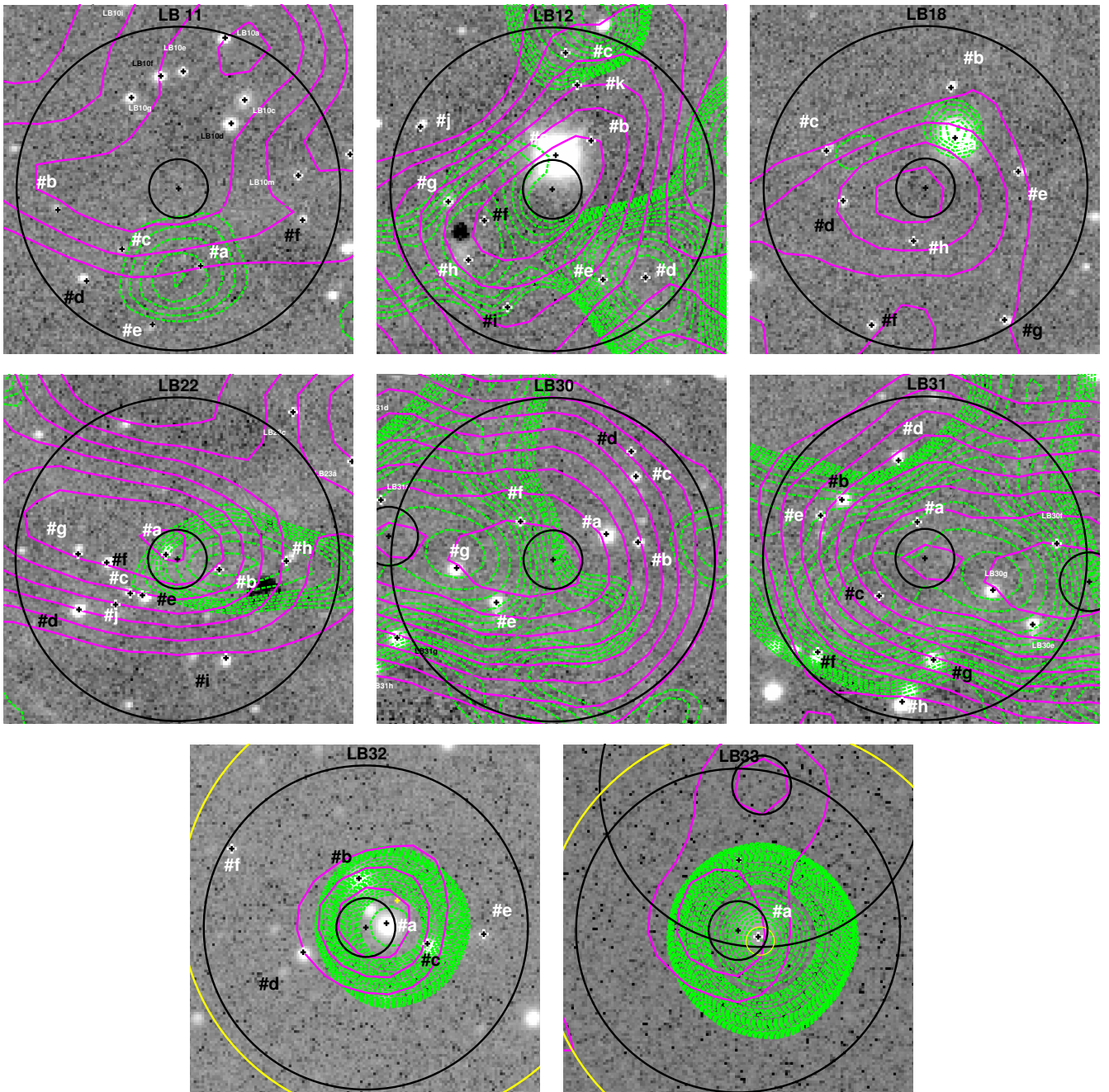


**Fig. A.8.** Finding charts for group C1 or sources outside the FOV of the MIPS M2 image. All have been detected at  $24\ \mu\text{m}$  with MIPS. Symbols as in Fig. A.1.

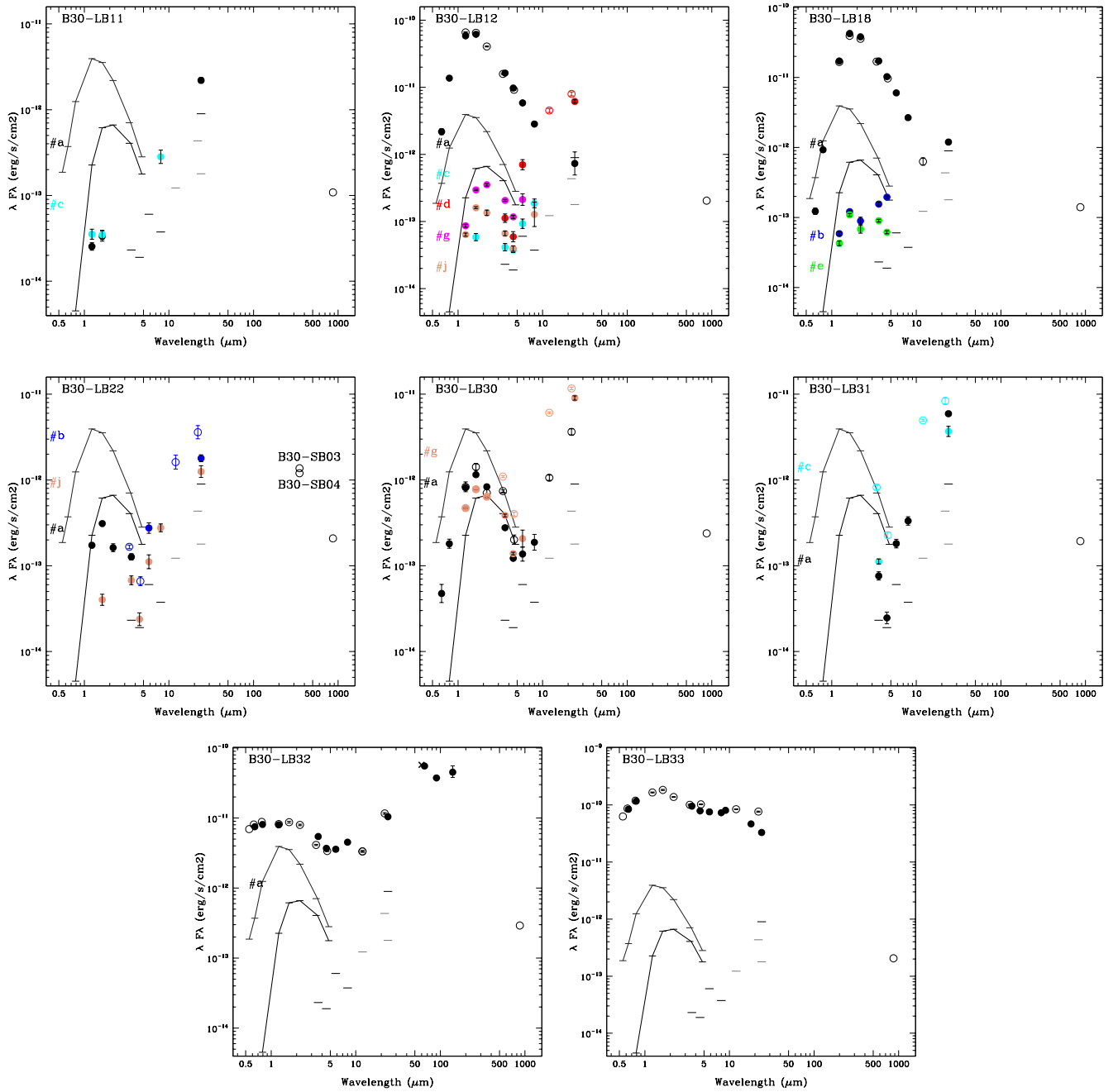


**Fig. A.9.** Spectral energy distribution for some relevant sources outside the FOV of the MIPS M2 image. All have been detected at  $24 \mu\text{m}$  with MIPS. Symbols as in Fig. A.2.

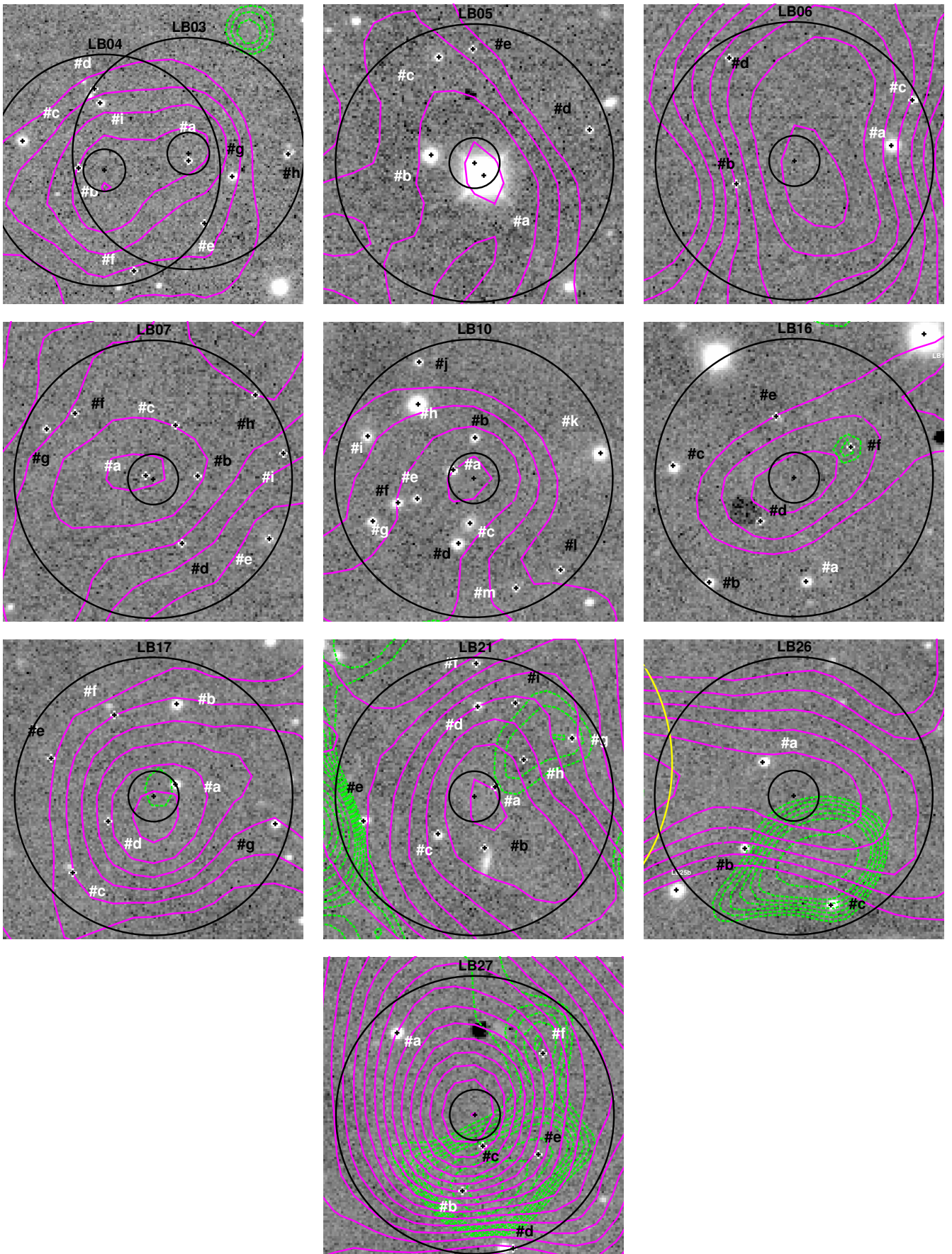


**Fig. A.10.** Finding charts for group C2 or sources outside the FOV of the MIPS M2 image. None of them have been detected  $24 \mu\text{m}$  with MIPS. Symbols as in Fig. A.1. We note that the feature displayed at  $24 \mu\text{m}$  for B30-LB16f corresponds to an artifact.

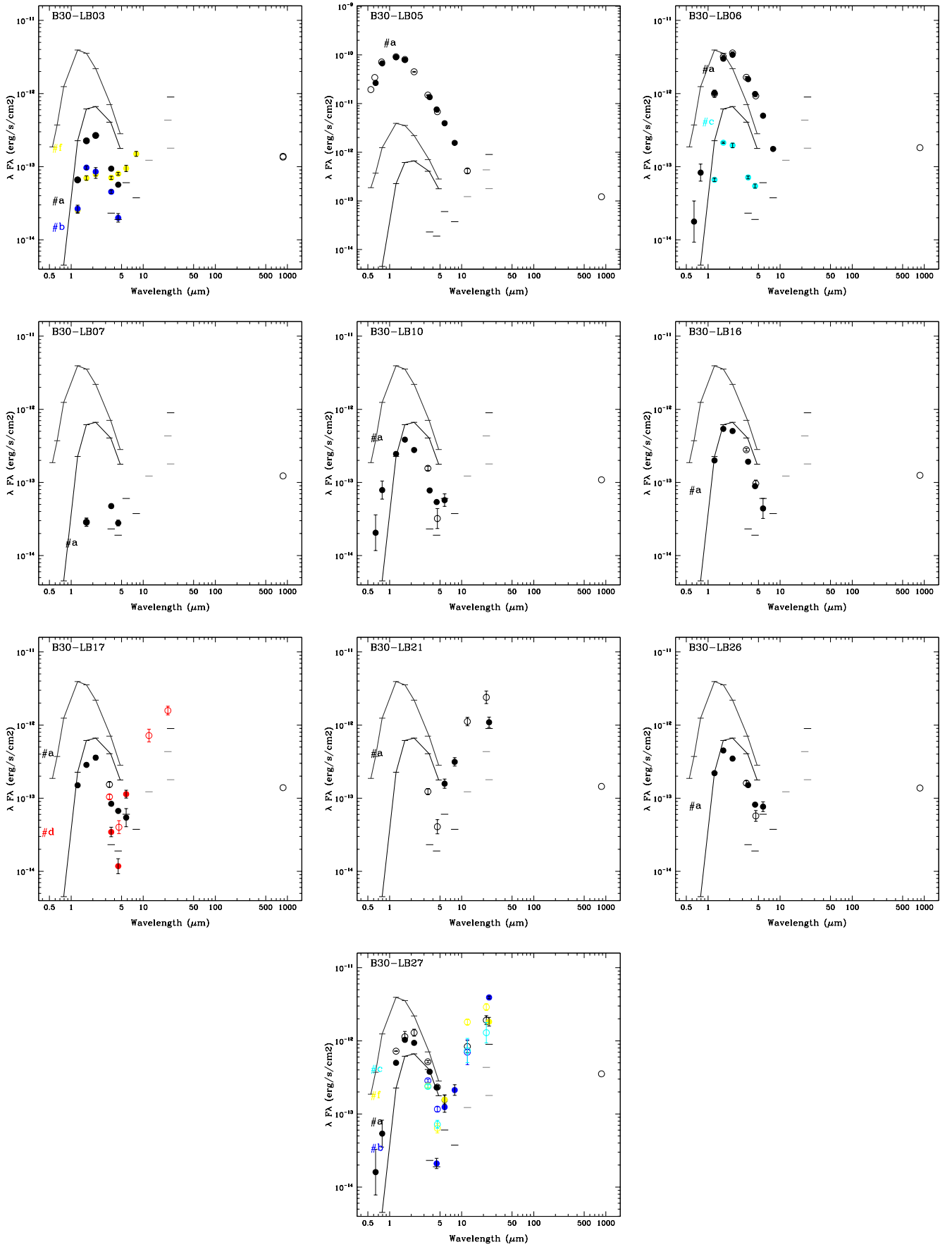


**Fig. A.11.** Spectral energy distribution for group C2 or sources outside the FOV of the MIPS M2 image. None of them have been detected at 24  $\mu\text{m}$  with MIPS. However, we note that B30-LB21 and B30-LB27 have a possible extended emission at 24  $\mu\text{m}$ . Symbols as in Fig. A.2.